

**Investigations on the Role of the  
Glucocorticoid-Induced Leucine Zipper  
in Macrophage Activation with a Focus on  
Sodium-Mediated Inflammation and Trained Immunity**

Dissertation

zur Erlangung des Grades des  
Doktors der Naturwissenschaften (Dr. rer. nat.) der  
Naturwissenschaftlich-Technischen Fakultät der  
Universität des Saarlandes

**Thierry Maxime Legroux**

Saarbrücken

2024

Tag des Kolloquiums: 24.09.2024

Dekan: Univ.-Prof. Dr.-Ing. Michael Vielhaber

Vorsitzender: Prof. Dr. Jörn Walter

Berichterstatter/in: Prof. Dr. Alexandra K. Kiemer

Prof. Dr. Andriy Luzhetskyy

Akad. Mitarbeiterin: Dr. Agnes-Valencia Weiß

## Zusammenfassung

Diese Doktorarbeit untersucht die vielschichtige Rolle des *glucocorticoid-induced leucine zipper*-Proteins (GILZ) in der Makrophagenbiologie und dessen mögliche therapeutische Anwendung bei entzündlichen Erkrankungen durch die Verwendung von *GILZ-knockout*- und *GILZ-transgenen* Makrophagen. Die Untersuchung der Auswirkungen von GILZ auf entzündliche Prozesse konzentriert sich speziell auf Entzündungen, die durch hohen Salzkonsum und die trainierte angeborene Immunität hervorgerufen werden. Der hohe Salzkonsum, der in modernen Ernährungsweisen verbreitet ist, steht in enger Verbindung mit kardiovaskulären Risiken und entzündlichen Erkrankungen. Die trainierte angeborene Immunität stellt einen neuen Rahmen für das Verständnis der Rolle von (patho-)physiologischen Entzündungen dar. Kapitel 1 zeigt, dass GILZ die Funktionen von Makrophagen hin zu einer Bereinigung der Entzündung verbessert, indem es die Abwehr von Bakterien und die Phagozytose verbessert, vor Pyroptose schützt und die mitochondrialen Aktivitäten moduliert. Diese Ergebnisse legen potenzielle therapeutische Anwendungen von GILZ zur Behandlung von entzündlichen Erkrankungen nahe. In Kapitel 2 wird die Interaktion zwischen GILZ und hohen Natriumkonzentrationen untersucht, wobei sich herausstellt, dass GILZ nur marginal Einfluss auf die Reaktionen von Makrophagen auf erhöhte Salzspiegel hat. Kapitel 3 untersucht die Rolle von GILZ in der trainierten angeborenen Immunität von Makrophagen und deutet unter unseren experimentellen Bedingungen auf kaum Einflussnahme hin, wobei die direkte Beteiligung von GILZ noch vollständig aufgeklärt werden muss. Insgesamt trägt diese Arbeit dazu bei, unser Verständnis von GILZ als entscheidendem Regulator bei der von Makrophagen vermittelten Entzündung zu vertiefen und betont dessen potenzielle therapeutische Anwendungen bei immunbezogenen Störungen.

## Abstract

This doctoral thesis explores the multifaceted role of glucocorticoid-induced leucine zipper (GILZ) in macrophage biology and its therapeutic implications for immune-related disorders, utilizing *GILZ knockout* and *GILZ transgenic* macrophages. The investigation of GILZ's effects on inflammatory processes specifically focuses on inflammation induced by high salt intake and trained immunity. High salt intake, prevalent in modern diets, is intricately linked to cardiovascular health risks and inflammatory diseases. Trained immunity emerges as a novel framework for understanding the role of inflammation in health and disease. Chapter 1 investigates how GILZ enhances macrophage functions, emphasizing its enhancement of phagocytosis, protection against pyroptosis, and modulation of mitochondrial activity. These findings suggest potential therapeutic applications of GILZ in managing inflammatory diseases. In Chapter 2, the interaction between GILZ and high sodium conditions is examined, revealing minimal impact on macrophage responses to elevated salt levels. Chapter 3 explores GILZ's role in trained innate immunity of macrophages, suggesting limited influence under our experimental conditions, although GILZ's direct involvement remains to be fully elucidated. Overall, this thesis advances our understanding of GILZ as a critical regulator in macrophage-mediated inflammation, underscoring its potential therapeutic applications in immune-related disorders.

## Table of contents

<b>Zusammenfassung</b> .....	<b>3</b>
<b>Abstract</b> .....	<b>3</b>
<b>Table of contents</b> .....	<b>4</b>
<b>Abbreviations</b> .....	<b>6</b>
<b>Chapter 1 Immunomodulation by Glucocorticoid-Induced Leucine Zipper (GILZ) in Macrophages: Enhanced Phagocytosis, Protection from Pyroptosis, and Altered Mitochondrial Function</b> .....	<b>8</b>
1.1 Published work in this dissertation .....	8
1.2 Contribution to the research field to a non-expert .....	25
1.3 Author contributions .....	25
<b>Chapter 2 The Interplay Between Sodium in the Microenvironment and the Glucocorticoid-Induced Leucine Zipper (GILZ): Determinants of Macrophage Activation</b> 26	
2.1 Introduction.....	26
2.1.1 Health Implications of High Salt Consumption .....	26
2.1.2 Sodium is Stored in the Human Skin.....	26
2.1.3 How Macrophages Sense and Respond to Sodium Chloride .....	27
2.1.4 GILZ Regulates the Sodium Balance in the Kidney .....	28
2.1.5 Hypothesis: GILZ Is Involved in High Salt-mediated Inflammation of Macrophages.....	28
2.2 Results.....	28
2.2.1 Characterization of GILZ Knockout and GILZ Transgenic Macrophages .....	28
2.2.2 Regulation of GILZ Expression by High Salt in Macrophages.....	29
2.2.3 No Detectable Involvement of GILZ in Short-Term High Salt Effects .....	30
2.2.4 No Detectable Involvement of GILZ in Long-Term High Salt Effects .....	31
2.2.5 Aldosterone Induces <i>Gilz</i> via the Glucocorticoid Receptor .....	32
2.3 Discussion .....	33
<b>Chapter 3 Investigating the Role of Glucocorticoid-Induced Leucine Zipper (GILZ) in Trained Immunity of Macrophages</b> .....	<b>34</b>
3.1 Introduction.....	34
3.1.1 Immune Memory .....	34
3.1.2 Trained Innate Immunity: Mechanisms and Molecular Pathways .....	34
3.1.3 Clinical Implications and Therapeutic Potential of Trained Innate Immunity.....	35
3.1.4 Hypothesis: Role of GILZ in Trained Innate Immunity.....	35
3.2 Results.....	37
3.2.1 Training Differentiated Macrophages .....	37
3.2.2 Training <i>in vivo</i> .....	38
3.2.3 Training Macrophage Progenitor Cells .....	39
3.3 Discussion .....	40
3.3.1 Training BMPCs vs. BMMs .....	40
3.3.2 Structural Diversity of $\beta$ -glucans and their Influence on TRIM .....	41
3.3.3 Sex-specific Differences in TRIM.....	42
<b>Chapter 4 Materials and Methods</b> .....	<b>44</b>
4.1.1 Materials .....	44
4.1.2 Mice .....	44
4.1.3 Cell Culture Conditions .....	44
4.1.4 Mouse Genotyping .....	44
4.1.5 Generation of BMMs.....	45
4.1.6 RNA Sequencing (RNA-Seq).....	45
4.1.7 RNA-Seq Data Processing and Analysis.....	45

4.1.8	RNA isolation, Reverse Transcription, and qRT-PCR.....	45
4.1.9	pHrodo™ Phagocytosis Assay .....	46
4.1.10	Salmonella enterica and Escherichia coli Infection Assay .....	46
4.1.11	Griess Assay .....	46
4.1.12	Real-time Caspase-3/7 Activity and Cytotoxicity Detection .....	47
4.1.13	ELISA .....	47
4.1.14	Detection of Reactive Oxygen Species (ROS).....	47
4.1.15	Agilent Seahorse Cell Mito Stress and Glycolysis Stress Test .....	47
4.1.16	Quantification of Mitochondrial DNA Copy Number .....	47
4.1.17	Flow Cytometry.....	47
4.1.18	BMM-Conditioned Media .....	47
4.1.19	Cell Migration and Proliferation Assays .....	48
4.1.20	Gelatin Zymography.....	48
4.1.21	L929-conditioned Media .....	48
4.1.22	Western Blot.....	48
4.1.23	<i>In vitro</i> BMM β-glucan Training.....	49
4.1.24	<i>In vivo</i> Induction of Trained Innate Immunity .....	49
4.1.25	RAW-Blue™ Reporter Cells .....	50
4.1.26	Data Representation and Statistics .....	50
	<b>Publications.....</b>	<b>51</b>
	<b>Curriculum Vitae .....</b>	<b>52</b>
	<b>Acknowledgements.....</b>	<b>53</b>
	<b>References (categorized).....</b>	<b>54</b>

Some figures included in this thesis are taken from articles published by the Springer Nature Portfolio Publishing Group. Permission to use these figures has been obtained through the Copyright Clearance Center's RightsLink® service, and appropriate credit is given. All figures have been used in accordance with the terms specified by the publisher under the license number #5824180710313, #5824181446990, #5824190131597, and #5824190251488.

## Abbreviations

2-DG	2-Desoxyglucose	GRE	Glucocorticoid response element
AA	Antimycin A	GSDMD	Gasdermin D
ACK	Ammonium-Chloride-Potassium	GSE	Gene Set Enrichment
ADAMTS2	A Disintegrin and Metalloproteinase with Thrombospondin Motifs 2	HAT	Histone Acetyltransferase
AIEC	Adherent-invasive Escherichia coli	HDAC	Histone Deacetylase
AKT	Protein Kinase B (also known as AKT)	HEPES	4-(2-Hydroxyethyl)-1-piperazineethane-sulfonic Acid
ANOVA	Analysis of Variance	HIF	Hypoxia-Inducible Factor
AP-1	Activator Protein 1	HMT	Histone Methyltransferase
Arg1	Arginase 1	HRP	Horseradish Peroxidase
Arg2	Arginase 2	HS	High Salt
ATAC	Assay for Transposase-Accessible Chromatin using Sequencing	IBD	Inflammatory Bowel Disease
ATCC	American Type Culture Collection	IFN	Interferon
ATP	Adenosine Triphosphate	IL	Interleukin
BCA	Bicinchoninic Acid	KO	Knockout
BCG	<i>Bacille Calmette-Guérin</i>	LPS	Lipopolysaccharide
BG	$\beta$ -Glucan	Ly6C	Lymphocyte Antigen 6 Family Member C1
BM	Bone Marrow	Ly6G	Lymphocyte Antigen 6 Family Member G
BMM	Bone Marrow-derived Macrophage	M-CSF	Macrophage Colony-Stimulating Factor
BMPC	Bone Marrow Progenitor Cell	MAPK	Mitogen-Activated Protein Kinase
CCL2	Chemokine (C-C motif) Ligand 2	MFI	Mean Fluorescence Intensity
CCR2	C-C chemokine receptor type 2	mitoROS	Mitochondrial reactive oxygen species
CD	Cluster of Differentiation	MMP	Matrix Metalloproteinase
CFU	Colony Forming Unit	MOI	Multiplicity of Infection
Co	Control	MR	Mineralocorticoid Receptor
CPM	Counts Per Million	Mrc1	Mannose Receptor C-type 1
DEG	Differentially Expressed Genes	MSC	Mesenchymal Stem Cells
DHE	Dihydroethidium	mtDNA	Mitochondrial DNA
DMSO	Dimethyl Sulfoxide	mTOR	Mammalian Target of Rapamycin
DNA	Deoxyribonucleic Acid	NADH	Nicotinamide Adenine Dinucleotide
DPP4	Dipeptidyl peptidase 4	NADPH	Nicotinamide Adenine Dinucleotide Phosphate
EAE	Experimental Autoimmune Encephalomyelitis	NCBI	National Center for Biotechnology Information
ECAR	Extracellular Acidification Rate	NCC	Na <sup>+</sup> -Cl <sup>-</sup> Cotransporter
ECM	Extracellular Matrix	NCLX	Mitochondrial Na <sup>+</sup> /Ca <sup>2+</sup> Exchanger
EDTA	Ethylenediaminetetraacetic Acid	NED	N-1-naphthylethylenediamine Dihydrochloride
EGFP	Enhanced Green Fluorescent Protein	NFAT	Nuclear Factor of Activated T-cells
ELISA	Enzyme-Linked Immunosorbent Assay	NF- $\kappa$ B	Nuclear factor kappa-light-chain-enhancer of activated B cells
ENaC	Epithelial Sodium Channel	NGS	Next-Generation Sequencing
F4/80	aka AGRE1 Adhesion G protein-coupled receptor E1	NLRP	NOD-like Receptor Protein
FACS	Fluorescence-Activated Cell Sorting	NO	Nitric Oxide
FBS	Fetal Bovine Serum aka FCS Fetal Calf Serum	Nos2	Nitric Oxide Synthase 2
FCCP	Carbonyl Cyanide-p-trifluoromethoxy-phenylhydrazone	<i>ns</i>	Not Significant
FDR	False Discovery Rate	NS	Normal Salt
FSC-A	Forward Scatter Area	O	Oligomycin
FSC-W	Forward Scatter Width	OCR	Oxygen Consumption Rate
GABA	Gamma-Aminobutyric Acid	OD	Optical Density
GC	Glucocorticoid	OXPHOS	Oxidative Phosphorylation
GCU	Green Calibrated Units	PAGE	Polyacrylamide Gel Electrophoresis
GEO	Gene Expression Omnibus	PBS	Phosphate-Buffered Saline
GILZ	Glucocorticoid-Induced Leucine Zipper	PCA	Principal Component Analysis
GO	Gene Ontology	PCR	Polymerase Chain Reaction
GR	Glucocorticoid Receptor	PFA	Paraformaldehyde

---

Ppia	Peptidylprolyl Isomerase A aka Cyclophilin A
PVDF	Polyvinylidene Fluoride
qRT-PCR	Real Time Quantitative Polymerase Chain Reaction
RA	Rotenone A
RCU	Red Calibrated Units
RNA	Ribonucleic Acid
ROS	Reactive Oxygen Species
RT	Reverse Transcription
SDS	Sodium Dodecyl Sulfate
SEAP	Secreted Alkaline Phosphatase
SEDIGRAM	Selective Dimerizing GC-Receptor Agonists or Modulators
SEM	Standard Error of the Mean
Sgk1	Serum- and Glucocorticoid-Regulated Kinase 1
SiglecF	Sialic Acid Binding Ig-like Lectin F
Slc6a12	Solute Carrier Family 6 (Neurotransmitter Transporter, Betaine/ GABA), Member 12
SSC-A	Side Scatter Area
TAT	Trans-Acting Activator of Transcription
TBS	Tris-Buffered Saline
TBST	Tris-Buffered Saline with Tween
TE	Tris-EDTA
TG	Transgenic
Tgfb	Transforming Growth Factor, Beta
TLR	Toll-Like Receptor
TMB	Tetramethylbenzidine
TNF	Tumor Necrosis Factor
TPM	Transcripts Per Million
TRIM	Trained Innate Immunity
Vegfa	Vascular Endothelial Growth Factor A
WGP	Whole Glucan Particles
WT	Wild Type
Ym1	aka Chitinase-Like Protein 3 (Chil3)

# Chapter 1 Immunomodulation by Glucocorticoid-Induced Leucine Zipper (GILZ) in Macrophages: Enhanced Phagocytosis, Protection from Pyroptosis, and Altered Mitochondrial Function

## 1.1 Published work in this dissertation

This chapter addresses the general characterization of glucocorticoid-induced leucine zipper (GILZ) by investigating gene expression in GILZ knockout (KO) and GILZ-overexpressing (TG) bone marrow-derived macrophages (BMMs) through bulk RNA sequencing and functional assays. GILZ is well-documented in the literature for its anti-inflammatory and immunosuppressive effects, acting as a downstream mediator of glucocorticoids and influencing various immune cell functions. It has been shown to regulate T cell activity, B cell function, and macrophage responses, making it a critical player in the immune system.

We found that GILZ plays a crucial role in modulating macrophage functions, including enhancing phagocytosis and antibacterial activity, providing protection from pyroptosis by modulating reactive oxygen species (ROS) production, altering mitochondrial function, and increasing matrix metalloproteinase activity, suggesting its involvement in tissue remodeling processes.

These findings underscore the therapeutic potential of GILZ in managing inflammatory and autoimmune diseases, aligning with its identified role as a mediator of glucocorticoid effects and its promise in therapeutic applications for conditions like inflammatory bowel disease (IBD), rheumatoid arthritis, and sepsis. Understanding GILZ's regulatory effects in macrophages could pave the way for novel treatments targeting macrophage-mediated inflammation.

The work in this project has been published in *Frontiers in Immunology* under this reference and is included in the PhD thesis:

**Thierry M Legroux**, Hanna S Schymik, Gilles Gasparoni, Saeed Mohammadi, Jörn Walter, Claude Libert, Britta Diesel, Jessica Hoppstädter and Alexandra K. Kiemer (2024):

Immunomodulation by glucocorticoid-induced leucine zipper in macrophages: enhanced phagocytosis, protection from pyroptosis, and altered mitochondrial function.

*Frontiers in Immunology* 15:1396827.

doi: [10.3389/fimmu.2024.1396827](https://doi.org/10.3389/fimmu.2024.1396827)





## OPEN ACCESS

## EDITED BY

Jagadeesh Bayry,  
Indian Institute of Technology Palakkad, India

## REVIEWED BY

Gajanan Katkar,  
University of California, San Diego,  
United States  
Susan Taylor Yeyeodu,  
Charles River Discovery Services,  
United States

## \*CORRESPONDENCE

Alexandra K. Kiemer

✉ pharm.bio.kiemer@mx.uni-saarland.de

RECEIVED 06 March 2024

ACCEPTED 07 May 2024

PUBLISHED 23 May 2024

## CITATION

Legroux TM, Schymik HS, Gasparoni G,  
Mohammadi S, Walter J, Libert C, Diesel B,  
Hoppstädter J and Kiemer AK (2024)  
Immunomodulation by glucocorticoid-  
induced leucine zipper in macrophages:  
enhanced phagocytosis, protection  
from pyroptosis, and altered  
mitochondrial function.  
*Front. Immunol.* 15:1396827.  
doi: 10.3389/fimmu.2024.1396827

## COPYRIGHT

© 2024 Legroux, Schymik, Gasparoni,  
Mohammadi, Walter, Libert, Diesel,  
Hoppstädter and Kiemer. This is an open-  
access article distributed under the terms of  
the [Creative Commons Attribution License  
\(CC BY\)](https://creativecommons.org/licenses/by/4.0/). The use, distribution or reproduction  
in other forums is permitted, provided the  
original author(s) and the copyright owner(s)  
are credited and that the original publication  
in this journal is cited, in accordance with  
accepted academic practice. No use,  
distribution or reproduction is permitted  
which does not comply with these terms.

# Immunomodulation by glucocorticoid-induced leucine zipper in macrophages: enhanced phagocytosis, protection from pyroptosis, and altered mitochondrial function

Thierry M. Legroux<sup>1</sup>, Hanna S. Schymik<sup>1</sup>, Gilles Gasparoni<sup>2</sup>,  
Saeed Mohammadi<sup>3</sup>, Jörn Walter<sup>2</sup>, Claude Libert<sup>4,5</sup>,  
Britta Diesel<sup>1</sup>, Jessica Hoppstädter<sup>1</sup> and Alexandra K. Kiemer<sup>1\*</sup>

<sup>1</sup>Department of Pharmacy, Pharmaceutical Biology, Saarland University, Saarbrücken, Germany,

<sup>2</sup>Department of Genetics, Saarland University, Saarbrücken, Germany, <sup>3</sup>Natural and Medical Sciences Research Center, University of Nizwa, Nizwa, Oman, <sup>4</sup>Flanders Institute for Biotechnology (VIB) Center for Inflammation Research, Ghent, Belgium, <sup>5</sup>Department of Biomedical Molecular Biology, Ghent University, Ghent, Belgium

Glucocorticoids, which have long served as fundamental therapeutics for diverse inflammatory conditions, are still widely used, despite associated side effects limiting their long-term use. Among their key mediators is glucocorticoid-induced leucine zipper (GILZ), recognized for its anti-inflammatory and immunosuppressive properties. Here, we explore the immunomodulatory effects of GILZ in macrophages through transcriptomic analysis and functional assays. Bulk RNA sequencing of GILZ knockout and GILZ-overexpressing macrophages revealed significant alterations in gene expression profiles, particularly impacting pathways associated with the inflammatory response, phagocytosis, cell death, mitochondrial function, and extracellular structure organization activity. GILZ-overexpression enhances phagocytic and antibacterial activity against *Salmonella typhimurium* and *Escherichia coli*, potentially mediated by increased nitric oxide production. In addition, GILZ protects macrophages from pyroptotic cell death, as indicated by a reduced production of reactive oxygen species (ROS) in GILZ transgenic macrophages. In contrast, GILZ KO macrophages produced more ROS, suggesting a regulatory role of GILZ in ROS-dependent pathways. Additionally, GILZ overexpression leads to decreased mitochondrial respiration and heightened matrix metalloproteinase activity, suggesting its involvement in tissue remodeling processes. These findings underscore the multifaceted role of GILZ in modulating macrophage functions and its potential as a therapeutic target for inflammatory disorders, offering insights into the development of novel therapeutic strategies aimed at optimizing the benefits of glucocorticoid therapy while minimizing adverse effects.

## KEYWORDS

RNA-seq, immunometabolism, extracellular matrix, lipopolysaccharide (LPS), reactive oxygen species (ROS), iNOS

## 1 Introduction

For over 60 years, glucocorticoids (GCs) have been a cornerstone in therapeutic strategies for their potent anti-inflammatory and immunosuppressive effects, addressing a spectrum of conditions such as rheumatic diseases, inflammatory bowel disease (IBD), autoimmune disorders, chronic inflammatory diseases, asthma, and cancer (1). Despite the emergence of more targeted biological therapies, GCs persist as widely utilized agents. In autoimmune and chronic inflammatory conditions, they are favored for providing symptomatic relief (2), and in the case of IBD, they serve as a fundamental treatment for moderate-to-severe cases (3). Additionally, in the oncological context, GCs play a pivotal role in managing cancer-related symptoms and addressing side effects of anti-cancer therapies and immune-related adverse events (4).

The use of GC therapy, despite its efficacy in mitigating inflammation and immune activation, is often constrained by a spectrum of side effects, frequently restricting its long-term application. These include musculoskeletal, gastrointestinal, cardiovascular, endocrine, neuropsychiatric, dermatologic, ocular, and immunologic issues (5). Of particular concern are the metabolic side effects, such as central adiposity, dyslipidemia, insulin resistance, and glucose intolerance, which can lead to diabetes (6). Other common side effects include weight gain, skin thinning, sleep disturbance, and neuropsychiatric disorders (7).

To optimize the benefits of GC therapy while minimizing adverse effects, several strategies are being explored. Metformin is being investigated as a promising drug for preventing metabolic side effects during systemic GC treatment (8). Targeted delivery of GCs to diseased tissues using antibody-glucocorticoid conjugates is being explored as a therapeutic alternative to overcome systemic side effects (9). In addition, the development of selective dimerizing GC-receptor agonists or modulators (SEDIGRAMs) aims to capitalize on specificities within the GC signaling pathway, potentially mitigating systemic side effects associated with monomeric activity (10).

GCs exert their actions on cells through a variety of mechanisms, including genomic and non-genomic pathways, tissue-specific effects, and interactions with other signaling pathways (11). Upon binding to the glucocorticoid receptor (GR) in the cytoplasm, the classical mechanism involves the hormone receptor complex modulating gene expression either positively or negatively by directly binding to GREs located in the promoter regions of target genes (12). The GR exhibits ubiquitous expression across cell types, thereby influencing the functionality of practically all immune cells (13). Approximately 20–30% of genes are deemed responsive to the GR, with the glucocorticoid-induced leucine zipper (GILZ, gene name TSC22D3) being among the earliest targets of GR, making it a promising GC-induced downstream effector molecule (10, 14, 15).

GILZ has been identified as a key mediator of the anti-inflammatory and immunosuppressive effects of GCs (16). GILZ is strongly upregulated by GCs and plays a crucial role in controlling major activities of T cells (17), B cells (18), MSCs (19), neutrophils (20), and macrophages (21).

Shortly following the characterization of GILZ in immune cells, the consideration of its therapeutic application emerged (22). Selective upregulation of GILZ and the use of recombinant GILZ protein have emerged as promising therapeutic approaches in diseases like inflammatory bowel disease (IBD), rheumatoid arthritis, psoriasis, sepsis, and diabetic retinopathy (2, 23–28). Leveraging its anti-inflammatory properties, GILZ holds the potential for therapeutic interventions in these conditions.

In macrophages, GILZ has been implicated in mediating typical GC effects, such as the regulation of macrophage activation (29). GCs aside, GILZ has demonstrated beneficial properties in combating inflammatory diseases. Transgenic mice that overexpress GILZ have been found to be more resistant to spinal cord injury, while GILZ knockout mice develop worse inflammatory conditions (30, 31). Furthermore, studies have demonstrated that selective GILZ overexpression in macrophages improves outcomes in septic animals by limiting systemic inflammation while increasing bacterial clearance (32, 33). The administration of a cell-permeable GILZ fusion protein (TAT-GILZ) facilitated the accelerated resolution of bacteria-induced pneumonia and peritonitis in mice, further underscoring the therapeutic potential of GILZ in modulating macrophage-mediated inflammation (34, 35).

Understanding the role of GILZ in macrophages and its potential therapeutic applications is crucial for advancing precision medicine in inflammatory disorders. In this context, our study employs RNA sequencing to investigate gene expression in GILZ knockout (KO) and GILZ-overexpressing (TG) macrophages (murine bone marrow-derived macrophages, BMMs), aiming to uncover the molecular mechanisms underlying GILZ-mediated effects and its therapeutic potential.

Here, we provide evidence for the immunomodulatory effects of GILZ overexpression in macrophages, demonstrating enhanced antibacterial activity, protection from pyroptosis, and altered mitochondrial function. Additionally, our findings reveal a significant impact on Matrix metalloproteinase (MMP) activity, suggesting a role for GILZ in influencing extracellular matrix remodeling and wound healing processes.

## 2 Materials and methods

### 2.1 Materials

RPMI-1640 cell culture media (#R0833), 200 mM L-glutamine (#G7513), 1% penicillin/streptomycin (#P4333), Accutase (#A6964), mitomycin C (#10107409001), antimycin A from *Streptomyces* sp. (#A8674), gentamicin (#G1397), dihydroethidium (DHE) (#37291), and gelatin type A (#G1890) were from Sigma-Aldrich. FBS (#P040–37500) and Panexin BMM Serum Substitute (#P04–951SA2) were obtained from PAN Biotech. Ultrapure lipopolysaccharide (LPS) from *E. coli* K12 (#tlrl-pekllps), and ATP (#tlrl-atpl) were purchased from Invivogen. TE buffer (#A0386.1000), and DMSO (#A3672-0250) were from AppliChem, M-CSF (#130–101-705) from Miltenyi Biotech, and mouse recombinant IFN- $\gamma$  (#87389.100) from Biomol.

Primers for qRT-PCR were purchased from Eurofins Genomics. Other chemicals were obtained from either Sigma-Aldrich or Carl Roth unless stated otherwise.

## 2.2 Mice

Animal housing and all experimental procedures were approved by the local animal welfare committee (AZ 2.4.1.1). C57BL/6J mice were housed in individually ventilated cages in a temperature and humidity-controlled room (22–24°C, 45–65 relative humidity) and a 12 h light/dark cycle. Water and food were provided *ad libitum*. Mice were age and sex-matched within experimental sets. B6.129P2-Lyz2<sup>tm1(cre)Ifo</sup>/J mice with Cre recombinase expression under the endogenous *Lyz2* promoter of the myeloid cell lineage were considered *wild-type* (WT). Crossing these animals with mice bearing loxP sites up and downstream of *Gilz* exon 6 resulted in a myeloid-specific *knockout* of GILZ (B6.129P2-Tsc22d3<sup>fl</sup> Lyz2<sup>tm1(cre)Ifo</sup>/J, GILZ KO). Both strains were described previously (36). In addition, mice bearing a *Tsc22d3/Gilz-1* cDNA knock-in under the control of the ROSA26 promoter preceded by a loxP-flanked stop cassette (37) were crossed with B6.129P2-Lyz2<sup>tm1(cre)Ifo</sup>/J mice, resulting in myeloid-specific GILZ overexpression. These animals (BL6Tsc22d3<sup>Rosa26EGFPtg</sup> Lyz2<sup>tm1(cre)Ifo</sup>/J) are designated as GILZ-overexpressing or transgenic (GILZ TG).

## 2.3 Cell culture conditions

Cells were cultured in a humidified incubator at 37°C and 5% CO<sub>2</sub> in RPMI-1640 cell culture media supplemented with 10% FBS, 1% 200 mM L-glutamine, and 100 units/ml penicillin/streptomycin (P/S) unless stated otherwise.

## 2.4 Generation and treatment of BMMs

BMMs were obtained from 10- to 23-week-old mice as described previously (38). Mice were sacrificed, and femurs and tibias were removed. The bone marrow was flushed out with cell culture medium using a 27G cannula and passed through a 100 µm cell strainer before erythrocyte lysis in hypotonic buffer (155 mM NH<sub>4</sub>Cl, 10 mM KHCO<sub>3</sub>, 1 mM Na<sub>2</sub>EDTA) at 37°C for 3 min. Cells were either resuspended in FBS with 10% DMSO for cryopreservation or kept in cell culture medium supplemented with M-CSF (50 ng/ml) for differentiation to BMMs (BMM medium). Cryopreserved cells were cooled to -80°C using the MrFrosty™ device (Thermo Scientific, #5100-0001) and transferred into liquid nitrogen for long-term storage. Bone marrow cells were incubated overnight in 30 ml of BMM medium in a T75 flask. On the next day, non-adherent cells were transferred to a fresh cell culture flask and incubated for 5 more days in 45 ml of BMM medium in a T175 flask. Subsequently, cells were washed once with PBS, detached with Accutase, and counted using the LUNA-FL™ Automated Fluorescence Cell Counter (Logos Biosystems) with Acridine Orange/Propidium Iodide

staining according to the manufacturer's protocol. The viable cell count was used to calculate seeding densities. All cell preparations had a viability of at least 95%. The identity of BMMs was verified by flow cytometric analysis using F4/80 as a macrophage marker, with purity levels > 95% (38, 39). Approximately 20–30 million differentiated BMMs were obtained per mouse. BMMs were seeded and treated in BMM medium according to the specified conditions for each assay.

BMM-conditioned media for migration and proliferation assays were generated by incubating 10<sup>6</sup> BMMs in a 6-well format with 3 ml per well of BMM medium for 24 h starting at the time of seeding. To assess MMP activity, 75,000 BMMs were incubated in a 96-well format with 150 µl of BMM media containing Panexin BMM serum substitute (PAN Biotech, #P04-951SA2) instead of FBS for 24 h, starting at the time of seeding.

## 2.5 RNA sequencing

For transcriptome analysis of BMMs from WT, GILZ KO, and GILZ TG mice, next-generation sequencing (NGS) was performed as described previously (40). 500,000 BMMs (1 ml/well) were seeded in a 12-well plate and treated for 4 h with LPS (100 ng/ml) on the next day. RNA was isolated using the High Pure RNA Isolation Kit (Roche, #11828665001) according to the manufacturer's protocol and stored at -80°C. All RNA samples used for further analysis had an RNA integrity number > 9 according to the analysis in a 2100 Bioanalyzer (Agilent) using the RNA 6000 Nano Kit (Agilent, #5067-1513). Libraries were prepared from 500 ng RNA. Poly(A) enrichment was performed on the input total RNA using the NEBNext Poly(A) mRNA Magnetic Isolation Module (New England Biolabs, #E7490) according to the manufacturer's instructions. The cDNA library preparation was conducted with the NEBNext Ultra Directional RNA Library Prep Kit for Illumina (New England Biolabs, #E7420) as recommended by the supplier. In brief, first- and second-strand cDNA synthesis was performed, followed by adapter ligation and PCR amplification of the final library (12 cycles). PCR cleanup was performed using Agencourt AM-Pure XP beads (Beckmann Coulter, #A63881). Libraries were sequenced for 1x 75 nt on a NextSeq500 (Illumina) sequencer.

## 2.6 RNA-seq data processing and analysis

Raw reads were demultiplexed and subjected to quality control through FastQC v0.11.2. Read processing was performed with grape-nf pipeline (v1.1.3) using Nextflow (v20.10.0) and mapped to GRC38mm10 assembly. The counts obtained after alignment were used to analyze differential expression using DESeq2 v1.40.2. Principle component analysis was performed using the CPM values of all annotated protein-coding genes. All analyses were conducted in the R programming language. DESeq2 analysis revealed differentially expressed genes (DEGs, *p* < 0.05) in the comparisons of GILZ KO vs. WT, GILZ TG vs. WT, and GILZ KO vs. GILZ TG under both untreated and LPS-treated conditions.

Subsequently, TPM values of the DEGs from all three contrasts were subjected to k-Means unsupervised clustering using iDEP 1.12, independently for untreated and LPS-treated cells (41). Processed and raw data were deposited in the Gene Expression Omnibus (GEO) database under the accession code GSE254137.

## 2.7 pHrodo™ phagocytosis assay

50,000 BMMs (150  $\mu$ l/well) were seeded into a 96-well plate and incubated overnight. pHrodo™ Red *S. aureus* Bioparticles™ (Thermo Scientific, #A10010) were suspended in PBS and treated in an ultrasonic water bath for 15 min at 37°C according to the manufacturer's protocol before adding 5  $\mu$ l of a 1  $\mu$ g/ $\mu$ l dilution to each well. Real-time imaging was started immediately in the Incucyte® S3 Live-Cell Analysis System (Essen BioScience) in the brightfield and red fluorescence channel (10x objective lens, 400 ms acquisition time). The phagocytic capacity was calculated as the total red object integrated intensity (RCU x  $\mu$ m<sup>2</sup>/Image) normalized to cell confluency [%] at the start of the assay as described previously (42).

## 2.8 *Salmonella enterica* and *Escherichia coli* infection assay

*Salmonella enterica* subsp. *enterica* serotype *Typhimurium* (NCTC® 12023) (43) and *Escherichia coli* TOP10 (Invitrogen™) were cultured overnight in LB at 37°C in an orbital shaker. Bacteria were washed once in PBS and resuspended in BMM media without P/S supplementation to infect BMMs at a multiplicity of infection (MOI) of 20 with *S. typhimurium* and an MOI of 100 with *E. coli*. Bacterial cell count was determined by OD<sub>600</sub> measurement assuming that an OD<sub>600</sub> of 1 equates to 10<sup>9</sup> colony-forming units (CFU). BMMs were seeded the day before in a 24-well plate (250,000 cells/well, 0.5 ml). Infection was synchronized by centrifuging for 5 min at 300 x g and maintained for 30 min. After the infection, BMMs were washed twice with PBS and cultured in cell culture media containing 100  $\mu$ g/ml gentamicin for 90 min to kill extracellular bacteria, after which the gentamicin concentration was reduced to 10  $\mu$ g/ml. BMMs were lysed in 1% Triton-X 100 after a total incubation time of 3 h for *E. coli* and 6 h for *S. typhimurium*. Lysis was stopped by adding LB media. The bacterial load of the infected BMMs was determined by serially diluting the lysates in PBS and plating them out on LB agar as described previously (44). Plates were incubated for 24 h at 37°C and CFUs were counted using ImageJ (Version 1.53k) (45).

## 2.9 Griess assay

Nitric oxide (NO) production was assessed by Griess assay as previously described (42). BMMs were seeded the day before in a 24-well plate (250,000 cells/well, 0.5 ml). On the next day, cells were treated with LPS (100 ng/ml) and IFN- $\gamma$  (25 ng/ml) for 24 h before 100  $\mu$ l of supernatant was incubated for 10 min at room temperature

with 90  $\mu$ l 1% sulfanilamide in 5% phosphoric acid, then 90  $\mu$ l 1% N-1-naphthylethylenediamine dihydrochloride (NED) was added and incubated for 5 min until absorbance was measured at  $\lambda = 560$  nm in a GloMax® Discover Microplate Reader (Promega). Absolute concentrations were determined by measuring a NaNO<sub>2</sub> standard curve in parallel for each assay. Data were normalized to protein contents measured by the Pierce™ BCA Protein Assay Kit according to the manufacturer's protocol (Thermo Scientific, #23227).

## 2.10 RNA isolation, reverse transcription, and qRT-PCR

Cells were infected with *S. typhimurium* as described above and subsequently stored at -80°C until RNA was isolated using the High Pure RNA Isolation Kit (Roche, #11828665001) or the Direct-Zol RNA Miniprep Kit (ZymoResearch, #R2052) according to the manufacturer's protocol. Reverse Transcription was performed using the High-Capacity cDNA Kit (Thermo Scientific, #4368813) according to the manufacturer's protocol using 300–500 ng of RNA per reaction. RT products were diluted in TE buffer. qRT-PCR reactions were performed in technical duplicates or triplicates using HOT FIREPol EvaGreen qPCR Mix Plus (no ROX) (Solis Biodyne, #082500020) according to the manufacturer's protocol as described previously (40, 46). The qRT-PCR reaction comprised 15 min at 95°C and 40 cycles of 15 s at 95°C, 20 s at 60°C, and 20 s at 72°C. Quantification was achieved by the 2<sup>- $\Delta\Delta$ Cq</sup> method. The primer sequences are depicted in Table 1.

## 2.11 Real-time caspase-3/7 activity and cytotoxicity detection

50,000 BMMs (150  $\mu$ l/well) were seeded in 96-well plates and incubated overnight. To induce pyroptosis, cells were treated for 4 h with LPS (100 ng/ml) and subsequently with ATP (2 mM). Real-time imaging was started immediately after LPS treatment using the Incucyte® S3 Live-Cell Analysis System (Essen BioScience) in brightfield, red, and green fluorescence channels (10x objective lens, 300 ms acquisition time for the green channel and 400 ms for the red channel). Culture media was supplemented with 4  $\mu$ M CellEvent™ Caspase-3/7 Green Detection Reagent (Invitrogen, #C10723) and 0.25  $\mu$ M Incucyte® Cytotox Red Reagent (Essen BioScience, #4632) as described previously (47). Total red and green object integrated intensities (RCU x  $\mu$ m<sup>2</sup>/Image) was normalized to the initial cell confluency [%] in each well. Background fluorescence at the beginning of the assay was uniformly set to 0 for all wells. Spectral unmixing was set to 1.5% removal of red signal from green as recommended by the manufacturer.

## 2.12 ELISA

500,000 BMMs (1 ml/well) were seeded in 12-well plates and incubated overnight. Cells were treated for 4 h with LPS (100 ng/ml)

TABLE 1 Primer sequences for qRT-PCR reactions.

Gene	Transcript RefSeq (NCBI)	Forward sequence (5'→3')	Reverse sequence (5'→3')
<i>Arg1</i>	NM_007482.3	ACAAGACAGGGCTCCTTCAG	GGCTTATGGTTACCCCTCCCG
<i>Arg2</i>	NM_009705.3	ATCCCCTCCCTGCCAATCAT	CTAGCTTCTTCTGTCCCGGA
<i>Nos2</i>	NM_010927.3	CTTCTGGACATTACGACCC	TACTCTGAGGGCTGACACAA
<i>Ppia</i>	NM_008907.1	GCGTCTCCTTCGAGCTGTTT	CACCCTGGACATGAATCCT

and subsequently for 30 min with ATP (2 mM) before supernatants were stored at -80°C. IL-1 $\beta$  secretion was measured by ELISA (BioLegend #432604) according to the manufacturer's protocol. Supernatants were diluted 1:25 in ELISA assay diluent.

## 2.13 Detection of reactive oxygen species

50,000 BMMs (150  $\mu$ l/well) were seeded in 96-well plates and incubated overnight. Cells were treated for 4 h with LPS (100 ng/ml). Then, culture medium was exchanged to medium containing ATP (2 mM) and 10  $\mu$ M dihydroethidium (DHE). Real-time imaging was started immediately in the Incucyte<sup>®</sup> S3 Live-Cell Analysis System (Essen BioScience) in the brightfield and red fluorescence channels (10x objective lens, 400 ms acquisition time) upon ATP treatment. Total ROS production was determined as the total red object integrated intensity (RCU  $\times$   $\mu$ m<sup>2</sup>/Image) after 30 min normalized to cell confluency [%] at the start of the assay. For the detection of mitochondrial ROS production, cells were incubated with 5  $\mu$ M red MitoSOX<sup>™</sup> mitochondrial superoxide indicator (Invitrogen, #M36008) in PBS with 2% FCS. ATP (2 mM) or antimycin A (AA, 10  $\mu$ M) were added as indicated.

## 2.14 Agilent Seahorse XF Cell Mito Stress and Glycolysis Stress Test

50,000 BMMs (150  $\mu$ l/well) were seeded in Seahorse 96-well cell culture plates (Agilent, #103793–100) the day before the assay. Cells were left untreated or treated for 4 h with LPS (100 ng/ml). The Mito Stress Test (Agilent, #103015–100) and Glycolysis Stress Test (Agilent, #103020–100) were performed according to the recommendations in the manufacturer's protocol in a Seahorse XFe96 Analyzer (Agilent). OCR and ECAR measurements were normalized to cell count as determined in a Cytation 1 Cell Imaging Reader (BioTek) from brightfield images taken after the assay using the Gen5 software (Version 3.14) as described previously (47).

## 2.15 Quantification of mitochondrial DNA copy number

Mitochondrial DNA (mtDNA) copy number was determined following the protocol by Quiros et al. (48). Briefly, DNA was extracted from 250,000 BMMs cultured in 0.5 ml of BMM media

per well (12-well plate) using the DNA Mini Prep Plus kit (ZymoResearch, #D4069) as per the manufacturer's instructions. Subsequently, qRT-PCR was employed to measure the gene expressions of *mt16S*, *mtND1*, and *Hk2*, utilizing primer sequences adapted from the referenced publication. The mitochondrial DNA (mtDNA) copy number was calculated as the ratio between mtDNA content (mean expression of *mt16S* and *mtND1*) and nuclear DNA (nDNA) represented by *Hk2* expression.

## 2.16 Flow cytometry

10<sup>6</sup> BMMs (2 ml/well) were seeded in 6-well plates. On the next day, cells were detached by gently scraping the wells with a cell scraper (TPP<sup>®</sup>), resuspended in 2% FCS-containing PBS, stained for 45 min at 37°C with 0.1  $\mu$ M MitoTracker Green FM and Deep Red FM (Invitrogen, #M22426 and #M7514 respectively), and washed with 2% FCS-containing PBS. Flow cytometry measurements were performed using an LSRFortessa<sup>™</sup> (BD Biosciences) operated by FACS Diva 8.0.1 (BD Biosciences). In each measurement, at least 50,000 events were recorded. MFI of unstained control cells was subtracted from corresponding stained cells, and background-subtracted MFI values for WT cells were set as 100%. The pseudocolor plots were generated utilizing FlowJo 10.10.0 software.

## 2.17 Cell migration and proliferation assays

Cell migration and proliferation capacity were measured using the Incucyte<sup>®</sup> S3 Live-Cell Analysis System (Essen BioScience) as described previously (47, 49).

To assess migration capacity, L929 cells (ATCC: CCL-1<sup>™</sup>) were seeded (50,000 cells per well in 100  $\mu$ l medium) in 96-well ImageLock<sup>™</sup> plates (Essen BioScience, #BA-04856) and grown to full confluency overnight. Cells were cultured as described above. On the next day, cells were treated for 2 h with 5  $\mu$ g/ml mitomycin C and washed with PBS before every well was scratched uniformly using the WoundMaker<sup>™</sup> (Essen BioScience). Detached cells were washed away with PBS before BMM-conditioned media were added to the cells (100  $\mu$ l/well). Plates were immediately placed into the Incucyte<sup>®</sup> S3 Live-Cell Analysis System (Essen BioScience) and imaged for relative wound closure [%] at indicated time points.

To assess proliferation capacity, L929 cells were seeded (5,000 cells/well, 100  $\mu$ l) and incubated overnight. On the next day, the medium was replaced by BMM-conditioned medium (100  $\mu$ l/well).

Cell confluency was measured over time in the Incucyte<sup>®</sup> S3 Live-Cell Analysis System (Essen BioScience) and normalized to starting confluency in each well.

## 2.18 Gelatin zymography

MMP activity was measured as previously described (50). In brief, BMM-conditioned media were loaded onto a 10% SDS-acrylamide gel containing 1 mg/ml gelatin and electrophoresis was performed. Gels were washed in 2.5% Triton-X 100 to remove SDS and after a 72-hour incubation at 37°C in a buffer conducive to enzyme activity (50 mM Tris, 5 mM CaCl<sub>2</sub> and 0.02% Brij-35), the gel was stained with Coomassie solution. After brief incubation in destaining solution, specific MMP activity, indicating gelatin degradation as clear bands on a dark background, was assessed based on their molecular weights. Conditioned media from each individual biological replicate was measured in technical duplicates. Gels were scanned with an Odyssey<sup>®</sup> CLX Infrared Imaging System (LI-COR Biosciences) and inverted to enhance visibility, presenting bands in black against a white background. Signals were quantified using the Odyssey<sup>®</sup> Image Studio software (Version 5.2).

## 2.19 Data representation and statistics

Visualization, advanced analysis, and all statistical tests were performed in Origin Lab 2018b. Data are presented as means ± standard error of the mean (bars). Each dot within the bar graphs represents one independent cell preparation. The mean of two groups was tested for statistical significance using the Mann-Whitney *U*-test. Statistical significance across all genotypes (mean of 3 groups) was assessed through one-way ANOVA (for single time point comparisons) and two-way ANOVA (for multiple time points) both followed by Bonferroni *post-hoc* tests.

## 3 Results

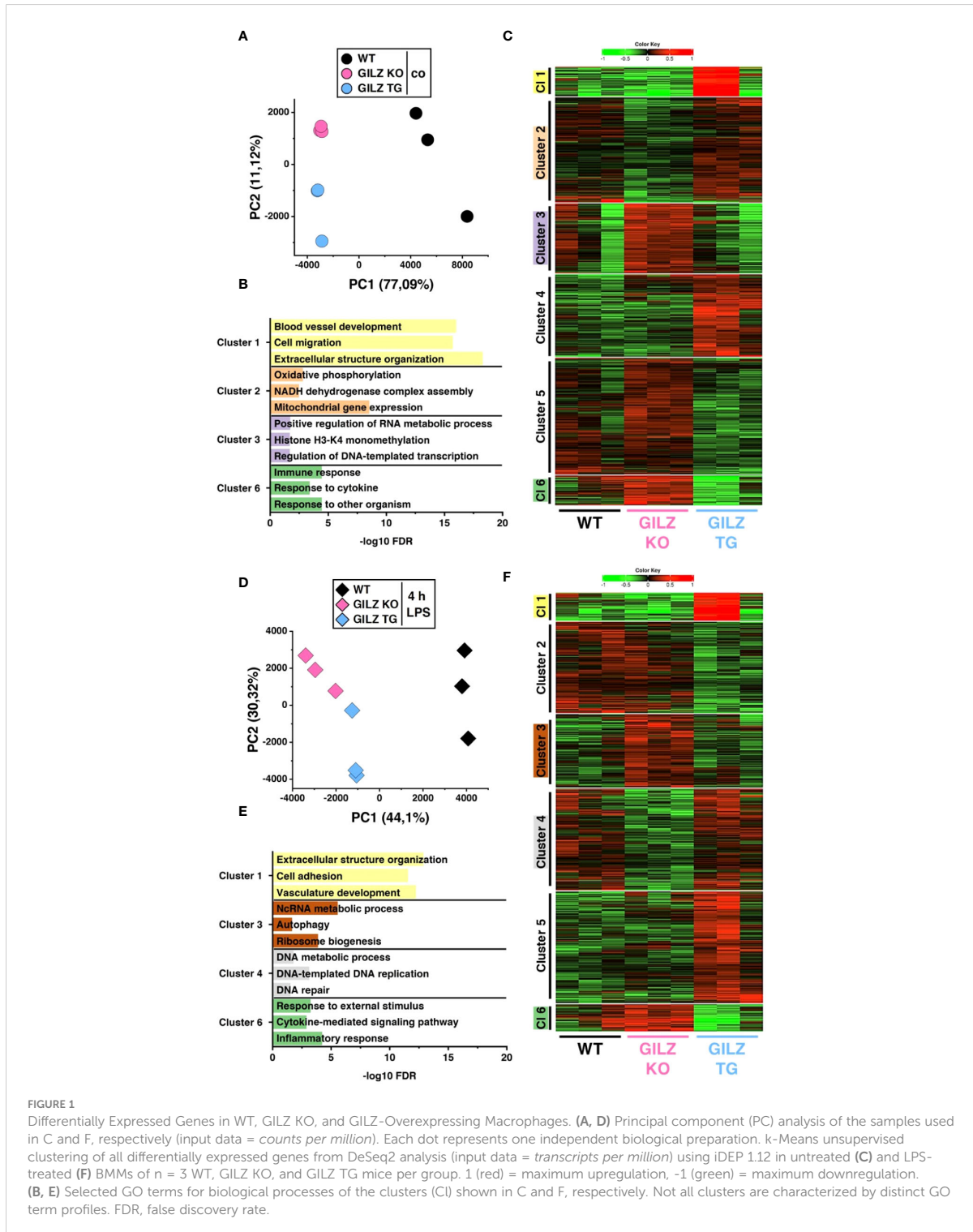
### 3.1 Differentially expressed genes in WT, GILZ KO, and GILZ-overexpressing macrophages

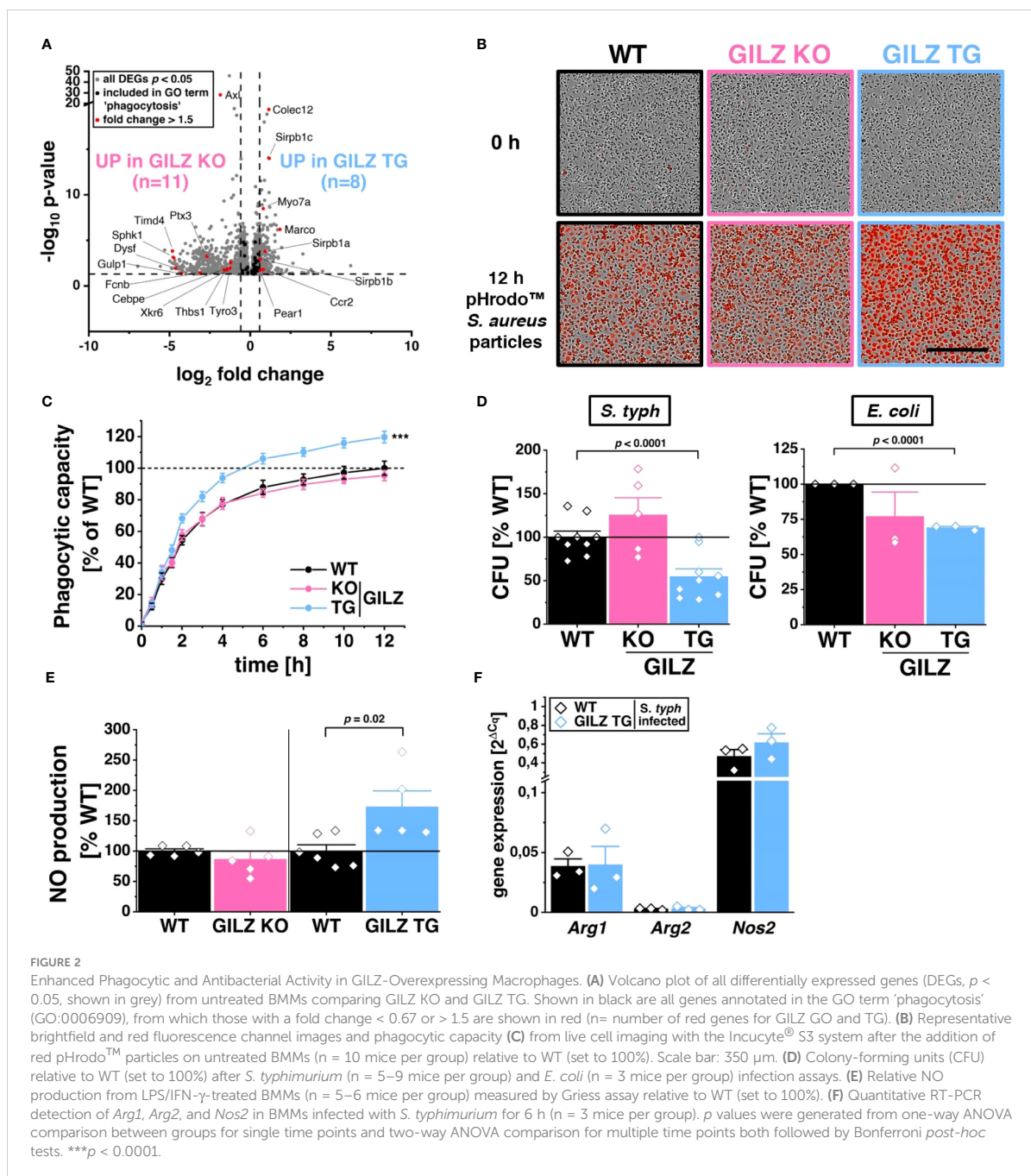
We conducted RNA-Seq with wild-type (WT), GILZ knockout (GILZ KO), and GILZ-overexpressing (GILZ TG) bone marrow-derived macrophages (BMMs), both under untreated conditions and following a 4 h LPS treatment. The RNA-Seq data, analyzed using the DESeq2 approach for the WT vs. KO, WT vs. TG, and KO vs. TG comparisons, revealed 3,286 differentially expressed genes (DEGs,  $p < 0.05$ ) in untreated cells. This number increased to 3,716 with LPS treatment, encompassing all three comparisons (Supplementary File S1). Principal component analysis (PCA) was employed to explore the variance in gene expression among samples. The obtained data revealed distinct grouping patterns based on the genotype,

underscoring that observed gene expression variations are closely associated with differences in GILZ abundance (Figures 1A, D). Next, we employed iDEP, a tool designed for identifying patterns in gene expression across all samples. The tool utilized *transcripts per million* (TPM) data of the DEGs, independently for untreated and LPS-treated cells, to conduct k-Mean hierarchical clustering. In Figures 1B, E, representative Gene Ontology (GO) terms for biological processes from hierarchical clustering are linked to their corresponding false discovery rates (FDRs), providing insights into the functional categories influenced by GILZ expression (Supplementary File S2). Genes involved in the inflammatory response of macrophages (Cluster 6) showed differential expression under both untreated and LPS-treated conditions. Moreover, two out of three GILZ TG samples exhibited a strong induction of genes associated with vasculature development, cell mobility, and extracellular structure organization (Cluster 1).

### 3.2 Enhanced phagocytic and antibacterial activity in GILZ-overexpressing macrophages

RNA-Seq analysis identified 55 differentially expressed genes associated with the GO term 'phagocytosis' (GO:0006909) in both GILZ KO and GILZ TG macrophages. Notably, these DEGs exhibited a balanced distribution of upregulation and downregulation in both cell types (Figure 2A). To elucidate the functional implications of these transcriptional changes, we conducted live cell imaging of macrophages after the addition of pHrodo<sup>™</sup> particles, emitting red fluorescent light upon engulfment (Figure 2B). Quantitative analysis revealed that GILZ-overexpressing macrophages exhibited a higher phagocytic capacity over 12 hours compared to WT macrophages, with a noticeable increase beginning at the 2-hour time point (Figure 2C). Given the observed alterations in phagocytosis, we investigated antibacterial activity in BMMs against *S. typhimurium* and *E. coli*. Notably, GILZ-overexpressing macrophages exhibited not only increased phagocytosis but also enhanced bacterial clearance against both tested pathogens (Figure 2D). In this context, GILZ KO cells exhibited a tendency of attenuated phagocytic capacity, albeit not reaching statistical significance, and results regarding bacterial clearance were inconclusive. Consequently, our focus shifted to GILZ-overexpressing macrophages, aiming to investigate whether the observed effects stem from increased NO production, which is one of the main antibacterial factors in murine macrophages (51). Indeed, GILZ TG macrophages demonstrated elevated NO production when polarized to M1 (Figure 2E). In M1 macrophages, inducible nitric oxide synthase (NOS2) is the main producer of NO, while arginases catalyze arginine hydrolysis to ornithine and urea, competing with NO synthases for arginine (52). Arginase 1 (ARG1) inhibits NO production and acts as an M2 marker, whereas Arginase 2 (ARG2) is involved in reducing M1 activation through metabolic reprogramming (53, 54). Upon infection, there was a tendency for increased expression of *Nos2* but neither altered expression of *Arg1* nor *Arg2* (Figure 2F).



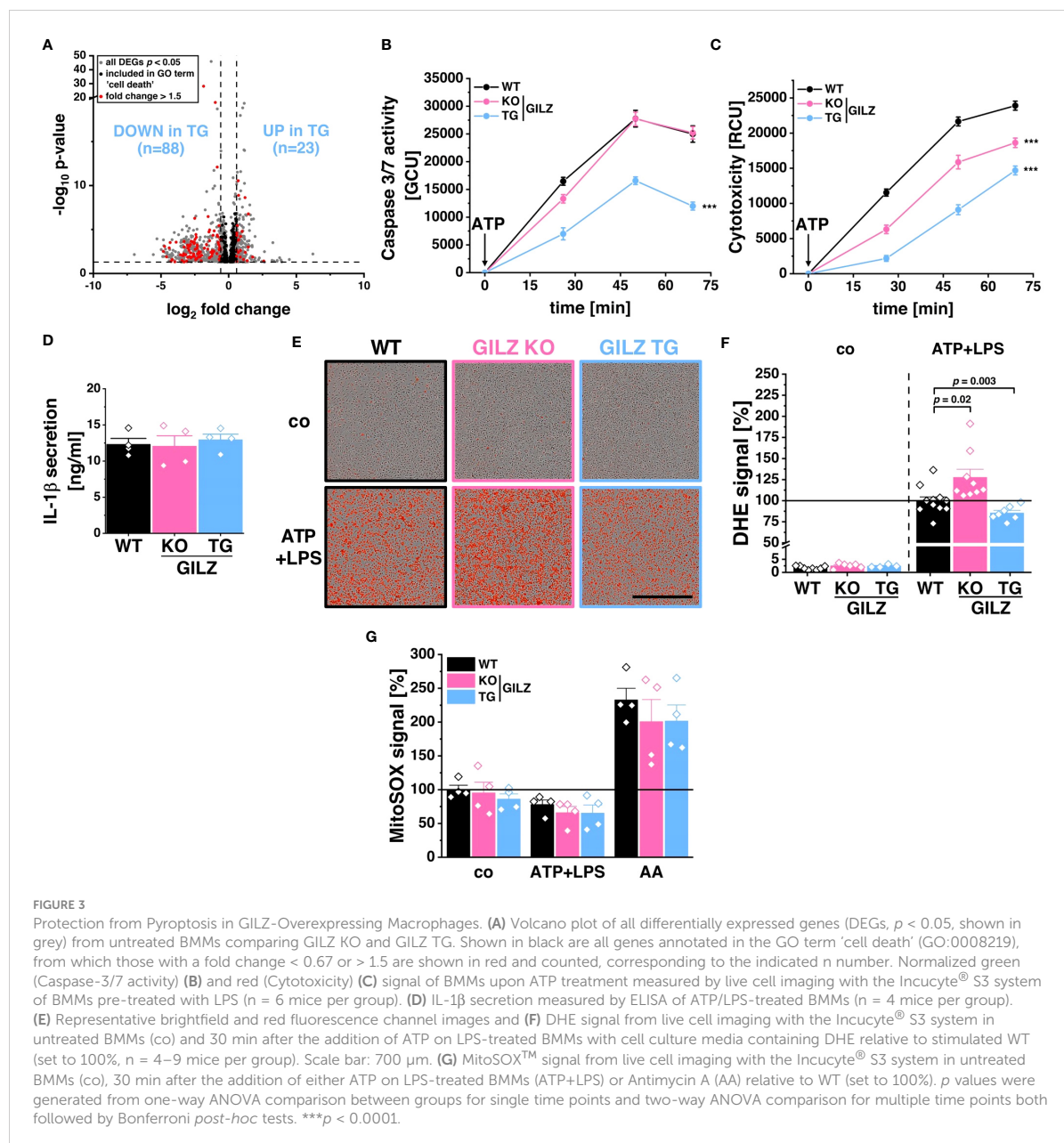


### 3.3 Protection from pyroptosis in GILZ-overexpressing macrophages

RNA-Seq analysis revealed 111 differentially expressed genes included in the 'cell death' GO term (GO:0008219), with 88 downregulated in GILZ TG macrophages (Figure 3A). This downregulation pattern prompted the hypothesis of a protective mechanism against specific forms of cell death. Upon inflammasome activation by ATP+LPS treatment, GILZ TG

macrophages exhibited a significant reduction in caspase-3/7 activation compared to WT (Figure 3B). Simultaneously, our evaluation of cell viability revealed enhanced cell survival in GILZ-overexpressing macrophages, as indicated by a substantial decrease in the cytotoxicity signal, originating from compromised plasma membrane integrity and a subsequent increase in fluorescence upon binding to DNA (Figure 3C). Given that ATP+LPS treatment induces pyroptotic cell death through caspase-1 activation, responsible for processing IL-1 $\beta$ , we explored IL-1 $\beta$  secretion under these conditions





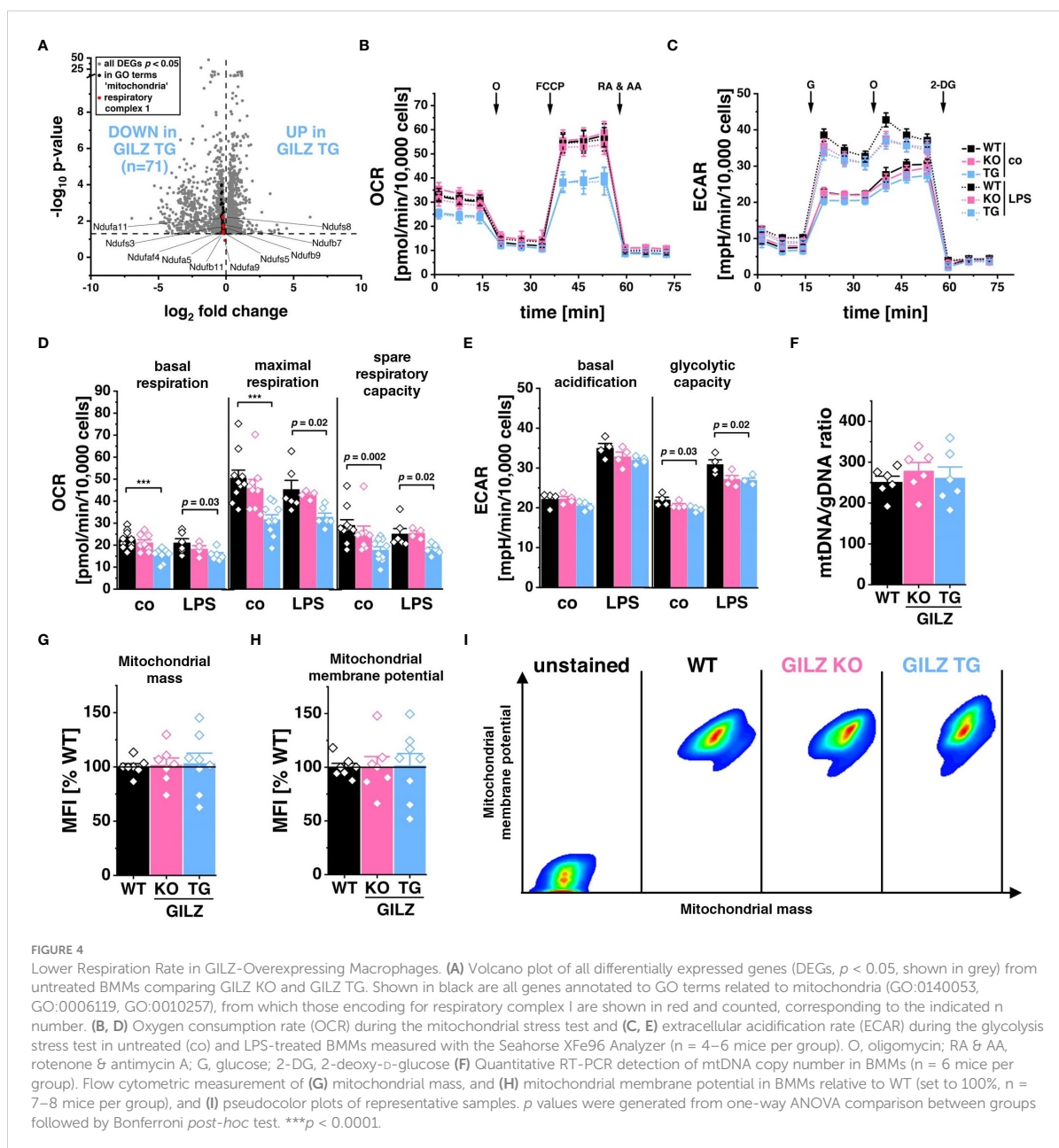
and found no significant differences between genotypes (Figure 3D). This led us to conclude that GILZ overexpression selectively influences specific facets of the signaling cascade following ATP+LPS treatment in macrophages. Given the pivotal role of reactive oxygen species (ROS) in promoting NLRP3 inflammasome activation and subsequent cell death, we investigated ROS production using DHE dye with live cell microscopy (Figure 3E). Notably, GILZ TG macrophages exhibited a significant reduction to 80% in ROS production, while GILZ KO macrophages displayed an increased production to 130% compared to WT macrophages (Figure 3F). Upon inflammasome activation, mitochondria are known to be both sources and targets of reactive oxygen species (55). We tracked

mitochondrial ROS (mitoROS) production under ATP+LPS treatment using mitoSOX fluorescence, a ROS dye specific for mitochondria. Intriguingly, across all genotypes, we observed a reduction of mitoROS production to 60% upon ATP+LPS treatment (Figure 3G), suggesting that mitoROS production may not be directly linked to cell viability. Additionally, we induced mitoROS production using Antimycin A (AA) as a positive control, and as expected, it elicited a substantial increase ( $p < 0.0001$ ) in mitoROS across all genotypes. Interestingly, we observed a trend of diminished mitoROS levels in GILZ TG macrophages under untreated conditions. This observation piqued our interest and warranted a characterization of mitochondria in these macrophages.

### 3.4 Lower respiration rate in GILZ-overexpressing macrophages

RNA-Seq analysis unveiled the significant downregulation of 71 genes associated with Gene Ontology terms related to 'mitochondria' (GO:0140053, GO:0006119, GO:0010257), corresponding to those depicted in Figure 1C as Cluster 2 and all specific to GILZ-overexpressing macrophages (Figure 4A). Particularly, among these genes, 15 of the 59 encode for subunits of the NADH:ubiquinone oxidoreductase, the key component of Complex I in the electron transport chain (GO:0010257, FDR =  $3.4 \times 10^{-3}$ ). Motivated by these

transcriptomic findings, we subsequently examined the functional implications by assessing the oxygen consumption rate (OCR) in these cells (Figure 4B). Interestingly, our analysis unveiled a significant reduction not only in basal respiration but also in maximal respiration and spare respiratory capacity in GILZ-overexpressing macrophages, both under untreated conditions and following LPS treatment (Figure 4D). When mitochondrial respiration is compromised, it often leads to compensatory adjustments in glycolytic activity (47, 56, 57). Therefore, to elucidate the glycolytic response, we performed a glycolysis stress test focusing on extracellular acidification rate (ECAR) (Figure 4C).

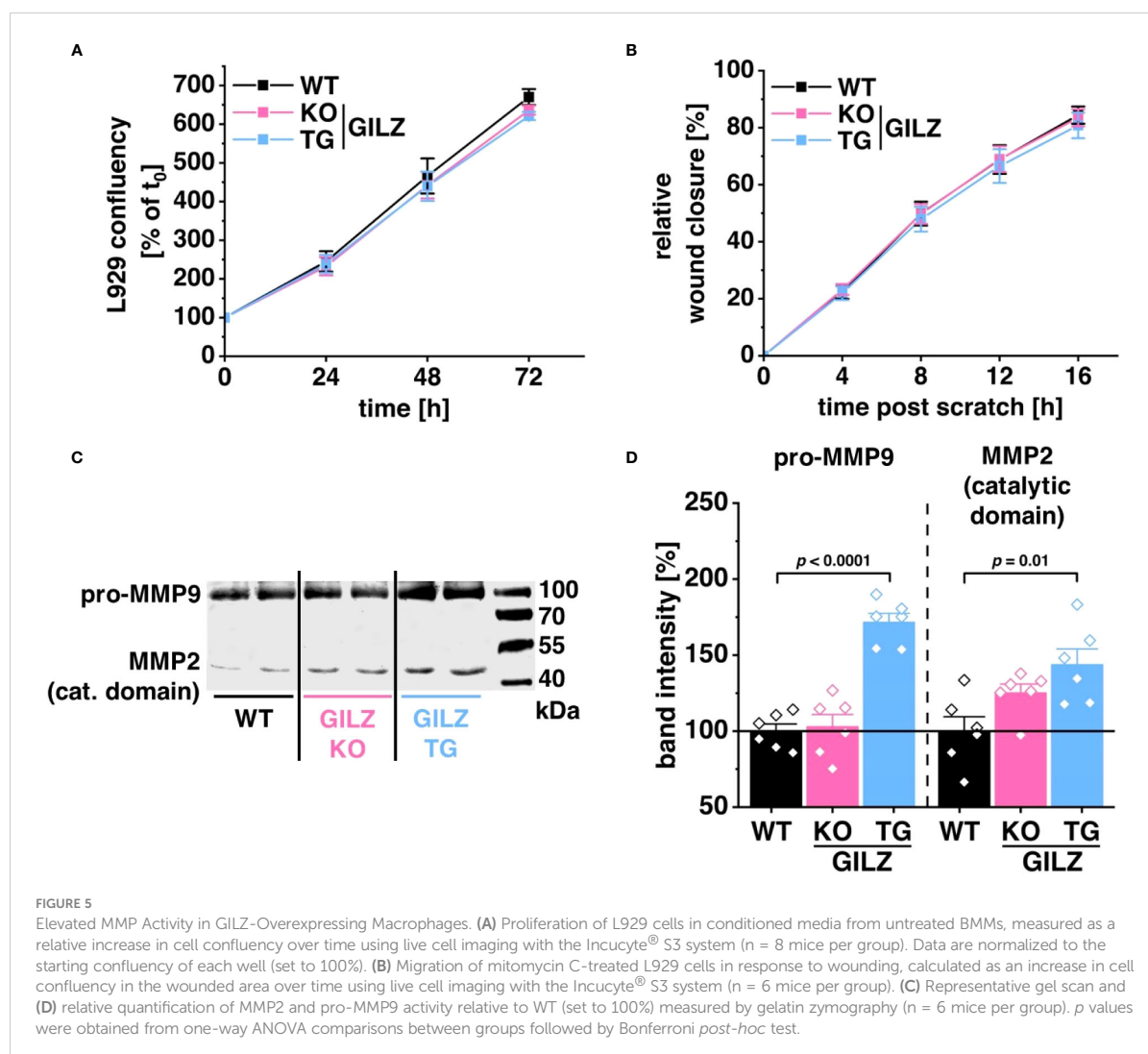


Our results demonstrated a slight reduction of glycolytic capacity in GILZ TG macrophages (Figure 4E). Notably, these metabolic alterations are not merely a consequence of a decrease in mitochondrial content, as indicated by equivalent mitochondrial DNA (mtDNA) content (Figure 4F), comparable mitochondrial mass (Figure 4G), and unchanged mitochondrial membrane potential (Figures 4H, I) in GILZ TG macrophages.

### 3.5 Elevated MMP activity in GILZ-overexpressing macrophages

RNA-Seq analysis disclosed 224 DEGs in untreated GILZ-overexpressing macrophages and 171 DEGs in LPS-treated cells associated with cell movement, wound healing, and extracellular structure organization forming Cluster 1 upon k-mean

unsupervised clustering of TPM values of DEGs ( $p < 0.05$ ) from DESeq2 analysis in all three comparisons (Figures 1C, F). Notably, among these DEGs forming Cluster 1, 80 genes were shared between untreated and LPS-treated BMMs. To discern the functional implications of these transcriptomic findings, we investigated their impact employing the murine fibroblast cell line L929. Surprisingly, cell proliferation (Figure 5A) or migration in response to wounding (Figure 5B) was unaffected by the macrophage genotype when L929 cells were exposed to media conditioned by WT, GILZ KO, or GILZ TG macrophages. Despite these outcomes, the RNA-Seq data, highlighting genes related to the extracellular matrix, prompted an investigation of MMP activity in the conditioned media using gelatin zymography (Figures 5C, D). The results unveiled heightened pro-MMP9 and MMP2 activity in media conditioned by GILZ TG macrophages. These findings correlate with the increased gene expression observed in the RNA-Seq data for these enzymes.



## 4 Discussion

In recent years, the exploration of therapeutic GILZ use has extended beyond its well-known anti-inflammatory effects, gaining interest for its potential pro-resolving actions. Traditionally, in macrophages, GILZ is postulated to confer an anti-inflammatory phenotype to monocytes and macrophages (58). It is recognized for inhibiting the expression of proinflammatory molecules, preventing toll-like receptor 2 production, and impeding NF- $\kappa$ B function (59). Moreover, GILZ can be induced by the natural product curcumin, contributing to its anti-inflammatory effects in macrophages (38). Additionally, GILZ plays a crucial role in modulating macrophage responses to LPS exposure; downregulation of GILZ is linked to heightened NF- $\kappa$ B and AP-1 activity, accompanied by increased pro-inflammatory cytokine production (36). Notably, M1-like macrophages from GILZ-deficient mice exhibit elevated expression of M1 markers and reduced expression of IL-10 compared to M1-like macrophages from wild-type mice (60). Consistent with these findings, our RNA-Seq data revealed that inflammatory pathways are upregulated in GILZ KO macrophages compared to GILZ-overexpressing macrophages both under control and inflammatory conditions.

Examining the resolution of inflammation, GILZ emerges as a pivotal mediator of the anti-inflammatory and immunomodulatory effects of GCs (15, 16). Moreover, GILZ demonstrates its potential in effectively resolving detrimental inflammation by regulating leptin production in osteoarthritis synovial fibroblasts (61), safeguarding myocardial cells (29), reducing spinal cord tissue damage and leukocyte infiltration (31), and inhibiting leukocyte recruitment in liver fibrosis (62). Notably, during the resolution phase of LPS-induced pleurisy, GILZ expression exhibits an increase, particularly in macrophages displaying resolving phenotypes, reinforcing its remarkable resolving actions (63). Nevertheless, the regulation of GILZ in macrophages appears to be intricate and contingent on the context. Various factors, including hypoxia (21), IL-10 (59), and proinflammatory cytokines (23), can influence the expression of GILZ in macrophages. Interestingly, GILZ levels are stabilized in macrophages characterized as LPS tolerant (36). Furthermore, the absence of GILZ has been linked to macrophage aging, which is linked to a low-grade inflammatory condition (46).

### 4.1 Antibacterial activity

In addition to its recognized anti-inflammatory effects, GILZ has demonstrated accompanying benefits in the context of bacterial infections, broadening its potential therapeutic applications. To characterize these additional effects, we conducted investigations involving GILZ KO and GILZ TG macrophages, aiming to uncover mechanistic insights through transcriptomic data analysis. Our study demonstrates enhanced phagocytic activity and increased killing efficacy of *S. typhimurium* [an intracellular pathogen (64)] and *E. coli* [using a non-invasive strain (65)] by GILZ-overexpressing macrophages, potentially mediated by an increased capacity to produce nitric oxide (NO). In this context,

it is noteworthy to examine analogous observations in existing literature. Notably, transgenic mice with heightened GILZ expression specifically in monocytes and macrophages exhibited lower frequencies of inflammatory monocytes, reduced plasma levels of inflammatory cytokines, and diminished blood bacterial counts when experiencing sepsis (32). This upregulation of GILZ in monocytes and macrophages improved their phagocytic capacity in *in vivo* assays and heightened the survival rates of septic mice. Additionally, TAT-GILZ, a fusion protein combining the cell-penetrating peptide TAT with GILZ, was found to induce the release of CCL2, facilitating monocyte/macrophage recruitment through the CCR2 receptor and resulting in accelerated resolution of *E. coli*-induced neutrophilic inflammation, increased peritoneal numbers of monocytes/macrophages, enhanced apoptosis/ efferocytosis counts, and improved bacterial clearance through phagocytosis (35). In the context of pneumococcal pneumonia, TAT-GILZ treatment reduced neutrophilic inflammation, enhanced macrophage efferocytosis, and improved bacterial clearance (34). Our findings in this study differ from our previous findings, which indicated enhanced phagocytosis and killing efficiency in GILZ KO macrophages (39). However, it is essential to note that different models were employed in the two studies. Specifically, phagocytic capacity was assessed using latex beads, emphasizing the material's impact on phagocytic activity, as highlighted by (66). Moreover, the measurements of NO production were conducted using a different cell type, and the infection conditions differed from those in our prior study. However, the precise molecular mechanisms through which GILZ exerts dual effects, enhancing antibacterial clearance and resolving inflammation effects, require further elucidation.

Contrary to GILZ, GCs have a negative impact on the antibacterial function of macrophages. They inhibit the phagocytic activity of macrophages, leading to an increase in the severity of bacterial infections such as tuberculosis (67). Furthermore, GCs have been found to directly upregulate the expression of DPP4, leading to the mobilization and enhanced activity of macrophages, which may exacerbate rather than mitigate macrophage-dominated inflammatory disorders in the context of GC therapy (68). GCs impair phagocytosis against Crohn's disease-associated adherent-invasive *E. coli* (AIEC) (69). Moreover, GCs have been demonstrated to suppress antimicrobial autophagy and nitric oxide production in macrophages, thereby facilitating mycobacterial survival (70).

### 4.2 Pyroptosis

Considering our discovery that GILZ overexpression protects macrophages from pyroptosis, we propose a potential regulatory role for GILZ in the pyroptotic cell death pathway. Pyroptosis is a lytic form of programmed cell death triggered by the detection of pathogens or host-derived danger signals. Gasdermin-D (GSDMD) functions as the central pyroptotic substrate for inflammatory caspases. This process results in the formation of pores, causing cell swelling until membrane rupture occurs. Consequently, this rupture leads to the release of inflammatory cytokines such as IL-

1 $\beta$ , IL-6, and IL-18 into the extracellular space (71). In our study, we observed that GILZ expression did not impact IL-1 $\beta$  secretion upon inflammasome activation, suggesting that GILZ may not influence cytokine processing by caspases within the pyroptosis cascade. Consequently, we redirected our focus to another well-established host-derived danger signal in this context. This signal centers on the detection of reactive oxygen species (ROS), known to induce the assembly of either noncanonical or canonical inflammasomes (72). Increasing levels of ROS by an upregulated NADPH oxidase have been shown to induce pyroptotic cell death (73). Recently, Devant and colleagues showed in macrophages that the terminal step in the pyroptosis pathway, namely pore formation, relies on ROS to oxidize the caspase cleaved GSDMD (74). Given the observed reduction in ROS levels in GILZ-overexpressing macrophages, our study suggests a potential interference by GILZ with ROS production, specifically after inflammasome assembly at a later stage in the pyroptotic cascade. As the exact origins of ROS production during pyroptosis and potential interaction partners for GILZ remain unclear, further investigations are needed. Notably, supporting our findings, previous research has established that decreased ROS levels confer protection against ATP-LPS-induced cell death in BMMs (75). Contrary to the common association of ROS generation with mitochondrial dysfunction, our study revealed no increase in mitochondrial ROS. Nonetheless, it is noteworthy that mitochondrial ROS have been identified as crucial contributors to pyroptosis via GSDMD oxidation (76). Additionally, TRAF3 was shown to amplify mitochondrial ROS production and pyroptosis through ULK1 ubiquitination (77). Ceramide-mediated regulation of mitochondrial ROS was observed to connect ROS, NLRP3-caspase-1 inflammasome activation, and pyroptosis in cancer cells (78). Furthermore, scavenging mitochondrial ROS effectively mitigated pyroptosis and IL-1 $\beta$  secretion in the context of hyperglycemia- and periodontitis-related pyroptosis (79).

With a focus on their potential to activate the NLRP3 inflammasome and induce pyroptosis, the detrimental effects of GCs have been extensively studied in various cellular and disease models. Studies on muscle cells suggest that GCs may induce pyroptosis through the NLRP3/GSDMD pathway, implying a role in muscle atrophy (80–82). Chronic GC exposure primes microglia to pro-inflammatory stimuli, inducing *Nlrp3* mRNA in the hippocampus, suggesting a link between GCs and neuroinflammation (83–85). In macrophages, sensitivity to GCs concerning the NLRP3 inflammasome appears model dependent. GCs enhance ATP-dependent NLRP3 expression in cultured human monocytes/macrophages, promoting pro-inflammation (86, 87). Conversely, under LPS stimulation, an inhibitory role is suggested in cultured murine macrophages (88). This once again emphasizes the need to explore alternative therapeutic options such as GILZ.

### 4.3 Respiration and mitochondria

Mitochondria are known to act as a signaling platform in macrophages, linking energy metabolism and macrophage polarization upon activation (89). In our study, we found that

macrophages overexpressing GILZ have significantly less mitochondrial oxidative phosphorylation capacity, which is linked to a downregulation of numerous genes encoding for complex I of the electron transport system. This contrasts with findings in cancer cells where GILZ has been implicated in enhancing mitochondrial oxidative phosphorylation, leading to increased susceptibility to death induced by mitochondrial pro-oxidants (90, 91). These contrasting effects underscore the context-dependent role of GILZ in mitochondrial function and warrant further investigation into its diverse mechanisms of action in different cellular contexts.

GCs have been shown to have a significant impact on mitochondrial function in macrophages. Mitochondrial GRs alter the expression of genes involved in oxidative phosphorylation, which can affect the activity and abundance of key enzymes in the electron transport chain, leading to changes in ATP production (92). Mitochondrial function is indispensable for GCs to exert their effects, as evidenced by studies demonstrating that the inhibition of complex V abolishes dexamethasone-mediated upregulation of *Gilz* (93). Chronic GC treatment of cortical neurons has been shown to reduce mitochondrial oxidation (94). Altogether, this leads us to speculate that GILZ may exert effects on macrophages similar to its primary inducers, GCs, suggesting potential molecular interactions that require elucidation in future studies.

### 4.4 Tissue remodeling

The versatility of macrophages allows them to participate across all phases of inflammation, from instigating the pro-inflammatory response to facilitating tissue repair post-injury. Considering this, we could identify a new aspect of GILZ's role in inflammatory conditions, particularly in its promotion of pro-resolving actions, such as the activation of matrix metalloproteinases (MMP) when GILZ is overexpressed in macrophages. The secretion of MMP9 and MMP2 by macrophages has been widely recognized as playing a crucial role in wound healing. These metalloproteinases are involved in the degradation and remodeling of the extracellular matrix (ECM), which is essential for various stages of the wound healing process (95–97). We detected pro-MMP9 via gelatin zymography. *In vivo*, macrophage-derived pro-MMP9 can be activated by MMP-3 or other MMPs (98). Although these gelatinase pro-forms are typically latent and catalytically inactive in the absence of their activating enzymes (99), they become activated during zymography due to the presence of the denaturing agent SDS (100). Overexpression of MMP9 in macrophages improves diastolic physiology and cardiac wound healing after myocardial infarction (101).

The effects of GCs on tissue repair extend beyond the activation of GRs but remain poorly understood (102). Findings in peripheral blood mononuclear cells suggest that GC-mediated monocyte/macrophage-specific induction of ADAMTS2, a secreted metalloproteinase involved in the processing of procollagen to collagen, may play a crucial role in the resolution of inflammation and wound repair (103). The precise mechanism by which GILZ might regulate MMP secretion in macrophages remains unclear and represents a novel area of investigation in the field.

## Data availability statement

Raw and processed data from the RNA-sequencing generated in the study were deposited in the Gene Expression Omnibus (GEO) database under the accession code GSE254137. Other original data in the present study are available from the corresponding author upon request.

## Ethics statement

The animal study was approved by the Landesamt für Verbraucherschutz, Saarbrücken, Germany. The study was conducted in accordance with the local legislation and institutional requirements.

## Author contributions

TL: Conceptualization, Data curation, Formal analysis, Funding acquisition, Investigation, Methodology, Validation, Visualization, Writing – original draft, Writing – review & editing. HS: Formal analysis, Investigation, Writing – review & editing. GG: Formal analysis, Software, Writing – review & editing. SM: Investigation, Writing – review & editing. JW: Funding acquisition, Project administration, Resources, Writing – review & editing. CL: Resources, Writing – review & editing. BD: Conceptualization, Funding acquisition, Methodology, Supervision, Writing – review & editing. JH: Conceptualization, Data curation, Funding acquisition, Methodology, Supervision, Validation, Writing – review & editing. AK: Conceptualization, Funding acquisition, Methodology, Project administration, Resources, Supervision, Writing – review & editing.

## Funding

The author(s) declare financial support was received for the research, authorship, and/or publication of this article. This

research was funded by the Deutsche Forschungsgemeinschaft (DFG, German Research Foundation), grants (KI702). TL was supported by the Studienstiftung des deutschen Volkes.

## Acknowledgments

The authors thank Matti Müller and Theo Ransweiler for their exceptional technical assistance, and Eva Dilly for her excellent animal care. Additionally, the authors acknowledge Stefano Bruscoli and Carlo Riccardi for providing GILZ knockout mice and Angelika M. Vollmar for support in the setup of gelatinase assays.

## Conflict of interest

The authors declare that the research was conducted in the absence of any commercial or financial relationships that could be construed as a potential conflict of interest.

## Publisher's note

All claims expressed in this article are solely those of the authors and do not necessarily represent those of their affiliated organizations, or those of the publisher, the editors and the reviewers. Any product that may be evaluated in this article, or claim that may be made by its manufacturer, is not guaranteed or endorsed by the publisher.

## Supplementary material

The Supplementary Material for this article can be found online at: <https://www.frontiersin.org/articles/10.3389/fimmu.2024.1396827/full#supplementary-material>

## References

- Hardy RS, Raza K, Cooper MS. Therapeutic glucocorticoids: mechanisms of actions in rheumatic diseases. *Nat Rev Rheumatol.* (2020) 16:133–44. doi: 10.1038/s41584-020-0371-y
- Ronchetti S, Ayroldi E, Ricci E, Gentili M, Migliorati G, Riccardi C. A glance at the use of glucocorticoids in rare inflammatory and autoimmune diseases: still an indispensable pharmacological tool? *Front Immunol.* (2020) 11:613435. doi: 10.3389/fimmu.2020.613435
- Bruscoli S, Febo M, Riccardi C, Migliorati G. Glucocorticoid therapy in inflammatory bowel disease: mechanisms and clinical practice. *Front Immunol.* (2021) 12:691480. doi: 10.3389/fimmu.2021.691480
- Kalfeist L, Galland L, Ledys F, Ghiringhelli F, Limagne E, Ladoire S. Impact of glucocorticoid use in oncology in the immunotherapy era. *Cells.* (2022) 11(5):770. doi: 10.3390/cells11050770
- Oray M, Abu Samra K, Ebrahimiadib N, Meese H, Foster CS. Long-term side effects of glucocorticoids. *Expert Opin Drug Saf.* (2016) 15:457–65. doi: 10.1517/14740338.2016.1140743
- van Raalte DH, Ouwens DM, Diamant M. Novel insights into glucocorticoid-mediated diabetogenic effects: towards expansion of therapeutic options? *Eur J Clin Invest.* (2009) 39:81–93. doi: 10.1111/j.1365-2362.2008.02067.x
- McDonough A, Curtis J, Saag K. The epidemiology of glucocorticoid-associated adverse events. *Curr Opin Rheumatol.* (2008) 20:131–7. doi: 10.1097/BOR.0b013e3282f51031
- Seelig E, Meyer S, Timper K, Nigro N, Bally M, Pernicova I, et al. Metformin prevents metabolic side effects during systemic glucocorticoid treatment. *Eur J Endocrinol.* (2017) 176:349–58. doi: 10.1530/eje-16-0653
- Han A, Olsen O, D'Souza C, Shan J, Zhao F, Yanolatos J, et al. Development of novel glucocorticoids for use in antibody-drug conjugates for the treatment of inflammatory diseases. *J Med Chem.* (2021) 64:11958–71. doi: 10.1021/acs.jmedchem.1c00541
- Timmermans S, Vandewalle J, Libert C. Dimerization of the glucocorticoid receptor and its importance in (Patho)physiology: A primer. *Cells.* (2022) 11(4):683. doi: 10.3390/cells11040683

11. Gerber AN, Newton R, Sasse SK. Repression of transcription by the glucocorticoid receptor: A parsimonious model for the genomics era. *J Biol Chem.* (2021) 296:100687. doi: 10.1016/j.jbc.2021.100687
12. Timmermans S, Souffriau J, Libert C. A general introduction to glucocorticoid biology. *Front Immunol.* (2019) 10:1545. doi: 10.3389/fimmu.2019.01545
13. Coutinho AE, Chapman KE. The anti-inflammatory and immunosuppressive effects of glucocorticoids, recent developments and mechanistic insights. *Mol Cell Endocrinol.* (2011) 335:2–13. doi: 10.1016/j.mce.2010.04.005
14. Maranville JC, Luca F, Richards AL, Wen X, Witonsky DB, Baxter S, et al. Interactions between glucocorticoid treatment and cis-regulatory polymorphisms contribute to cellular response phenotypes. *PLoS Genet.* (2011) 7:e1002162. doi: 10.1371/journal.pgen.1002162
15. Bereshchenko O, Migliorati G, Bruscoli S, Riccardi C. Glucocorticoid-induced leucine zipper: A novel anti-inflammatory molecule. *Front Pharmacol.* (2019) 10:308. doi: 10.3389/fphar.2019.00308
16. Ayroldi E, Riccardi C. Glucocorticoid-induced leucine zipper (GILZ): a new important mediator of glucocorticoid action. *FASEB J.* (2009) 23:3649–58. doi: 10.1096/fj.09-134684
17. Cannarile L, Delfino DV, Adorasio S, Riccardi C, Ayroldi E. Implicating the role of GILZ in glucocorticoid modulation of T-cell activation. *Front Immunol.* (2019) 10:1823. doi: 10.3389/fimmu.2019.01823
18. Bruscoli S, Biagioli M, Sorcini D, Frammartino T, Cimino M, Sportoletti P, et al. Lack of glucocorticoid-induced leucine zipper (GILZ) deregulates B-cell survival and results in B-cell lymphocytosis in mice. *Blood.* (2015) 126:1790–801. doi: 10.1182/blood-2015-03-631580
19. Yang N, Zhang W, Shi XM. Glucocorticoid-induced leucine zipper (GILZ) mediates glucocorticoid action and inhibits inflammatory cytokine-induced COX-2 expression. *J Cell Biochem.* (2008) 103:1760–71. doi: 10.1002/jcb.21562
20. Espinasse MA, Pepin A, Virault-Rocroy P, Szely N, Chollet-Martin S, Pallardy M, et al. Glucocorticoid-induced leucine zipper is expressed in human neutrophils and promotes apoptosis through mcl-1 down-regulation. *J Innate Immun.* (2016) 8:81–96. doi: 10.1159/000439052
21. Wang Y, Ma YY, Song XL, Cai HY, Chen JC, Song LN, et al. Upregulations of glucocorticoid-induced leucine zipper by hypoxia and glucocorticoid inhibit proinflammatory cytokines under hypoxic conditions in macrophages. *J Immunol.* (2012) 188:222–9. doi: 10.4049/jimmunol.1002958
22. Beaulieu E, Morand EF. Role of GILZ in immune regulation, glucocorticoid actions and rheumatoid arthritis. *Nat Rev Rheumatol.* (2011) 7:340–8. doi: 10.1038/nrrheum.2011.59
23. Beaulieu E, Ngo D, Santos L, Yang YH, Smith M, Jorgensen C, et al. Glucocorticoid-induced leucine zipper is an endogenous antiinflammatory mediator in arthritis. *Arthritis Rheum.* (2010) 62:2651–61. doi: 10.1002/art.27566
24. Luz-Crawford P, Tejedor G, Mauselet-Bonnefont AL, Beaulieu E, Morand EF, Jorgensen C, et al. Glucocorticoid-induced leucine zipper governs the therapeutic potential of mesenchymal stem cells by inducing a switch from pathogenic to regulatory Th17 cells in a mouse model of collagen-induced arthritis. *Arthritis Rheumatol.* (2015) 67:1514–24. doi: 10.1002/art.39069
25. Sevilla LM, Perez P. Glucocorticoids and glucocorticoid-induced-leucine-zipper (GILZ) in psoriasis. *Front Immunol.* (2019) 10:2220. doi: 10.3389/fimmu.2019.02220
26. He YJ, Xu JQ, Sun MM, Fang XZ, Peng ZK, Pan SW, et al. Glucocorticoid-induced leucine zipper: A promising marker for monitoring and treating sepsis. *Front Immunol.* (2020) 11:606649. doi: 10.3389/fimmu.2020.606649
27. Yang S, Qi S, Wang C. The role of retinal Muller cells in diabetic retinopathy and related therapeutic advances. *Front Cell Dev Biol.* (2022) 10:1047487. doi: 10.3389/fcell.2022.1047487
28. Pagliarlunga M, Flamini S, Contini R, Febo M, Ricci E, Ronchetti S, et al. Anti-inflammatory effects of synthetic peptides based on glucocorticoid-induced leucine zipper (GILZ) protein for the treatment of inflammatory bowel diseases (IBDs). *Cells.* (2023) 12(18):2294. doi: 10.3390/cells12182294
29. Cappetta D, Bereshchenko O, Cianflone E, Rossi F, Riccardi C, Torella D, et al. Glucocorticoid-induced leucine zipper (GILZ) in cardiovascular health and disease. *Cells.* (2021) 10(8):2155. doi: 10.3390/cells10082155
30. Esposito E, Bruscoli S, Mazzon E, Paterniti I, Coppo M, Velardi E, et al. Glucocorticoid-induced leucine zipper (GILZ) over-expression in T lymphocytes inhibits inflammation and tissue damage in spinal cord injury. *Neurotherapeutics.* (2012) 9:210–25. doi: 10.1007/s13311-011-0084-7
31. Mazzon E, Bruscoli S, Galuppo M, Biagioli M, Sorcini D, Bereshchenko O, et al. Glucocorticoid-induced leucine zipper (GILZ) controls inflammation and tissue damage after spinal cord injury. *CNS Neurosci Ther.* (2014) 20:973–81. doi: 10.1111/cns.12315
32. Ellouze M, Vigouroux L, Tcherakian C, Woerther PL, Guguin A, Robert O, et al. Overexpression of GILZ in macrophages limits systemic inflammation while increasing bacterial clearance in sepsis in mice. *Eur J Immunol.* (2020) 50:589–602. doi: 10.1002/eji.201948278
33. Vandewalle J, Libert C. GILZ in sepsis: "Poor is the pupil who does not surpass his master". *Eur J Immunol.* (2020) 50:490–3. doi: 10.1002/eji.202048582
34. Souza JAM, Carvalho AFS, Grossi LC, Zaidan I, de Oliveira LC, Vago JP, et al. Glucocorticoid-induced leucine zipper alleviates lung inflammation and enhances bacterial clearance during pneumococcal pneumonia. *Cells.* (2022) 11(3):532. doi: 10.3390/cells11030532
35. Grossi LC, Zaidan I, Souza JAM, Carvalho AFS, Sanches RCO, Cardoso C, et al. GILZ modulates the recruitment of monocytes/macrophages endowed with a resolving phenotype and favors resolution of *Escherichia coli* infection. *Cells.* (2023) 12(10):1403. doi: 10.3390/cells12101403
36. Hoppstädter J, Kessler SM, Bruscoli S, Huwer H, Riccardi C, Kierner AK. Glucocorticoid-induced leucine zipper: a critical factor in macrophage endotoxin tolerance. *J Immunol.* (2015) 194:6057–67. doi: 10.4049/jimmunol.1403207
37. Carceller E, Balleger M, Deckers J, Riccardi C, Bruscoli S, Hocheppied T, et al. Overexpression of Glucocorticoid-induced Leucine Zipper (GILZ) increases susceptibility to Imiquimod-induced psoriasis and involves cutaneous activation of TGF- $\beta$ 1. *Sci Rep.* (2016) 6:38825. doi: 10.1038/srep38825
38. Hoppstädter J, Hachenthal N, Valbuena-Perez JV, Lampe S, Astanina K, Kunze MM, et al. Induction of glucocorticoid-induced leucine zipper (GILZ) contributes to anti-inflammatory effects of the natural product curcumin in macrophages. *J Biol Chem.* (2016) 291:22949–60. doi: 10.1074/jbc.M116.733253
39. Hoppstädter J, Diesel B, Linnenberger R, Hachenthal N, Flamini S, Minet M, et al. Amplified host defense by toll-like receptor-mediated downregulation of the glucocorticoid-induced leucine zipper (GILZ) in macrophages. *Front Immunol.* (2019) 9:3111. doi: 10.3389/fimmu.2018.03111
40. Hoppstädter J, Dembek A, Höring M, Schymik HS, Dahlem C, Sultan A, et al. Dysregulation of cholesterol homeostasis in human lung cancer tissue and tumour-associated macrophages. *EBioMedicine.* (2021) 72:103578. doi: 10.1016/j.ebiom.2021.103578
41. Ge SX, Son EW, Yao R. iDEP: an integrated web application for differential expression and pathway analysis of RNA-Seq data. *BMC Bioinf.* (2018) 19:534. doi: 10.1186/s12859-018-2486-6
42. Linnenberger R, Hoppstädter J, Wrublewski S, Ampofo E, Kierner AK. Statins and Bempedoic acid: different actions of cholesterol inhibitors on macrophage activation. *Int J Mol Sci.* (2021) 22(22):12480. doi: 10.3390/ijms222212480
43. Helaine S, Thompson JA, Watson KG, Liu M, Boyle C, Holden DW. Dynamics of intracellular bacterial replication at the single cell level. *Proc Natl Acad Sci U.S.A.* (2010) 107:3746–51. doi: 10.1073/pnas.1000041107
44. Hoppstädter J, Diesel B, Linnenberger R, Hachenthal N, Flamini S, Minet M, et al. Amplified host defense by toll-like receptor-mediated downregulation of the glucocorticoid-induced leucine zipper (GILZ) in macrophages. *Front Immunol.* (2019) 9:3111. doi: 10.3389/fimmu.2018.03111
45. Schneider CA, Rasband WS, Eliceiri KW. NIH Image to ImageJ: 25 years of image analysis. *Nat Methods.* (2012) 9:671–5. doi: 10.1038/nmeth.2089
46. Valbuena Perez JV, Linnenberger R, Dembek A, Bruscoli S, Riccardi C, Schulz MH, et al. Altered glucocorticoid metabolism represents a feature of macrophage-aging. *Aging Cell.* (2020) 19:e13156. doi: 10.1111/acel.13156
47. Dahlem C, Siow WX, Lopatniuk M, Tse WKF, Kessler SM, Kirsch SH, et al. Thiohologamide A, a new anti-proliferative anti-tumor agent, modulates macrophage polarization and metabolism. *Cancers (Basel).* (2020) 12(5):1288. doi: 10.3390/cancers12051288
48. Quiros PM, Goyal A, Jha P, Auwerx J. Analysis of mtDNA/nDNA ratio in mice. *Curr Protoc Mouse Biol.* (2017) 7:47–54. doi: 10.1002/cpmo.21
49. Chanda S, Lepikhov K, Dahlem C, Schymik HS, Hoppstädter J, Geber AK, et al. Gene editing and small molecule inhibitors of the RNA binding protein IGF2BP2/IMP2 show its potential as an anti-cancer drug target. *Front Biosci (Landmark Ed).* (2024) 29:41. doi: 10.31083/j.fbl2901041
50. Toth M, Fridman R. Assessment of gelatinases (MMP-2 and MMP-9) by gelatin zymography. *Methods Mol Med.* (2001) 57:163–74. doi: 10.1385/1-59259-136-1:163
51. Bogdan C. Nitric oxide and the immune response. *Nat Immunol.* (2001) 2:907–16. doi: 10.1038/ni1001-907
52. Silva MT. When two is better than one: macrophages and neutrophils work in concert in innate immunity as complementary and cooperative partners of a myeloid phagocyte system. *J Leukoc Biol.* (2010) 87:93–106. doi: 10.1189/jlb.0809549
53. Palmieri EM, Gonzalez-Cotto M, Baseler WA, Davies LC, Ghesquiere B, Maio N, et al. Nitric oxide orchestrates metabolic rewiring in M1 macrophages by targeting aconitase 2 and pyruvate dehydrogenase. *Nat Commun.* (2020) 11:698. doi: 10.1038/s41467-020-14433-7
54. Dowling JK, Afzal R, Gearing LJ, Cervantes-Silva MP, Annett S, Davis GM, et al. Mitochondrial arginase-2 is essential for IL-10 metabolic reprogramming of inflammatory macrophages. *Nat Commun.* (2021) 12:1460. doi: 10.1038/s41467-021-21617-2
55. Iyer SS, He Q, Janczy JR, Elliott EI, Zhong Z, Olivier AK, et al. Mitochondrial cardiolipin is required for Nlrp3 inflammasome activation. *Immunity.* (2013) 39:311–23. doi: 10.1016/j.immuni.2013.08.001
56. Andrzejewski S, Gravel S-P, Pollak M, St-Pierre J. Metformin directly acts on mitochondria to alter cellular bioenergetics. *Cancer Metab.* (2014) 2:12. doi: 10.1186/2049-3002-2-12
57. Bhatt AN, Chauhan A, Khanna S, Rai Y, Singh S, Soni R, et al. Transient elevation of glycolysis confers radio-resistance by facilitating DNA repair in cells. *BMC Cancer.* (2015) 15:335. doi: 10.1186/s12885-015-1368-9
58. Veitillard M, Schlecht-Louf G. Glucocorticoid-induced leucine zipper: fine-tuning of dendritic cells function. *Front Immunol.* (2018) 9:1232. doi: 10.3389/fimmu.2018.01232

59. Berberi D, Bruscoli S, Cohen N, Foussat A, Migliorati G, Bouchet-Delbos L, et al. Synthesis of glucocorticoid-induced leucine zipper (GILZ) by macrophages: an anti-inflammatory and immunosuppressive mechanism shared by glucocorticoids and IL-10. *Blood*. (2003) 101:729–38. doi: 10.1182/blood-2002-02-0538
60. Vago JP, Galvão I, Negreiros-Lima GL, Teixeira LCR, Lima KM, Sugimoto MA, et al. Glucocorticoid-induced leucine zipper modulates macrophage polarization and apoptotic cell clearance. *Pharmacol Res*. (2020) 158:104842. doi: 10.1016/j.phrs.2020.104842
61. Malaise O, Relic B, Charlier E, Zeddou M, Neuville S, Deroeyer C, et al. Glucocorticoid-induced leucine zipper is involved in glucocorticoid-induced and mineralocorticoid-induced leptin production by osteoarthritis synovial fibroblasts. *Arthritis Res Ther*. (2016) 18:219. doi: 10.1186/s13075-016-1119-6
62. Flamini S, Sergeev P, Viana de Barros Z, Mello T, Biagioli M, Paglialunga M, et al. Glucocorticoid-induced leucine zipper regulates liver fibrosis by suppressing CCL2-mediated leukocyte recruitment. *Cell Death Dis*. (2021) 12:421. doi: 10.1038/s41419-021-03704-w
63. Vago JP, Tavares LP, Garcia CC, Lima KM, Perucci LO, Vieira É L, et al. The role and effects of glucocorticoid-induced leucine zipper in the context of inflammation resolution. *J Immunol*. (2015) 194:4940–50. doi: 10.4049/jimmunol.1401722
64. Jiang L, Wang P, Song X, Zhang H, Ma S, Wang J, et al. Salmonella Typhimurium reprograms macrophage metabolism via T3SS effector SopE2 to promote intracellular replication and virulence. *Nat Commun*. (2021) 12:879. doi: 10.1038/s41467-021-21186-4
65. Gokulan K, Khare S, Rooney AW, Han J, Lynne AM, Foley SL. Impact of plasmids, including those encoding VirB4/D4 type IV secretion systems, on Salmonella enterica serovar Heidelberg virulence in macrophages and epithelial cells. *PLoS One*. (2013) 8:e77866. doi: 10.1371/journal.pone.0077866
66. Kapellos TS, Taylor L, Lee H, Cowley SA, James WS, Iqbal AJ, et al. A novel real time imaging platform to quantify macrophage phagocytosis. *Biochem Pharmacol*. (2016) 116:107–19. doi: 10.1016/j.bcp.2016.07.011
67. Xie Y, Xie J, Meijer AH, Schaaf MJM. Glucocorticoid-induced exacerbation of mycobacterial infection is associated with a reduced phagocytic capacity of macrophages. *Front Immunol*. (2021) 12:618569. doi: 10.3389/fimmu.2021.618569
68. Diaz-Jiménez D, Petrillo MG, Busada JT, Hermoso M, Cidlowski JA. Glucocorticoids mobilize macrophages by transcriptionally up-regulating the exopeptidase DPP4. *J Biol Chem*. (2020) 295:3213–3227. doi: 10.1074/jbc.RA119.010894
69. Olivares-Morales MJ, de la Fuente MK, Dubois-Camacho K, Parada D, Diaz-Jiménez D, Torres-Riquelme A, et al. Glucocorticoids impair phagocytosis and inflammatory response against crohn's disease-associated adherent-invasive *Escherichia coli*. *Front Immunol*. (2018) 9:1026. doi: 10.3389/fimmu.2018.01026
70. Wang J, Wang R, Wang H, Yang X, Xiong W, et al. Glucocorticoids suppress antimicrobial autophagy and nitric oxide production and facilitate mycobacterial survival in macrophages. *Sci Rep*. (2017) 7:982. doi: 10.1038/s41598-017-01174-9
71. Zheng D, Liwinski T, Elinav E. Inflammasome activation and regulation: toward a better understanding of complex mechanisms. *Cell Discovery*. (2020) 6:36. doi: 10.1038/s41421-020-0167-x
72. Muñoz-Wolf N, Ward RW, Hearnden CH, Sharp FA, Geoghegan J, O'Grady K, et al. Non-canonical inflammasome activation mediates the adjuvanticity of nanoparticles. *Cell Rep Med*. (2023) 4:100899. doi: 10.1016/j.xcrm.2022.100899
73. Basiorka AA, McGraw KL, Eksioglou EA, Chen X, Johnson J, Zhang L, et al. The NLRP3 inflammasome functions as a driver of the myelodysplastic syndrome phenotype. *Blood*. (2016) 128:2960–75. doi: 10.1182/blood-2016-07-730556
74. Devant P, Borsic E, Ngwa EM, Xiao H, Chouchani ET, Thiagarajah JR, et al. Gasdermin D pore-forming activity is redox-sensitive. *Cell Rep*. (2023) 42:112008. doi: 10.1016/j.celrep.2023.112008
75. Wang H, Zhou X, Li H, Qian X, Wang Y, Ma L. Transient receptor potential melastatin 2 negatively regulates LPS-ATP-induced caspase-1-dependent pyroptosis of bone marrow-derived macrophage by modulating ROS production. *BioMed Res Int*. (2017) 2017:2975648. doi: 10.1155/2017/2975648
76. Wang Y, Shi P, Chen Q, Huang Z, Zou D, Zhang J, et al. Mitochondrial ROS promote macrophage pyroptosis by inducing GSDMD oxidation. *J Mol Cell Biol*. (2019) 11:1069–82. doi: 10.1093/jmcb/mjz020
77. Shen Y, Liu WW, Zhang X, Shi JG, Jiang S, Zheng L, et al. TRAF3 promotes ROS production and pyroptosis by targeting ULK1 ubiquitination in macrophages. *FASEB J*. (2020) 34:7144–59. doi: 10.1096/fj.201903073R
78. Su L, Chen Y, Huang C, Wu S, Wang X, Zhao X, et al. Targeting Src reactivates pyroptosis to reverse chemoresistance in lung and pancreatic cancer models. *Sci Trans Med*. (2023) 15:eabl7895. doi: 10.1126/scitranslmed.abl7895
79. Zhao Z, Ming Y, Li X, Tan H, He X, Yang L, et al. Hyperglycemia aggravates periodontitis via autophagy impairment and ROS-inflammasome-mediated macrophage pyroptosis. *Int J Mol Sci*. (2023) 24(7):6309. doi: 10.3390/ijms24076309
80. Oh S, Yang J, Park C, Son K, Byun K. Dieckol attenuated glucocorticoid-induced muscle atrophy by decreasing NLRP3 inflammasome and pyroptosis. *Int J Mol Sci*. (2021) 22(15):8057. doi: 10.3390/ijms22158057
81. Wang L, Jiao XF, Wu C, Li XQ, Sun HX, Shen XY, et al. Trimetazidine attenuates dexamethasone-induced muscle atrophy via inhibiting NLRP3/GSDMD pathway-mediated pyroptosis. *Cell Death Discovery*. (2021) 7:251. doi: 10.1038/s41420-021-00648-0
82. Yang B, Zhang T, Wei L, Zhao B, Wang Q, Yao Z, et al. Glucocorticoid induces GSDMD-dependent pyrolysis in PC12 cells via endoplasmic reticulum stress. *PLoS One*. (2022) 17:e0274057. doi: 10.1371/journal.pone.0274057
83. Frank MG, Hershman SA, Weber MD, Watkins LR, Maier SF. Chronic exposure to exogenous glucocorticoids primes microglia to pro-inflammatory stimuli and induces NLRP3 mRNA in the hippocampus. *Psychoneuroendocrinology*. (2014) 40:191–200. doi: 10.1016/j.psyneuen.2013.11.006
84. Svensson M, Rosvall P, Boza-Serrano A, Andersson E, Lexell J, Deierborg T. Forced treadmill exercise can induce stress and increase neuronal damage in a mouse model of global cerebral ischemia. *Neurobiol Stress*. (2016) 5:8–18. doi: 10.1016/j.jynstr.2016.09.002
85. Canet G, Zussy C, Hernandez C, Chevallier N, Marchi N, Desrumaux C, et al. Chronic glucocorticoids consumption triggers and worsens experimental Alzheimer's disease-like pathology by detrimental immune modulations. *Neuroendocrinology*. (2022) 112:982–97. doi: 10.1159/000521559
86. Busillo JM, Azzam KM, Cidlowski JA. Glucocorticoids sensitize the innate immune system through regulation of the NLRP3 inflammasome. *J Biol Chem*. (2011) 286:38703–13. doi: 10.1074/jbc.M111.275370
87. Slusher AL, Acevedo EO. Stress induced proinflammatory adaptations: Plausible mechanisms for the link between stress and cardiovascular disease. *Front Physiol*. (2023) 14:1124121. doi: 10.3389/fphys.2023.1124121
88. Wu L, Zhou C, Wu J, Chen S, Tian Z, Du Q. Corticosterone inhibits LPS-induced NLRP3 inflammasome priming in macrophages by suppressing xanthine oxidase. *Mediators Inflammation*. (2020) 2020:6959741. doi: 10.1155/2020/6959741
89. Harry GJ, Childers G, Giridharan S, Hernandez IL. An association between mitochondria and microglia effector function. What do we think we know? *Neuroimmunol Neuroinflamm*. (2020) 7:150–65. doi: 10.20517/2347-8659.2020.07
90. André F, Corazao-Rozas P, Idziorek T, Quesnel B, Kluz J, Marchetti P. GILZ overexpression attenuates endoplasmic reticulum stress-mediated cell death via the activation of mitochondrial oxidative phosphorylation. *Biochem Biophys Res Commun*. (2016) 478:513–20. doi: 10.1016/j.bbrc.2016.07.053
91. André F, Trinh A, Balayssac S, Maboudou P, Dekiok S, Malet-Martino M, et al. Metabolic rewiring in cancer cells overexpressing the glucocorticoid-induced leucine zipper protein (GILZ): Activation of mitochondrial oxidative phosphorylation and sensitization to oxidative cell death induced by mitochondrial targeted drugs. *Int J Biochem Cell Biol*. (2017) 85:166–74. doi: 10.1016/j.biocel.2017.02.011
92. Kokkinopoulou I, Moutsatsou P. Mitochondrial glucocorticoid receptors and their actions. *Int J Mol Sci*. (2021) 22(11):6054. doi: 10.3390/ijms22116054
93. Stifel U, Wolfschmitt EM, Vogt J, Wächter U, Vettorazzi S, Tews D, et al. Glucocorticoids coordinate macrophage metabolism through the regulation of the tricarboxylic acid cycle. *Mol Metab*. (2022) 57:101424. doi: 10.1016/j.molmet.2021.101424
94. Du J, Wang Y, Hunter R, Wei Y, Blumenthal R, Falke C, et al. Dynamic regulation of mitochondrial function by glucocorticoids. *Proc Natl Acad Sci U.S.A.* (2009) 106:3543–8. doi: 10.1073/pnas.0812671106
95. Hartenstein B, Dittlich BT, Stickens D, Heyer B, Vu TH, Teurich S, et al. Epidermal development and wound healing in matrix metalloproteinase 13-deficient mice. *J Invest Dermatol*. (2006) 126:486–96. doi: 10.1038/sj.jid.5700084
96. Manuel JA, Gawronska-Kozak B. Matrix metalloproteinase 9 (MMP-9) is upregulated during scarless wound healing in athymic nude mice. *Matrix Biol*. (2006) 25:505–14. doi: 10.1016/j.matbio.2006.07.008
97. Page-McCaw A, Ewald AJ, Werb Z. Matrix metalloproteinases and the regulation of tissue remodelling. *Nat Rev Mol Cell Biol*. (2007) 8:221–33. doi: 10.1038/nrm2125
98. Dreier R, Grassel S, Fuchs S, Schaumburger J, Bruckner P. Pro-MMP-9 is a specific macrophage product and is activated by osteoarthritic chondrocytes via MMP-3 or a MT1-MMP/MMP-13 cascade. *Experimental Cell Research* (2004) 297(2):303–12. doi: 10.1016/j.yexcr.2004.02.027
99. Egorov D, Kopaliani I, Ameln AK-V, Speier S, Deussen A. Mechanism of pro-MMP9 activation in co-culture of pro-inflammatory macrophages and cardiomyocytes. *Experimental Cell Research* (2024) 434(1):113868. doi: 10.1016/j.yexcr.2023.113868
100. Vandooen J, Geurts N, Martens E, Van den Steen PE, Opdenakker G. Zymography methods for visualizing hydrolytic enzymes. *Nat Methods* (2013) 10(3):211–20. doi: 10.1038/nmeth.2371
101. Meschiari CA, Jung M, Iyer RP, Yabluchanskiy A, Toba H, Garrett MR, et al. Macrophage overexpression of matrix metalloproteinase-9 in aged mice improves diastolic physiology and cardiac wound healing after myocardial infarction. *Am J Physiol Heart Circ Physiol*. (2018) 314:H224–35. doi: 10.1152/ajpheart.00453.2017
102. Desgeorges T, Caratti G, Mounier R, Tuckermann J, Chazaud B. Glucocorticoids shape macrophage phenotype for tissue repair. *Front Immunol*. (2019) 10:1591. doi: 10.3389/fimmu.2019.01591
103. Hofer TP, Frankenberger M, Mages J, Lang R, Meyer P, Hoffmann R, et al. Tissue-specific induction of ADAMTS2 in monocytes and macrophages by glucocorticoids. *J Mol Med (Berl)*. (2008) 86:323–32. doi: 10.1007/s00109-007-0284-0



## 1.2 Contribution to the research field to a non-expert

Our research in this publication investigates how the protein GILZ influences inflammation, a critical process in the body's response to infection and injury. Glucocorticoids (GCs), widely used to treat inflammation, often cause side effects that limit their effectiveness. GILZ, a key mediator of GC effects, has garnered attention for its potential therapeutic benefits. We studied how altering GILZ levels affects macrophage behavior. Macrophages are central immune cells orchestrating pathogen elimination, facilitating tissue repair, and maintaining physiological balance within the body. Through genetic modifications affecting GILZ expression, wherein we engineered macrophages to either express no GILZ or large amounts of GILZ, we uncovered significant effects on inflammation, cell death, and other immune processes. Increased GILZ levels promoted pathogen elimination and wound healing and protected against cell death, while GILZ deficiency intensified inflammatory reactions. Our work on GILZ contributes to the understanding of immune processes, which could drive the development of safer and more effective treatments for inflammatory diseases such as inflammatory bowel disease or arthritis.

## 1.3 Author contributions

I specifically contributed to this publication by designing and performing all experiments unless otherwise stated, conducting data analysis and interpretation, writing the manuscript draft, and preparing figures. Additionally, I coordinated with co-authors throughout the review and revision process. I extend my gratitude to Hanna Schymik for her preparation of the RNA library, to Gilles Gasparoni for conducting RNA sequencing and preparing the raw files, and to Saeed Mohammadi for the assistance in performing the infection and Griess assays. Throughout the project, Jessica Hoppstädter, Britta Diesel, and Alexandra K. Kiemer provided extensive support and supervision, ensuring the smooth progression of our research. Claude Libert proof-read the manuscript and generously provided the GILZ transgenic mice, which were further bred by Rebecca Linnenberger and me. Funding for this project was acquired by Alexandra K. Kiemer and Jörn Walter, with additional support from the *Studienstiftung des deutschen Volkes*, which provided me with a stipend to pursue this research. Please note that other acknowledgments are listed in the paper itself.

## Chapter 2 The Interplay Between Sodium in the Microenvironment and the Glucocorticoid-Induced Leucine Zipper (GILZ): Determinants of Macrophage Activation

### 2.1 Introduction

#### 2.1.1 Health Implications of High Salt Consumption

The consumption of salt (sodium chloride, NaCl) in food is deeply rooted in global traditions and societal norms. Nonetheless, overconsumption of salt is linked to hypertension, a condition strongly associated with cardiovascular complications (Ellison & Welling, 2021; Huang *et al.*, 2020; Mozaffarian *et al.*, 2014). This heightened risk of cardiovascular diseases contributes significantly to global morbidity and mortality, with an estimated annual toll of approximately five million deaths worldwide caused by a high salt diet (Hunter *et al.*, 2022; O'Donnell *et al.*, 2014). Public health initiatives and campaigns have been implemented to raise awareness about the health risks associated with high salt intake.

The impact of high salt intake extends beyond cardiovascular health, with studies indicating associations with autoimmune and inflammatory diseases (Jung *et al.*, 2019; McDonald *et al.*, 2016). Specifically, high salt intake has been associated with increased pathogenic Th17 cell differentiation in both humans and mice, facilitated by the p38/MAPK, NFAT5, and SGK1 pathways, with *in vivo* studies in mice demonstrating that a high-salt diet exacerbates experimental autoimmune encephalomyelitis (EAE) by expanding Th17 cells in gut-associated lymphoid tissue and the central nervous system (Figure 1) (Kleinewietfeld *et al.*, 2013; Wu *et al.*, 2013).

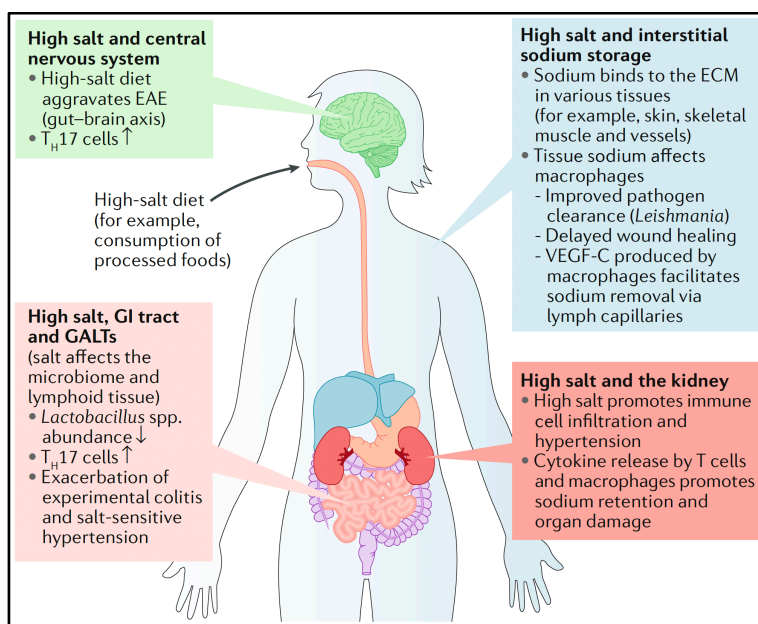


**Figure 1: High salt conditions affect cells in different organs (Wilck *et al.*, 2019)**

Copyright © 2019, Springer Nature Limited

Recent research has highlighted that high salt intake indirectly regulates immunity by impacting the gut microbiota, leading to a depletion of *Lactobacillus* spp. in both mice and humans (Hamad *et al.*, 2022; Miranda *et al.*, 2018). This depletion correlates with elevated frequencies of Th17 cells in multiple tissues, heightened blood pressure, and worsened disease progression in mice, yet replenishing *Lactobacillus* spp. has been demonstrated to alleviate exacerbations of EAE and salt-sensitive hypertension through the regulation of Th17 cells (Wilck *et al.*, 2017).

#### 2.1.2 Sodium is Stored in the Human Skin

Studies by Titze *et al.* revealed unexpected findings on sodium accumulation independent of water accumulation, highlighting the skin as a site for osmotically inactive sodium accumulation influenced by dietary salt intake (Rakova *et al.*, 2013; Titze *et al.*, 2002). The tissue sodium content in humans can be visualized and quantified using magnetic resonance imaging, revealing higher sodium content in skin than in muscle, with variations based on sex and health conditions (Kopp *et al.*, 2012; Miyauchi *et al.*, 2024). Notably, skin sodium content increases

with age, suggesting a link between sodium accumulation and age-related inflammation and diseases known as inflammaging (Furman *et al.*, 2019; Guimarães *et al.*, 2021; Linz *et al.*, 2015; López-Otín *et al.*, 2013). Macrophages play a crucial role in maintaining sodium homeostasis within the skin independent of renal function. This process is mediated by an NFAT5/VEGF-C mechanism, which increases lymphatic capillary density to maintain local electrolyte balance and normal blood pressure (Machnik *et al.*, 2009; Titze *et al.*, 2014). Furthermore, macrophages are recruited by sodium gradients in the renal medulla, establishing a defense zone against infections through epithelial chemokine (CCL2) production (Berry *et al.*, 2017). Additionally, Jantsch *et al.* revealed that macrophages are pivotal in strengthening the skin's antimicrobial barrier by facilitating sodium storage at the site of bacterial infections, thus enhancing host defense mechanisms (Jantsch *et al.*, 2015).

### 2.1.3 How Macrophages Sense and Respond to Sodium Chloride

First findings demonstrating the impact of sodium on immune cell activity came by accident in the 1990s. Using increases in sodium chloride as a osmolarity control, researchers found that the addition of NaCl triggered proinflammatory responses in peripheral blood mononuclear cells (Shapiro & Dinarello, 1995).

More recently, researchers found that the skin stores an additional 40 mM NaCl due to dietary and inflammatory stimuli (Jantsch *et al.*, 2015; Kopp *et al.*, 2012; Machnik *et al.*, 2009). Since then, it has become evident that high salt (HS) favors the pro-inflammatory polarization of macrophages (Figure 2) (Müller *et al.*, 2019).

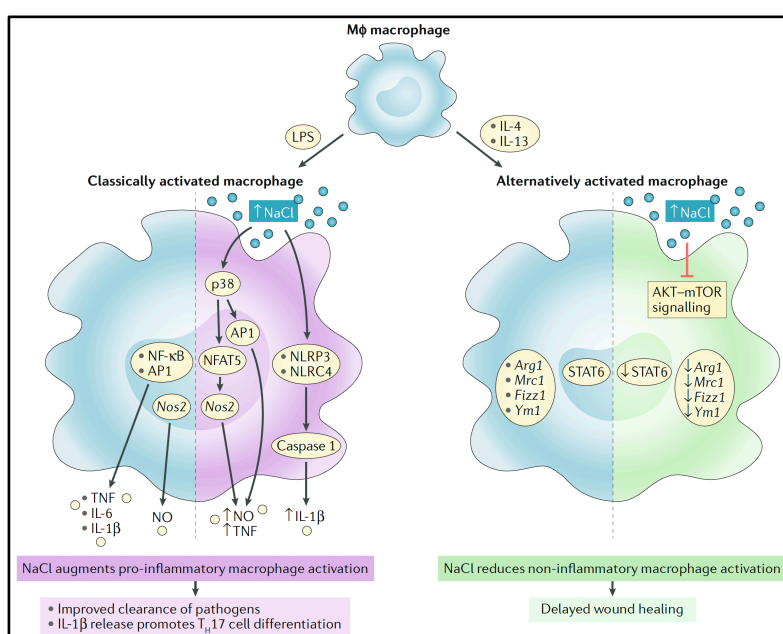


**Figure 2: How macrophages respond to high salt conditions (Wilck *et al.*, 2019)**

Copyright © 2019, Springer Nature Limited

Sensing changes in sodium balance involves macrophages utilizing the  $\text{Na}^+/\text{Ca}^{2+}$  exchanger NCLX and the Na/Cl betaine/GABA transporter (BGT-1, encoded by *Slc6a12*) to trigger NFAT5 signaling pathways and an inflammasome-dependent activation of caspase-1 (Ip & Medzhitov, 2015; Neubert *et al.*, 2020; Zhang *et al.*, 2024). In response, profound metabolic adaptations occur in macrophages, heavily impacting their immune activation status and plasticity. Sodium transiently inhibits complex II/III of the electron transport chain with a subsequent reduction of the oxygen consumption rate (OCR) and ATP production (Geisberger *et al.*, 2021; Hernansanz-Agustín *et al.*, 2020). Increased stabilization of hypoxia-inducible factor 1 $\alpha$  (HIF-1 $\alpha$ ) and enhanced autophagy contribute to improved antibacterial activity (Neubert *et al.*, 2019). However, sodium limits macrophages' role in orchestrating wound healing processes and reduces phagocytosis (Müller *et al.*, 2024). Under classical polarization towards the pro-inflammatory M1 phenotype, HS intensifies the phenotype, resulting in increased NO production and heightened bactericidal activity (Jantsch *et al.*, 2015; Krampert *et al.*, 2023). Conversely, when polarized to the classical M2 phenotype, HS diminishes the anti-inflammatory plasticity, leading to reduced expression of signature genes, impaired wound healing capacities, suppressed T effector cell proliferation, and alterations in immunometabolic pathways (Binger *et al.*, 2015). Mitochondrial function is crucial for early macrophage activation and function under HS conditions, as pharmacological inhibition of mitochondrial complexes mimics the HS effect on Nos2 expression and accelerated bacterial defenses (Geisberger *et al.*, 2021). Interestingly, the use of mannitol or urea as tonicity controls failed to replicate the effects observed with sodium chloride, underscoring the specificity of the impact (Jantsch *et al.*, 2015; Neubert *et al.*, 2019).

### 2.1.4 GILZ Regulates the Sodium Balance in the Kidney

Originally identified as a pivotal mediator of the anti-inflammatory properties of glucocorticoids in immune cells, GILZ governs essential functions of macrophages, including cytokine production, host defense, and polarization - key markers for high salt-mediated inflammation (Ayroldi & Riccardi, 2009; Ellouze *et al.*, 2020; Hoppstädter *et al.*, 2015; Legroux *et al.*, 2024; Souza *et al.*, 2022; Vago *et al.*, 2020).

The generation of total GILZ KO mice revealed various unexpected phenotypes, including infertility in male mice due to impaired sperm maturation and cardiomyocyte hypertrophic growth (Cappetta *et al.*, 2021; Venanzi *et al.*, 2014). In the kidney, aldosterone regulates sodium and potassium balance *via* induction of target genes by binding to the mineralocorticoid receptor (MR), such as the serum and glucocorticoid-regulated kinase 1 (SGK1) and GILZ (Bruscoli *et al.*, 2022). GILZ inhibits the Na<sup>+</sup>-Cl<sup>-</sup> cotransporter (NCC) and activates the epithelial sodium channel (ENaC), which changes the electrochemical gradient and facilitates potassium secretion. This explains why GILZ KO mice exhibit elevated plasma potassium concentrations compared to WT mice, without alterations in blood pressure (Mozaffari, 2020; Rashmi *et al.*, 2017; Soundararajan *et al.*, 2010).

Research indicates that MR signaling in macrophages plays a significant role in various physiological and pathological processes, including cardiac tissue inflammation, fibrosis, and atherosclerosis (Belden *et al.*, 2017; Fraccarollo *et al.*, 2019). Aldosterone can also induce GILZ *via* the glucocorticoid receptor (GR) in human synovial fibroblasts, where GILZ mediates leptin production by corticoids, an important adipokine (Malaise *et al.*, 2016).

### 2.1.5 Hypothesis: GILZ Is Involved in High Salt-mediated Inflammation of Macrophages

Given GILZ's significance as a major player in macrophage signaling and its role in regulating sodium balance in the kidney, we sought to investigate the interplay between GILZ and sodium in inflammation. We hypothesized that high salt conditions trigger an inflammatory response modulated by GILZ, significantly influencing inflammatory processes and infection defense. To test this hypothesis, we compared typical markers of HS-mediated inflammation in WT, GILZ KO, and GILZ TG macrophages.

## 2.2 Results

### 2.2.1 Characterization of GILZ Knockout and GILZ Transgenic Macrophages

In our investigation into the role of GILZ in HS-mediated inflammation, we used WT, GILZ KO, and GILZ TG BMMs. GILZ KO macrophages were confirmed to lack detectable GILZ mRNA expression (gene: *Gilz* or *Tsc22d3*), while GILZ TG macrophages displayed a constitutive 10-fold increase in *Gilz* expression, which persisted under inflammatory conditions and was further inducible by the glucocorticoid dexamethasone (Figure 3A). Western Blot analysis demonstrated that the constitutive GILZ protein levels (15 kDa) in GILZ TG macrophages were comparable to those observed in dexamethasone-treated WT macrophages (Figure 3B). However, attempts to confirm the absence of GILZ in KO macrophages were unsuccessful (Figure 3C). Both the near-infrared-based fluorescent secondary antibody and horseradish peroxidase-conjugated secondary antibody mistakenly detected proteins of the same size as GILZ, producing two bands at 15 kDa, raising questions about the method's validity. This led us to conclude that the commercially available primary antibody lacked the necessary specificity and selectivity for its target protein under our experimental conditions.

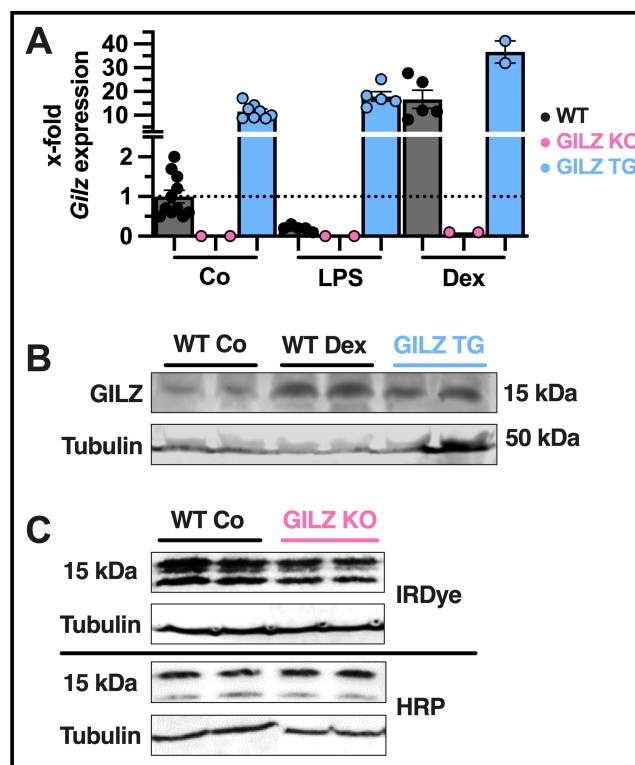


**Figure 3: Characterization of GILZ knockout and GILZ transgenic macrophages**

(A) qRT-PCR detection of *Gilz/Tsc22d3* expression in WT, GILZ KO, and GILZ TG BMMs relative to untreated WT cells after 4 hours of treatment with 100 ng/ml LPS or 1 μM dexamethasone for 24 hours (n = 2-8 BMM preparations per group). (B), (C) Western Blot of GILZ and α-tubulin in untreated (Co) and treated for 24 hours with 1 μM dexamethasone (Dex) WT, GILZ KO and GILZ TG BMMs (n = 2 BMM preparations per group). Blots were stained overnight at 4 °C with primary antibodies (1:1000 dilution for GILZ and 1:2000 dilution for α-tubulin) and stained for 2 hours at room temperature with IRDye secondary antibodies (1:10,000 dilution) or 1 hour in HRP-conjugated secondary antibody for GILZ (1:1000 dilution).

### 2.2.2 Regulation of GILZ Expression by High Salt in Macrophages

To assess the impact of HS on macrophage activation, we elevated the NaCl concentration in the media by an additional 40 mM, increasing it from 140 mM (normal media) to 180 mM (HS). This adjustment mimics the interstitial accumulation of NaCl observed under pathophysiological conditions (Müller *et al.*, 2019; Wilck *et al.*, 2019). Upon short-term exposure (4 h) to HS conditions, a significant downregulation of GILZ mRNA levels by approximately 65% was observed (Figure 4A). However, upon prolonged exposure (24 h) to HS conditions, we noted restoration of *Gilz* levels (Figure 4B). As previously described, acute LPS exposure alone downregulated *Gilz* expression (Figure 3), with no additional alteration upon concurrent HS exposure, while long-term LPS stimulation induced an immunotolerant state characterized by restoration of GILZ mRNA levels (Hopstädter *et al.*, 2015). The addition of HS upon long-term LPS stimulation elevated *Gilz* levels (Figure 4B).

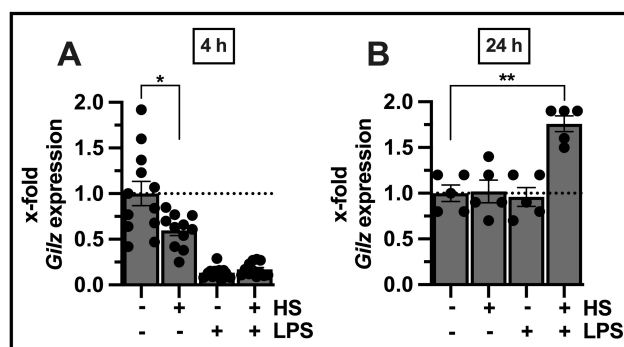


**Figure 4: Regulation of *Gilz/Tsc22d3* expression by high salt in macrophages**

(A) qRT-PCR detection of *Gilz/Tsc22d3* expression in BMMs after 4 hours and (B) 24 hours of treatment with high salt (HS; +40 mM NaCl) and/or 100 ng/ml LPS, relative to untreated control cells (n = 5-12 BMM preparations per group). *p* values were generated from one-way ANOVA comparison between groups, followed by Bonferroni *post-hoc* tests. \* *p* < 0.05, \*\* *p* < 0.01

### 2.2.3 No Detectable Involvement of GILZ in Short-Term High Salt Effects

We conducted gene expression analysis in WT, GILZ KO, and GILZ TG BMMs treated with LPS and HS for 4 hours to investigate GILZ's role in HS-mediated inflammation upon short-term exposure. Independent of GILZ abundance in the cells, HS conditions significantly increased the expression of several signature genes under inflammatory conditions (Figure 5A, F-H).

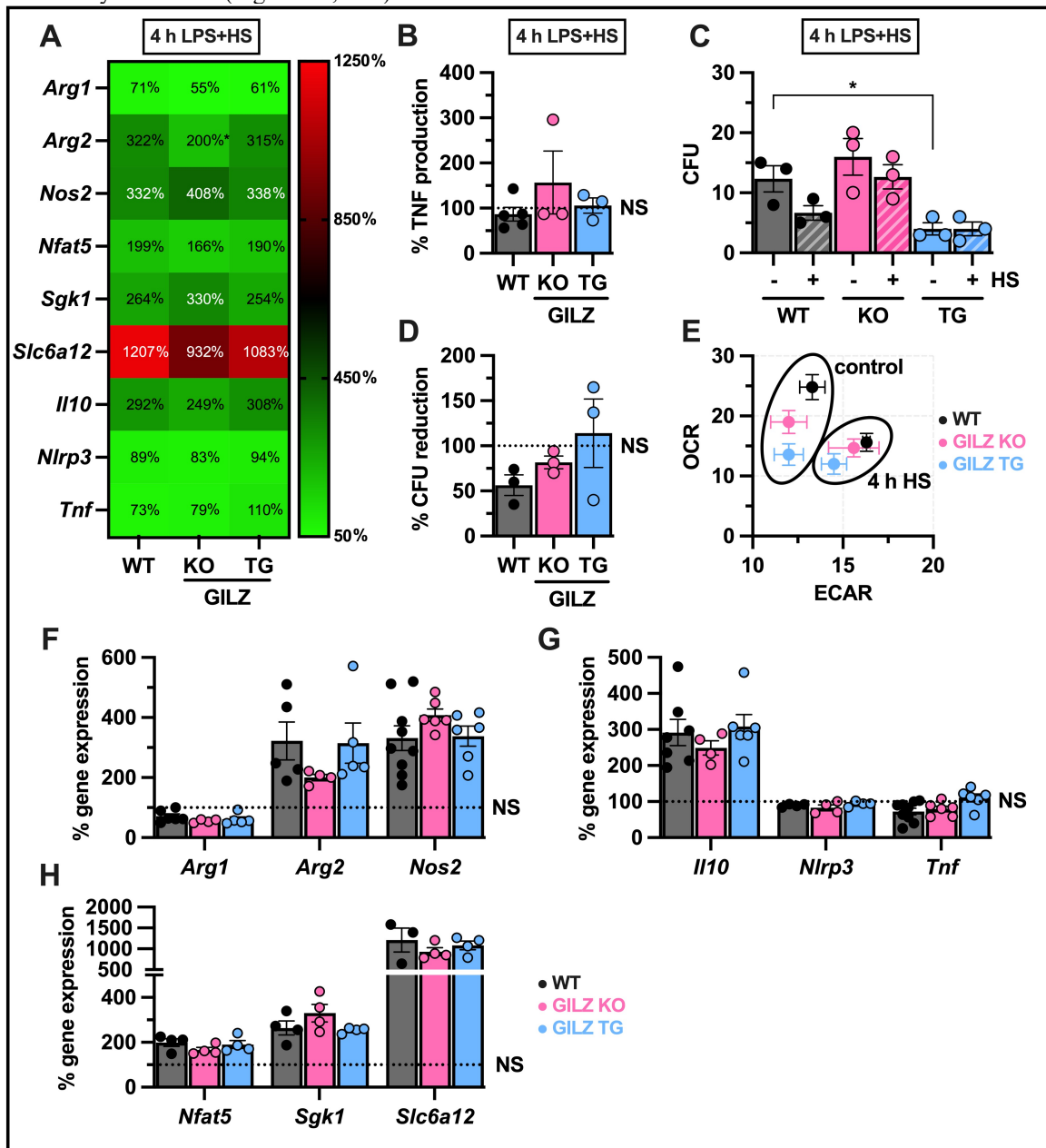


**Figure 5: No detectable involvement of GILZ in short-term high salt effects**

(A) qRT-PCR detection of depicted gene expression in WT, GILZ KO, and GILZ TG BMMs treated (4 h) with high salt (HS; +40 mM NaCl) and 100 ng/ml lipopolysaccharide (LPS), relative to respective LPS-treated cells of the same genotype ( $n = 4-9$  BMM preparations per group). (B) Normalized TNF secretion of WT, GILZ KO, and GILZ TG BMMs treated with LPS+HS (4 h) measured by ELISA, relative to respective LPS-treated cells of the same genotype ( $n = 3-5$  BMM preparations per group). (C) Colony-forming units (CFU) after 6 h infection of WT, GILZ KO, and GILZ TG BMMs with *S. typhimurium* treated with HS (4 h) before infection, and (D) reduction in CFU by HS relative to respective control ( $n = 3$  BMM preparations per group). (E) Basal oxygen consumption rate (OCR) and extracellular acidification rate (ECAR) of WT, GILZ KO, and GILZ TG BMMs treated with HS (4 h) measured with the Seahorse XFe96 Analyzer ( $n = 4$  BMM preparations per group). (F), (G), (H) gene expression data of (A) showing variability between biological replicates.  $p$  values were generated from one-way ANOVA comparison between groups, followed by Bonferroni *post-hoc* tests. Where no significance is indicated, differences between groups were not statistically significant. \*  $p < 0.05$

*Nos2*, the gene coding for the nitric oxide-synthesizing enzyme, a crucial marker in HS-mediated inflammation, was highly upregulated (Figure 5A, F). As expected from literature (Binger *et al.*, 2015), *Arg1*, which competes

with *Nos2* for the substrate L-arginine, was downregulated, although *Arg2*, more involved in NO metabolism than antimicrobial defense, was significantly upregulated (Figure 5A, F). *Nfat5* and *Nlrp3*, both key regulators in the osmoregulatory response and inflammasome activation, were also upregulated under HS conditions (Figure 5A, G-H). *Sgk1*, involved in sodium homeostasis and potentially influencing macrophage inflammatory responses, was upregulated by HS (Figure 5A, H). We measured *Slc6a12* expression, encoding a critical sodium channel, and found it to be drastically upregulated by HS (Figure 5A, H). Furthermore, *Il10*, a major anti-inflammatory cytokine, showed increased expression under HS conditions (Figure 5A, G). We assessed *Tnf* expression to evaluate the pro-inflammatory response, as TNF is a key cytokine in macrophage-mediated inflammation and observed a decrease in *Tnf* expression under HS conditions (Figure 5A, G).

Taken together, we surprisingly found no significant differences in gene expression of key mediators between genotypes.

We next assessed the secretion of TNF following a 4-hour LPS stimulation under HS conditions, where we observed neither elevated TNF levels nor significant differences between genotypes, which supports our findings from gene expression analysis (Figure 5B).

We further investigated bacterial clearance of BMMs in a *Salmonella typhimurium* infection assay, since antibacterial activity is the most important marker of HS-mediated inflammation (Jantsch *et al.*, 2015). As expected, pre-cultivating cells in HS for 4 hours prior to the 6-hour infection significantly enhanced the antibacterial activity of the macrophages, as evidenced by a lower CFU count (Figure 5C). GILZ TG macrophages did not exhibit a substantial increase in antibacterial activity, but as described in Chapter 1, already displayed heightened antibacterial activity under control conditions. There was no significant difference in antibacterial activity between genotypes, as GILZ KO macrophages also did not exert higher antibacterial activity compared to WT macrophages. (Figure 5D).

High salt conditions have been demonstrated to inhibit mitochondrial activity in macrophages. To investigate whether the abundance of GILZ in macrophages renders them less or more susceptible to this effect, we assessed the oxygen consumption rate (OCR) upon HS treatment (Figure 5E). Confirming previous findings (Geisberger *et al.*, 2021), we observed a significant shift in macrophage metabolism towards glycolysis, characterized by a lower OCR and a higher extracellular acidification rate (ECAR), typical for pro-inflammatory macrophage polarization. The extent to which the OCR was reduced was highest in WT cells. Given that GILZ-overexpressing macrophages already exhibit a lower respiration rate, as demonstrated in Chapter 1, the reduction in OCR by HS was limited in these cells.

Taken together, these findings indicate that GILZ does not play a significant role in the gene expression changes or functional responses induced by short-term HS exposure in macrophages. The observed effects on bacterial clearance and metabolic shifts are primarily attributable to HS itself, rather than the presence or absence of GILZ.

#### 2.2.4 No Detectable Involvement of GILZ in Long-Term High Salt Effects

Having found no detectable involvement of GILZ in short-term HS effects, we next investigated the role of GILZ in long-term HS exposure, focusing on comparisons between WT and GILZ TG macrophages.

Prolonged incubation of BMMs in HS media has been shown to enhance antibacterial activity against *S. typhimurium* (Neubert *et al.*, 2019), which we confirmed (Figure 6A). Notably, while GILZ TG macrophages exhibited higher efficacy in bacterial killing, HS conditioning resulted in a less pronounced increase in antibacterial activity in these cells compared to WT macrophages. Gene expression analysis under prolonged LPS and HS exposure revealed no significant alterations attributable to GILZ overexpression in BMMs (Figure 6B). However, this exposure notably increased the expression of *Nos2*, *Nlrp3*, and *Slc6a12* (Figure 6B).

We then polarized cells to classically activated M1 macrophages through a 24-hour stimulation with interferon- $\gamma$  (IFN) and LPS. M1-polarized BMMs demonstrated enhanced bacterial clearance when infected with *S. typhimurium* for 24 h (Figure 6C). Interestingly, additional HS further strengthened this effect in WT macrophages, while GILZ TG macrophages maintained heightened bactericidal activity even in an unpolarized state, as described in Chapter 1 (Legroux *et al.*, 2024). This observation correlates with increased NO production, a key bactericidal agent, in both WT and GILZ TG macrophages upon additional HS exposure (Figure 6D), occurring to a similar extent in both groups.

HS exposure triggered significant activation of NF- $\kappa$ B, the principal transcription factor governing pro-inflammatory gene expression in innate immune cells, in a murine macrophage reporter cell line (Figure 6E). Lastly, we investigated the involvement of GILZ in HS effects under IL-4 polarization. Gene expression comparison between WT and GILZ TG cells revealed downregulation of M2 signature genes *Arg1*, *Mrc1*, and *Ym1* by HS, with no significant differences between genotypes (Figure 6F). Nevertheless, *Nos2* was highly upregulated under HS conditions.

Taken together, our findings suggest that while HS enhances bactericidal activity and pro-inflammatory gene expression in macrophages, constitutive GILZ overexpression does not significantly alter these responses under long-term HS exposure.

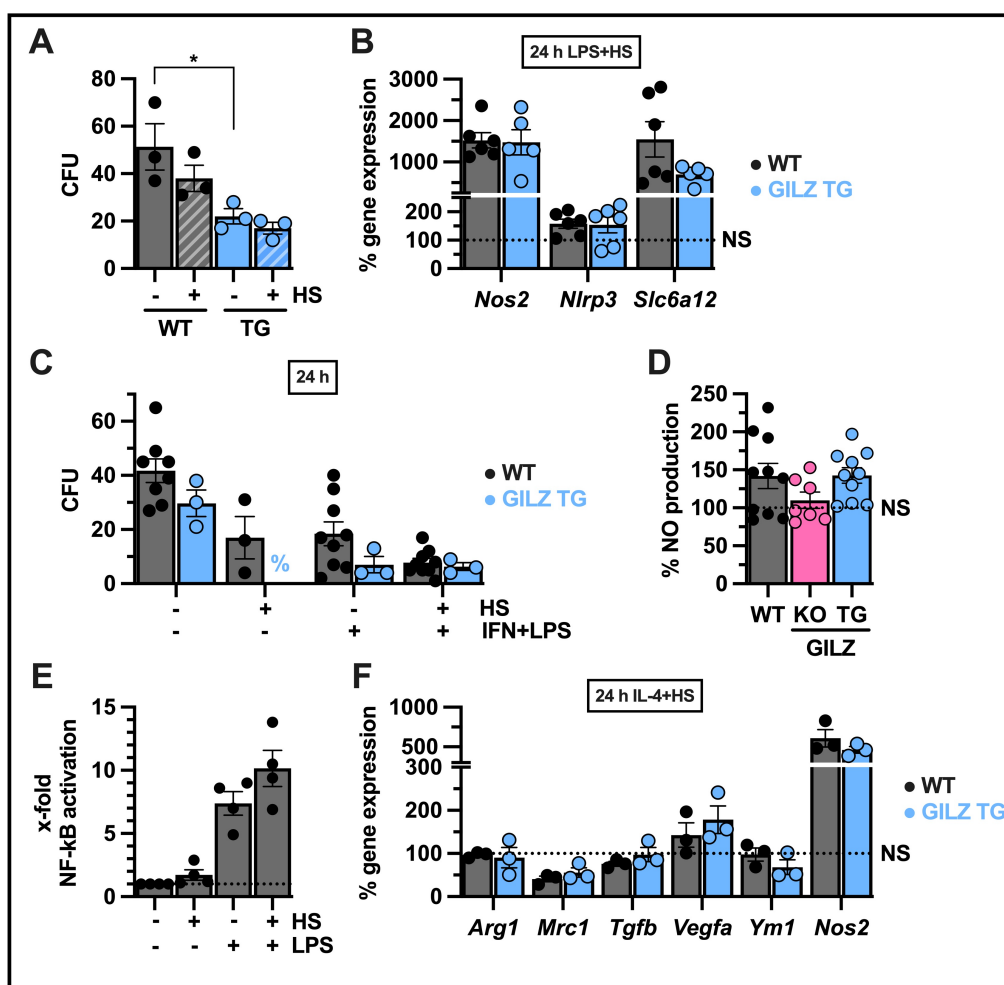


**Figure 6:** No detectable involvement of GILZ in long-term high salt effects

(A) Colony-forming units (CFU) after 6 h infection of WT and GILZ TG BMMs with *S. typhimurium* treated (16 h) with high salt (HS; +40 mM NaCl) before infection (n = 3 BMM preparations per group). (B) qRT-PCR detection of depicted gene expression in WT and GILZ TG BMMs treated (24 h) with high salt (HS; +40 mM NaCl) and 10 ng/ml LPS, relative to respective LPS-treated cells of the same genotype (n = 4-9 BMM preparations per group). (C) CFU after 24 h infection of WT and GILZ TG BMMs treated (24 h) with HS and/or 10 ng/ml LPS + 5 ng/ml IFN- $\gamma$  before infection (n = 3-9 BMM preparations per group). (D) Relative NO production from IFN+LPS+HS-treated WT, GILZ KO, and GILZ TG BMMs (24 h) measured by Griess assay relative to respective IFN+LPS-treated cells from the same genotype. (E) NF- $\kappa$ B/AP-1 activation of RAW-Blue™ reporter cells after 24 h HS  $\pm$  LPS treatment, relative to respective untreated controls (n = 4 independent experiments). (F) qRT-PCR detection of depicted gene expression in WT and GILZ TG BMMs treated (24 h) with HS and 20 ng/ml interleukin 4 (IL-4), relative to respective IL-4-treated cells of the same genotype (n = 3 BMM preparations per group). *p* values were generated from one-way ANOVA comparison between groups, followed by Bonferroni *post-hoc* tests. Where no significance is indicated, differences between groups were not statistically significant. \* *p* < 0.05, % = not measured, NS = normal salt.

### 2.2.5 Aldosterone Induces *Gilz* via the Glucocorticoid Receptor

Aldosterone regulates sodium and potassium balance in part by inducing the expression of GILZ in kidney epithelial cells (Bruscoli *et al.*, 2022). GILZ, in turn, modulates ion transport *via* transporters like NCC and ENaC (Rashmi *et al.*, 2017; Soundararajan *et al.*, 2010). Given the incomplete understanding of how macrophages sense sodium-mediated inflammation and the pivotal role of the aldosterone-MR axis in sodium-mediated effects, we wanted to investigate whether GILZ might also mediate sodium sensing by ion transporters in macrophages. To explore this, we investigated the induction of *Gilz* by aldosterone and whether this induction is mediated through binding to the MR or the GR. We treated BMMs with aldosterone in the presence of eplerenone, an MR antagonist, and mifepristone, a GR antagonist. We observed that aldosterone induced *Gilz* in macrophages, but that mifepristone, and not eplerenone, abolished this induction (Figure 7). This suggests that the induction occurs *via* binding to the GR rather than the MR, as mifepristone alone did not induce *Gilz* and blockade of the GR by mifepristone prevented *Gilz* induction by aldosterone. Although GR activation is known to modulate ion transport in some tissues, it is not known to do so in macrophages (Laube *et al.*, 2020). Therefore, if *Gilz* was induced by



GR, it would unlikely modulate ion transport in macrophages. We concluded that the MR is not involved in potential GILZ-mediated effects under HS conditions.

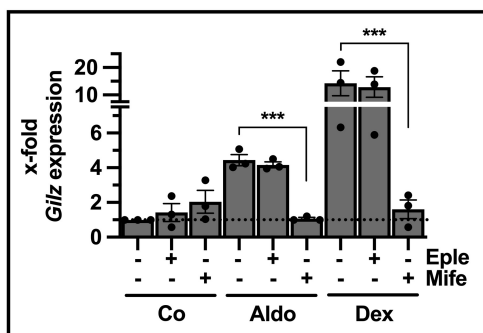


**Figure 7: Aldosterone induces *Gilz* via the glucocorticoid receptor**

qRT-PCR detection of *Gilz* expression in BMMs treated (4 h) with 1  $\mu$ mol aldosterone, 1  $\mu$ mol dexamethasone, and pre-treated (1 h) with either 10  $\mu$ mol mifepristone (Mife) or 10  $\mu$ mol eplerenone (Eple) as indicated relative to solvent-controlled (0.001% DMSO) cells ( $n = 3$  BMM preparations per group).  $p$  values were generated from one-way ANOVA comparison between groups, followed by Bonferroni *post-hoc* tests. \*\*\*  $p < 0.0001$

## 2.3 Discussion

We successfully replicated the effects of HS conditions on macrophage biology as described in the literature. Short-term HS exposure significantly induced high salt signature genes, including *Nos2*, *Sgk1*, *Nfat5*, and *Slc6a12*, which encode pivotal proteins involved in sensing, mediating, and executing functions upon HS treatment (Neubert *et al.*, 2020). Among these, *Slc6a12*, a tonicity-responsive channel, exhibited very high upregulation in gene expression, consistent with previous findings attributing it with the highest upregulation of all genes under HS conditions (Binger *et al.*, 2015).

We also reproduced the observation that some proinflammatory markers, such as TNF or *Nlrp3* expression, are paradoxically unaffected or even downregulated by HS initially, with a definitive shift towards inflammation occurring only after 24 hours (Geisberger *et al.*, 2021). The upregulation of *Il10*, an important marker for anti-inflammatory polarization, indicates that HS treatment does not merely enhance classical M1 polarization but leads to a distinct macrophage polarization subtype, aligning with existing literature (Zhang *et al.*, 2015).

HS is known to blunt anti-inflammatory activation rather than invert polarization towards the canonical M1 state (Binger *et al.*, 2015). This is confirmed by the blunted expression of M2 signature genes *Mrc1*, *Tgfb*, and *Ym1*. Additionally, the heavy upregulation of *Nos2*, a typical marker for M1 activation in macrophages, under HS conditions suggests that HS influences NO synthesis more strongly than IL-4 can diminish it through inducing anti-inflammatory polarization.

We could not detect any involvement of GILZ in HS-mediated inflammation or sensing mechanisms. Manipulating GILZ abundance in macrophages affected neither short-term nor long-term polarization or functionality under high salt treatment. However, it is important to clarify the challenges encountered during our study. While GILZ is recognized as a significant factor in macrophage signaling pathways, its levels are substantially reduced during acute inflammation (Hoppstädter *et al.*, 2019). This natural suppression of GILZ expression during acute inflammation may have influenced the insights gained from GILZ KO macrophages in short-term inflammation studies. The observed differences in baseline conditions prior to LPS challenge under HS suggest potential relevance of GILZ, warranting further exploration using GILZ TG macrophages. However, the overexpression of GILZ notably influenced macrophage functionalities, as previously reported (Legroux *et al.*, 2024), introducing variability that complicates the interpretation of GILZ's specific role under high salt treatment. Moreover, HS-induced reduction of *Gilz* expression in BMMs, although transient, raises questions about the sustained relevance of GILZ in macrophages under prolonged HS conditions. Of note, the viability of macrophages under HS conditions is not impaired in WT, GILZ KO, or GILZ TG macrophages (data not shown).

Recent literature has highlighted the induction of pyroptosis by HS conditions, presenting new opportunities for further research. One study has shown that hypertonic saline induces inflammation in macrophages through the NLRP1 inflammasome (Sposito *et al.*, 2023). Another study suggests that sodium entering cells through the BGT-1 (the transporter encoded by *Slc6a12*) activates SGK1, promotes the expression of the NLRP3 inflammasome, and activates the MAPK/NF- $\kappa$ B pathways, thereby causing inflammatory damage through membrane rupture (Zhang *et al.*, 2024). These findings are particularly interesting in the context of our research, as GILZ has been shown to protect against pyroptosis, and SGK1, just like GILZ is an important gene in GC-signaling (Legroux *et al.*, 2024).

## Chapter 3 Investigating the Role of Glucocorticoid-Induced Leucine Zipper (GILZ) in Trained Immunity of Macrophages

### 3.1 Introduction

#### 3.1.1 Immune Memory

The human immune system comprises both innate and adaptive immune components, traditionally associating immune memory with the advanced capabilities of the adaptive immune response (Bonilla & Oettgen, 2010). However, it is essential to acknowledge that immune memory is not exclusive to vertebrates or solely reliant on adaptive immunity (Netea *et al.*, 2011). Indeed, immune memory is a fundamental characteristic observed across all living organisms, including plants and non-vertebrates (Gourbal *et al.*, 2018).

Conceptually, immune memory properties are defined by the amplitude and specificity of the immune response upon re-exposure to pathogens. This phenomenon, observed in both primitive or innate and adaptive immune systems, significantly relies on epigenetic reprogramming during the initial encounter with non-host signals, shaping the magnitude and speed of the immune response (Lau *et al.*, 2018; Netea *et al.*, 2019). Specificity, on the other hand, is a feature unique to the adaptive immune response and arises from somatic gene recombination and clonal selection in B- and T-lymphocytes (De Silva & Klein, 2015).

#### 3.1.2 Trained Innate Immunity: Mechanisms and Molecular Pathways

Trained innate immunity (TRIM) emerges as a form of innate immunological memory (Hajishengallis *et al.*, 2023). Well-established inducers of TRIM, such as the tuberculosis vaccine *Bacille Calmette-Guérin* (BCG), the fungal cell wall component  $\beta$ -glucan, and certain viral infections, prime innate immune cells like monocytes, macrophages, dendritic cells, and natural killer cells through initial infection or stimulation, leading to augmented but nonspecific responses to subsequent infections or stimuli, characterized by an increased production of inflammatory cytokines and enhanced antimicrobial defense (Figure 8) (R. J. W. Arts *et al.*, 2016; Bekkering *et al.*, 2018; Covián *et al.*, 2021; Hole *et al.*, 2019; Kalafati *et al.*, 2020; Kleinnijenhuis *et al.*, 2012; Netea & Meer, 2017; Quintin *et al.*, 2012; Vivier *et al.*, 2011).

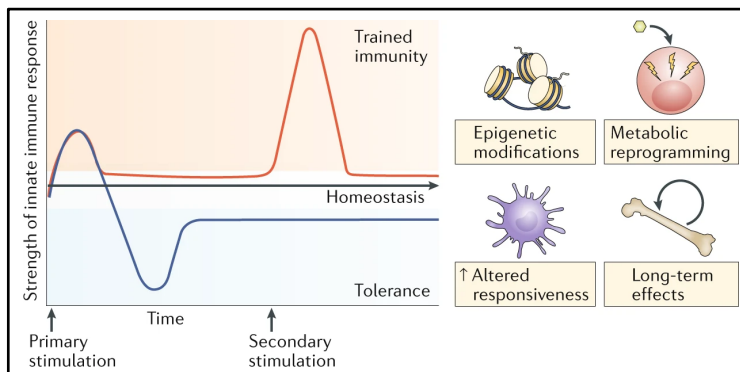


**Figure 8: Defining trained immunity as a functional program of innate memory in contrast to immune tolerance (Netea *et al.*, 2020)**

Copyright © 2020, Springer Nature Limited

It is notable that in TRIM, cells return to their baseline state after the initial stimulus, which induced persistent epigenetic changes (Divangahi *et al.*, 2021). While activating resting monocytes and macrophages, *e.g.*, through toll-like receptor (TLR) signaling also induces histone modifications that promote transcription of inflammatory genes by enriching open-chromatin regions, these modifications are transient and diminish when ligands are no longer binding (Medzhitov, 2001). Re-stimulation of these activated cells before the initial stimulus subsides results in an enhanced inflammatory response, referred to as priming (Divangahi *et al.*, 2021). In contrast, innate immune tolerance leads to functional deficits associated with temporary epigenetic changes, resulting in reduced function upon restimulation (Figure 8) (Cheng *et al.*, 2016). While the induction of tolerance serves as a counter-regulatory mechanism to decrease potential harmful collateral damage in tissues in response to inflammation (Hamdi *et al.*, 2007), prolonged or excessive activation can induce immune paralysis. This state may have detrimental effects, increasing susceptibility to secondary infections (Medzhitov *et al.*, 2012). Resolution of inflammation is a coordinated and active process aimed at restoration of tissue integrity and function (Ortega - Gómez *et al.*, 2013).

The molecular mechanisms underlying the acquisition and maintenance of a 'trained' state are not completely understood (Hajishengallis *et al.*, 2023). However, the altered responsiveness to a specific subset of inflammatory

genes responsible for the enhanced response is characterized by changes in chromatin organization, transcription of long non-coding RNAs (lncRNAs), DNA methylation, and reprogramming of cellular metabolism (Divangahi *et al.*, 2021; Netea *et al.*, 2020). Glycolysis, glutaminolysis, mevalonate synthesis, fatty acid metabolism, and cholesterol metabolism, along with changes in oxygen consumption and oxidative phosphorylation (OXPHOS), are indispensable for the induction of the epigenetic changes associated with trained immunity (R. J. Arts, B. Novakovic, *et al.*, 2016; Cheng *et al.*, 2014; Domínguez-Andrés *et al.*, 2019).

### 3.1.3 Clinical Implications and Therapeutic Potential of Trained Innate Immunity

Given the relatively brief life span of tissue-resident cells of the innate immune system, with a half-life of 5-7 days according to literature (Yona *et al.*, 2013), it is not unexpected that systemic induction of TRIM relies not only on tissue cell populations (peripheral trained immunity), but on profound changes in metabolic and epigenetic pathways in bone-marrow progenitor cells (central trained immunity) to induce long-lasting effects (Cirovic *et al.*, 2020; Geckin *et al.*, 2022; Kleinnijenhuis *et al.*, 2013).

TRIM can be seen as a novel framework for understanding the role of chronic inflammation in health and disease (Figure 9). Regulating trained immunity therapeutically can be applied not only to address immunodeficiencies, in the form of counteracting immunosuppression or immune paralysis, and enhancing resistance to infections, but also for managing hyperinflammation, autoimmune diseases, and chronic kidney disease. The inhibition of trained immunity serves also as a potential strategy against lifestyle-related risk factors, which have been shown to induce trained immunity in both *in vitro* and in experimental animal models (Bekkering *et al.*, 2021; Christ *et al.*, 2018; Ochando *et al.*, 2023; Riksen *et al.*, 2023; Sviridov *et al.*, 2022). Identifying molecular targets is indispensable for developing potential pharmacological therapies.

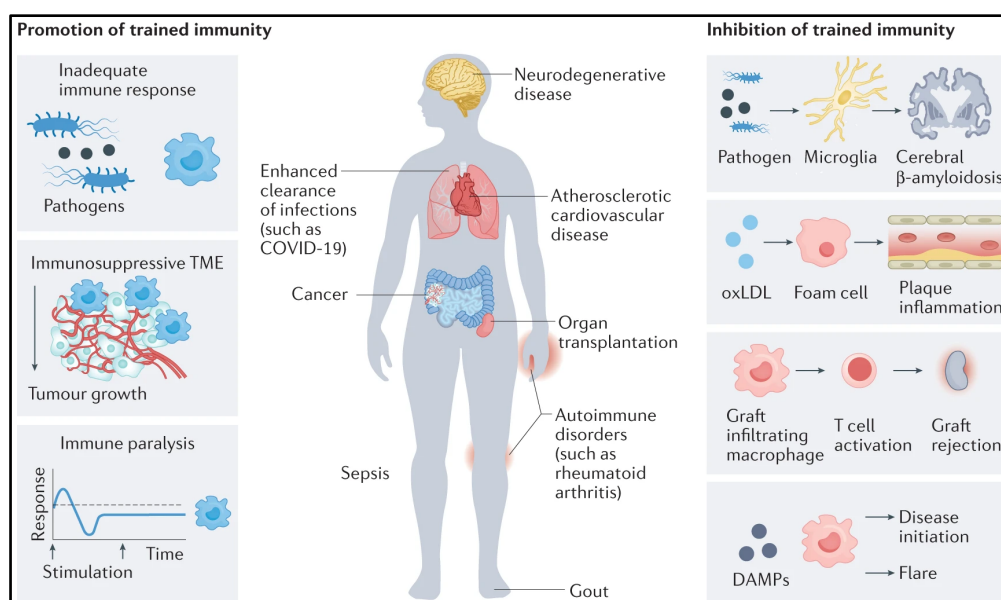


**Figure 9: The role of trained immunity in health and disease (van Leent *et al.*, 2022)**

Copyright © 2022, Springer Nature Limited

Recent research has uncovered fascinating insights into the transmission of trained immunity across generations. In murine models, descendants of ancestors who survived *Candida albicans* infections inherited cellular, developmental, transcriptional, and epigenetic alterations that enhanced immune responsiveness and provided increased protection against infections in subsequent generations (Katzmarski *et al.*, 2021). Kaufmann *et al.* attempted to reproduce these findings but observed no significant difference in infection outcomes between the offspring of trained and non-trained parents, suggesting variability in the heritability and expression of trained immunity across different experimental conditions (Kaufmann *et al.*, 2022).

### 3.1.4 Hypothesis: Role of GILZ in Trained Innate Immunity

Originally identified as a pivotal mediator of the anti-inflammatory properties of glucocorticoids in immune cells, the glucocorticoid-induced leucine zipper (GILZ) governs essential functions of macrophages, including cytokine production and host defense (Ayroldi & Riccardi, 2009; Ellouze *et al.*, 2020; Hoppstädter *et al.*, 2015; Souza *et al.*, 2022; Vago *et al.*, 2020). Alterations in immunometabolism can also be attributed to GILZ activity (Legroux *et al.*, 2024). Based on the dual roles of GILZ in promoting resolution of inflammation, as discussed in Chapter 1, and its established association with immune tolerance (Cohen *et al.*, 2006; Hoppstädter *et al.*, 2015), we hypothesized that low levels of GILZ may induce trained immunity. This hypothesis is grounded in the potential for reduced GILZ expression to skew macrophage phenotypes toward a heightened inflammatory state, thereby

augmenting their responsiveness and memory to subsequent pathogen encounters. It is noteworthy that trained immunity and immune tolerance represent distinct yet interconnected processes, with recent studies highlighting the itaconate synthesis pathway as a pivotal regulatory hub linking these two immunological phenomena (Domínguez - Andrés *et al.*, 2019).

TRIM relies heavily on the establishment of epigenetic modifications, primarily through posttranslational histone modifications, DNA methylation, chromatin remodeling, and the production of lncRNAs (Hu *et al.*, 2022). Histone methyltransferases (HMTs) and histone acetyltransferases (HATs) are particularly critical in this process (Saeed *et al.*, 2014). However, histone deacetylases (HDACs) also play a significant role, given the tight interconnection between immunometabolism and epigenetics in TRIM (Robinson *et al.*, 2023). Lactate, the end product of anaerobic glycolysis, inhibits HDAC activity (Arts, Joosten, Netea, 2016). Furthermore, critical metabolic intermediates such as NAD<sup>+</sup> and acetyl-CoA, altered in trained monocytes, serve as cofactors or substrates for numerous HDACs and HATs, affecting their activity (van der Heijden *et al.*, 2018). The fatty acid metabolite butyrate, related to trained immunity, has also been shown to inhibit HDAC activity (Fanucchi *et al.*, 2021). GILZ has been previously investigated for its role in HDAC-mediated transcriptional repression. A study showed co-immunoprecipitation of GILZ with HDAC1, but not other HDACs, suggesting that GILZ recruits class I HDACs to inhibit transcriptional activity (Shi *et al.*, 2003). Supporting this, Bruscoli *et al.* (2010) demonstrated that GILZ specifically interacts with HDAC1, but not HDAC2, mediating the antimyogenic effects of glucocorticoids (Bruscoli *et al.*, 2010). These findings support our hypothesis that GILZ is involved in TRIM, through its interactions with HDACs.

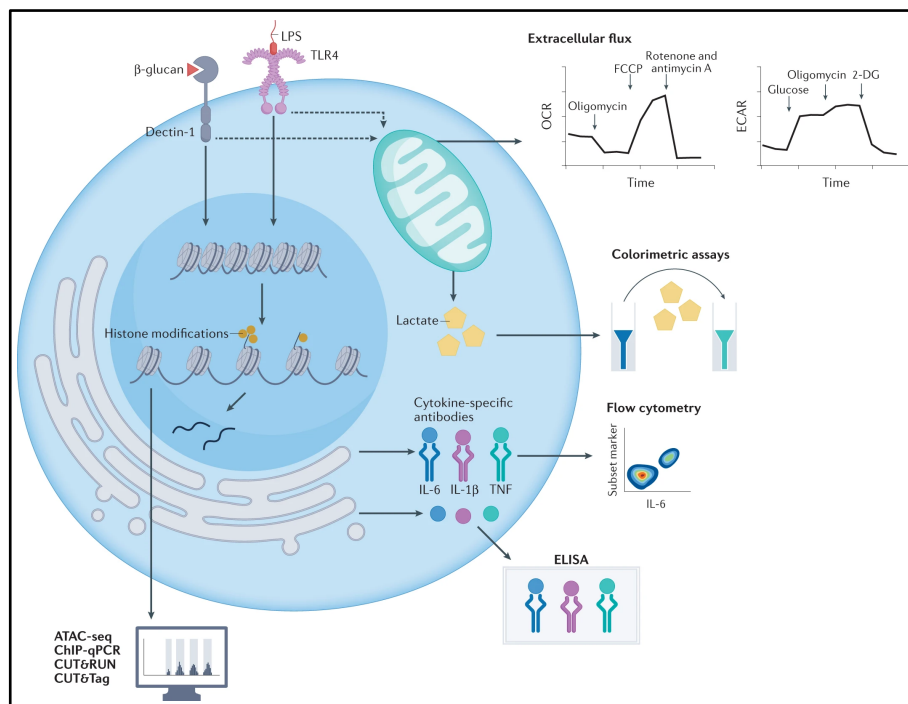


**Figure 10: Cellular, molecular, metabolic, and epigenetic approaches to study trained immunity (Ochando *et al.*, 2023)**

Copyright © 2022, Springer Nature Limited

Given its influence on essential functions of macrophages, we hypothesized that GILZ plays a role in modulating the trained immunity process. Initially, we tried to investigate the role of GILZ in the induction of trained immune memory in fully differentiated macrophages. Subsequently, we explored the effects of *in vivo* β-glucan vaccination in a mouse model of LPS-induced sepsis, assessing TNF and IL-6 serum levels, as well as immune cell composition in the lungs. Finally, we successfully induced TRIM in bone marrow (BM) cells obtained from WT, GILZ KO, and GILZ TG mice to compare the extent of training in macrophages based on GILZ abundance measuring immunometabolism, cytokine production, and antimicrobial defense (Figure 10).

## 3.2 Results

### 3.2.1 Training Differentiated Macrophages

In our investigation of trained immunity induction in fully differentiated macrophages, we explored different training protocols based on literature to evaluate their effectiveness and identify a potential role for GILZ. We used commercially available whole glucan particles (WGP) as the  $\beta$ -glucan preparation.

We first measured *Gilz* mRNA levels over the course of the protocol proposed for differentiated macrophages (Benjaskulluecha *et al.*, 2024). Interestingly, *Gilz* expression significantly increased throughout the resting period after 24 h of WGP treatment (Figure 11A). Cells going through the entire protocol (WGP for 24 h, followed by 72 h resting before 2 h of LPS stimulation) were trained consistently but to a minimal extent, with a modest increase of 1.3-fold in TNF levels compared to untrained macrophages (Figure 11B). We hypothesized that the viability of BMMs after more than 4 days in culture might be negatively affected and thus reduced the resting period to 48 h, while shortening the stressful WGP treatment to 8 h and prolonging LPS treatment, hoping to see more pronounced differences in TNF secretion. Unfortunately, we could not induce TRIM under these conditions (Figure 11C), potentially highlighting the importance of an appropriate rest period to induce the characteristic epigenetic modifications.

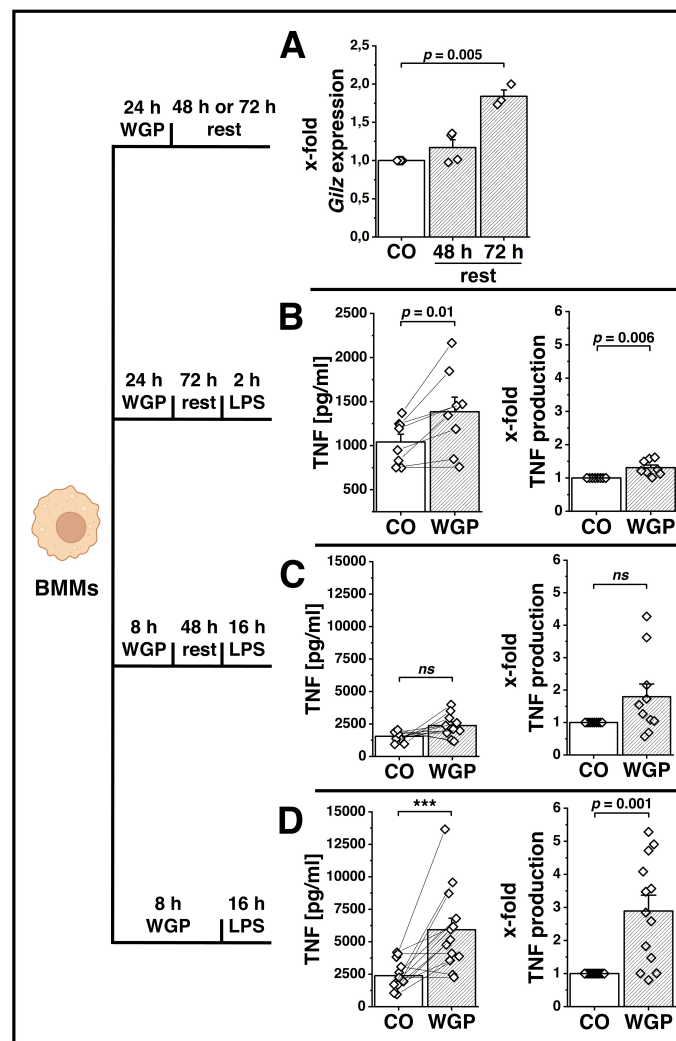


**Figure 11: Training differentiated macrophages**

(A) qRT-PCR detection of *Gilz/Tsc2dd3* expression in BMMs after 48 and 72 h of rest after 24 h treatment with 100  $\mu$ g/ml WGP, relative to untreated cells ( $n = 3-4$  BMM preparations). (B) Cells were treated with 100  $\mu$ g/ml WGP for 24 h, followed by 10 ng/ml LPS stimulation for 2 h after 72 h of rest in cell culture media ( $n = 8$  BMM preparations). (C) Cells were treated with 100  $\mu$ g/ml WGP for 8 h, followed by 100 ng/ml LPS stimulation for 16 h after 48 h of rest in cell culture media ( $n = 10$  BMM preparations), or (D) without rest ( $n = 13$  BMM preparations). TNF secretion was measured by ELISA. Each dot represents one independent biological replicate (mean  $\pm$  SEM), and connected dots represent paired samples indicating the respective untreated control.  $p$ -values were determined by Mann-Whitney U-test. \*\*\*  $p < 0.0001$

Finally, we tried a short-term training protocol that has been proposed, involving exposure to WGP for 8 h, followed by 16 h LPS stimulation (Walachowski *et al.*, 2017). This approach resulted in significantly elevated TNF levels compared to LPS treatment alone (Figure 11D). But considering the nature of TRIM, it is likely due to additive rather than sustained effects, aligning more with inflammatory priming (Divangahi *et al.*, 2021), of the cells rather than trained immunity. We decided not to proceed with GILZ KO and GILZ TG BMMs since none of these protocols led to a robust and reliable training phenotype in the BMMs.

### 3.2.2 Training *in vivo*

We investigated the effects of *in vivo* training by intraperitoneally injecting mice with  $\beta$ -glucan following an established protocol (Kalafati *et al.*, 2020; Moorlag *et al.*, 2020). Seven days post-injection, we assessed the response to systemic inflammation induced by intraperitoneal LPS administration (4 h), focusing on TNF and IL-6 serum levels and immune cell composition in the lungs (Figure 12A). LPS-induced sepsis significantly increased systemic TNF and IL-6 secretion to a similar extent in both  $\beta$ -glucan vaccinated and control animals (Figure 12B). Flow cytometry analysis revealed that LPS injection dramatically promoted leukocyte recruitment into the lungs, increasing from 40% to 70%, regardless of  $\beta$ -glucan vaccination (Figure 13). Since  $\beta$ -glucan vaccination is known to induce trained immunity, which is independent of B and T cells, it was unsurprising to observe no changes in B or T cell frequencies. Gating on viable cells to account for the higher abundance of leukocytes from LPS-induced sepsis, we found that alveolar macrophages were reduced by the LPS challenge, independent of  $\beta$ -glucan vaccination. Neutrophils, highly recruited, represented around 50% of the leukocytes detected in the lungs after the LPS challenge. Interestingly, there was a significantly higher frequency of neutrophils in mice vaccinated with  $\beta$ -glucan 7 days prior, possibly indicating an inflamed state before the LPS injection. Although less frequent, monocytes more than doubled in abundance in response to LPS, regardless of vaccination status. Macrophage recruitment did not seem to be affected by the LPS challenge; however,  $\beta$ -glucan vaccinated mice showed significantly fewer macrophages 7 days post-vaccination (Figure 13). Overall, while the LPS challenge effectively induced systemic inflammation,  $\beta$ -glucan vaccination did not influence the recruitment of leukocytes under septic conditions, suggesting that TRIM has not been induced in the mice.

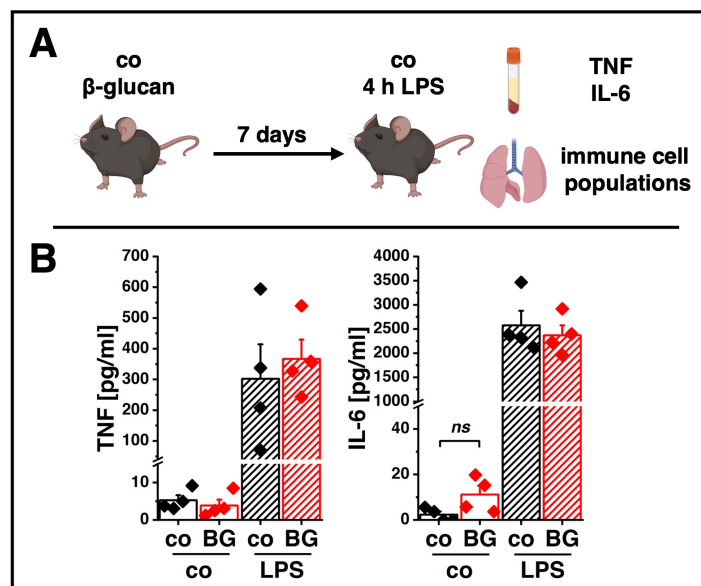


**Figure 12: Training *in vivo*: serum levels**

(A) Experimental protocol in 6 months old, male mice. (B) TNF and IL-6 serum concentrations of mice ( $n = 4$ ) measured by ELISA. Each dot represents one independent biological replicate (mean  $\pm$  SEM).  $p$  values were generated from one-way ANOVA comparison between groups, followed by Bonferroni *post-hoc* tests.

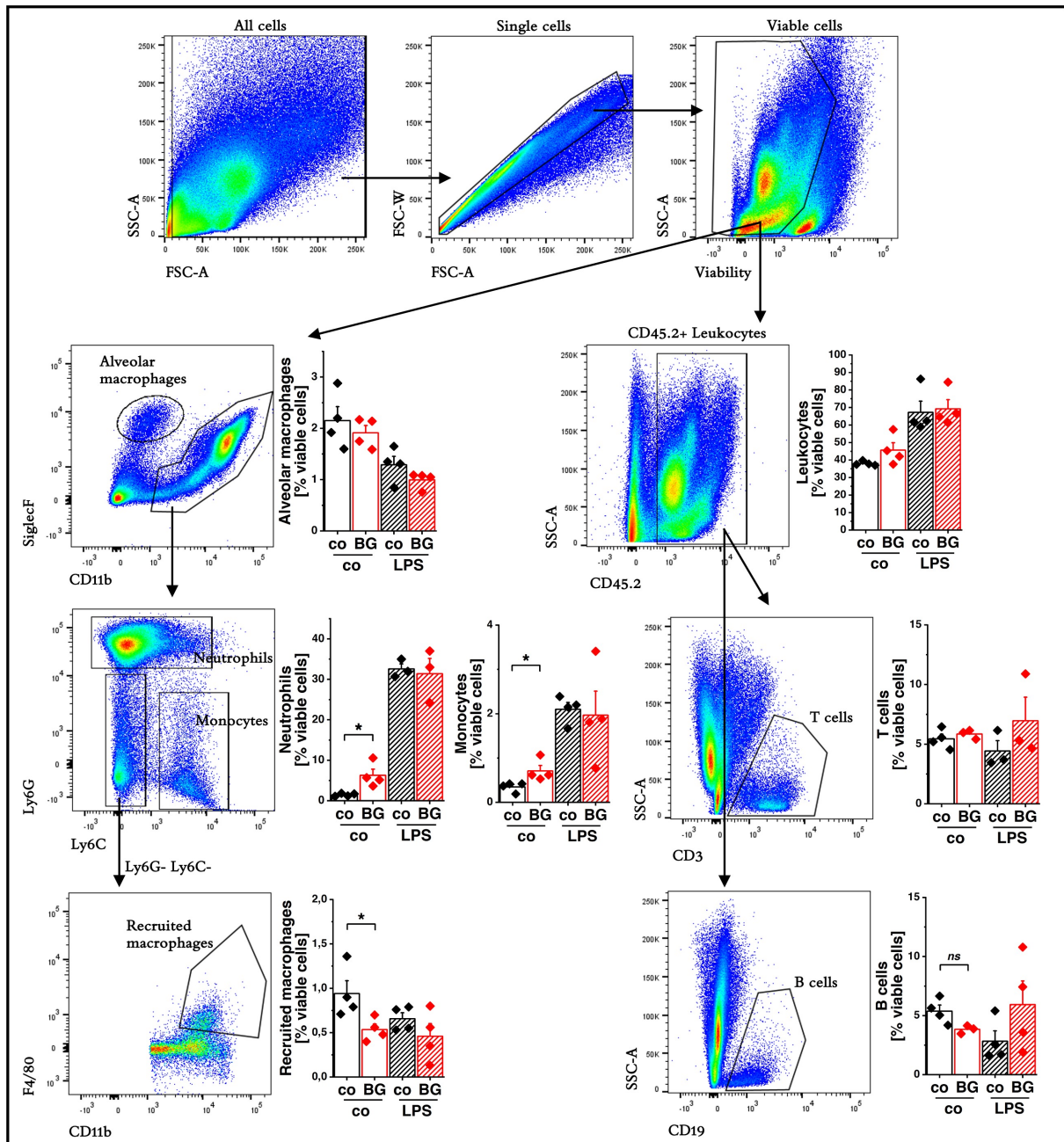


**Figure 13: Training *in vivo*: immune cell populations in the lungs**

Frequency and the gating strategy to determine of immune cell populations in the lungs of mice injected with PBS (co) or  $\beta$ -glucan (BG) 7 days prior to a 4 h LPS challenge (LPS) or PBS control (co) ( $n = 4$ ). Each dot represents one independent biological replicate (mean  $\pm$  SEM).  $p$  values were generated from one-way ANOVA comparison between groups, followed by Bonferroni *post-hoc* tests. \*  $p < 0.05$

### 3.2.3 Training Macrophage Progenitor Cells

Lastly, we conducted experiments involving the training of bone marrow progenitor cells (BMPCs) with  $\beta$ -glucan derived from baker's yeast (Invivogen) following a validated and recognized protocol (Bekkering *et al.*, 2016; Domínguez-Andrés *et al.*, 2021). Bone marrow cells were isolated from the femurs and tibias of WT, GILZ KO, and GILZ TG mice and cultured in the presence of  $\beta$ -glucan for 24 hours. Subsequently, the cells were differentiated into macrophages for an additional 5 days using L929-conditioned media as the source for M-CSF. After the training period, macrophages were subjected to functional assays to evaluate their cytokine production, phagocytic activity, and immunometabolism (Figure 14A). To evaluate the impact of trained immunity induction on macrophage functions, we assessed TNF production levels in trained and untrained macrophages following LPS stimulation. Trained macrophages exhibited approximately 150% TNF production compared to untrained macrophages, indicating the successful induction of trained immunity (Figure 14B). We investigated the metabolic alterations associated with trained immunity induction by measuring the Oxygen Consumption Rate (OCR) and

Extracellular Acidification Rate (ECAR) in trained macrophages:  $\beta$ -glucan priming led to a significant reduction in OCR to approximately 75% of control macrophages, while maintaining spare respiratory capacity, accompanied by an increase in ECAR to around 120% of control levels (Figure 14C). These findings suggest a metabolic shift towards glycolysis in trained macrophages, indicative of enhanced immune activation and effector functions (Cheng *et al.*, 2014). To assess the antibacterial activity of trained macrophages, we conducted *S. typhimurium* and *E. coli* infection assays. Contrary to our expectations (Ochando *et al.*, 2023), training did not significantly enhance their ability to combat *S. typhimurium* and *E. coli* infections. However, GILZ overexpression enhanced antibacterial activity in control macrophages, consistent with previous reports (Figure 14D). This observation complicates the interpretation of our training experiments, as GILZ expression levels can influence the antibacterial response of macrophages independently of  $\beta$ -glucan priming.

Notably, the observed effects of trained immunity induction were consistent across all genotypes, including WT, GILZ KO, and GILZ TG macrophages. TNF production in untrained cells was comparable across the different genotypes. This suggests that the absence or excess of GILZ did not inherently predispose the progenitor cells to altered baseline TNF production levels in the macrophages. Consequently, these results indicate that the lack or overexpression of GILZ did not significantly influence the extent of trained immunity induction in bone marrow cells.

### 3.3 Discussion

#### 3.3.1 Training BMPCs vs. BMMs

We successfully induced a state of trained immunity in BMMs by treating BMPCs with  $\beta$ -glucan prior to their differentiation into BMMs, following the widely recognized and validated protocol established by the most renowned groups in the field (Bekkering *et al.*, 2016; Domínguez-Andrés *et al.*, 2021). We therefore adopted it for our experiments with WT, GILZ KO, and GILZ TG macrophages. However, we did not observe a role for GILZ in trained immunity using this protocol.

Manipulating GILZ abundance affects multiple stages of the training protocol. Upon  $\beta$ -glucan treatment, the establishment and maintenance of the trained state can be influenced through epigenetic mechanisms and signaling following Dectin-1 receptor activation. Additionally, effector functions such as responses to secondary LPS treatment, antibacterial activity, or energy profiles, can be altered independently from training. GILZ KO macrophages are known to secrete higher levels of TNF upon LPS treatment, whereas GILZ overexpression reduces the oxygen consumption rate (Hoppstädter *et al.*, 2015; Legroux *et al.*, 2024).

Conversely, training differentiated BMMs is less established in the field. We also attempted to train differentiated BMMs using protocols described in the literature (Benjaskulluecha *et al.*, 2024; Saz-Leal *et al.*, 2018; Walachowski *et al.*, 2017). However, we were unable to successfully induce a state of trained immunity.

Induction of trained immunity in BMMs has also been proposed using a short-term protocol (Walachowski *et al.*, 2017). In this model, there is no resting period between the 8-hour WGP treatment and the 16-hour LPS stimulation, suggesting that the impacts of the stimuli may simply be additive. During immune priming, the initial stimulus activates macrophages and prevents their immune status from returning to baseline before a secondary challenge. As a result, the response to a second challenge is often additive or synergistic with the initial stimulus (Foster *et al.*, 2007). Given that the induction of trained immunity is characterized by long-lasting epigenetic changes, which typically cannot occur within such a short time period, this model may be more aligned with the concept of priming rather than trained immunity (Divangahi *et al.*, 2021).

Intraperitoneal injection of 500  $\mu$ g BG did not induce a state of trained immunity in mice, as evidenced by cytokine production and immune cell recruitment following LPS-induced sepsis. Several factors could have influenced these results. The mice used were six months old, while most *in vivo* vaccinations are conducted on younger mice, suggesting age-related differences in the ability to acquire a trained state (Kalafati *et al.*, 2020; Moorlag *et al.*, 2020). Additionally, the reproducibility of *in vivo* experiments can be significantly impacted by the microbiome, with variations in gut microbiota potentially leading to differing results and contributing to poor reproducibility in rodent models (Beura *et al.*, 2016; Rosshart *et al.*, 2019). Specifically, research has shown that the gut microbiome can influence BCG-induced trained immunity, with certain microbes altering immune responses and potentially affecting the efficacy of immune training (Stražar *et al.*, 2021).



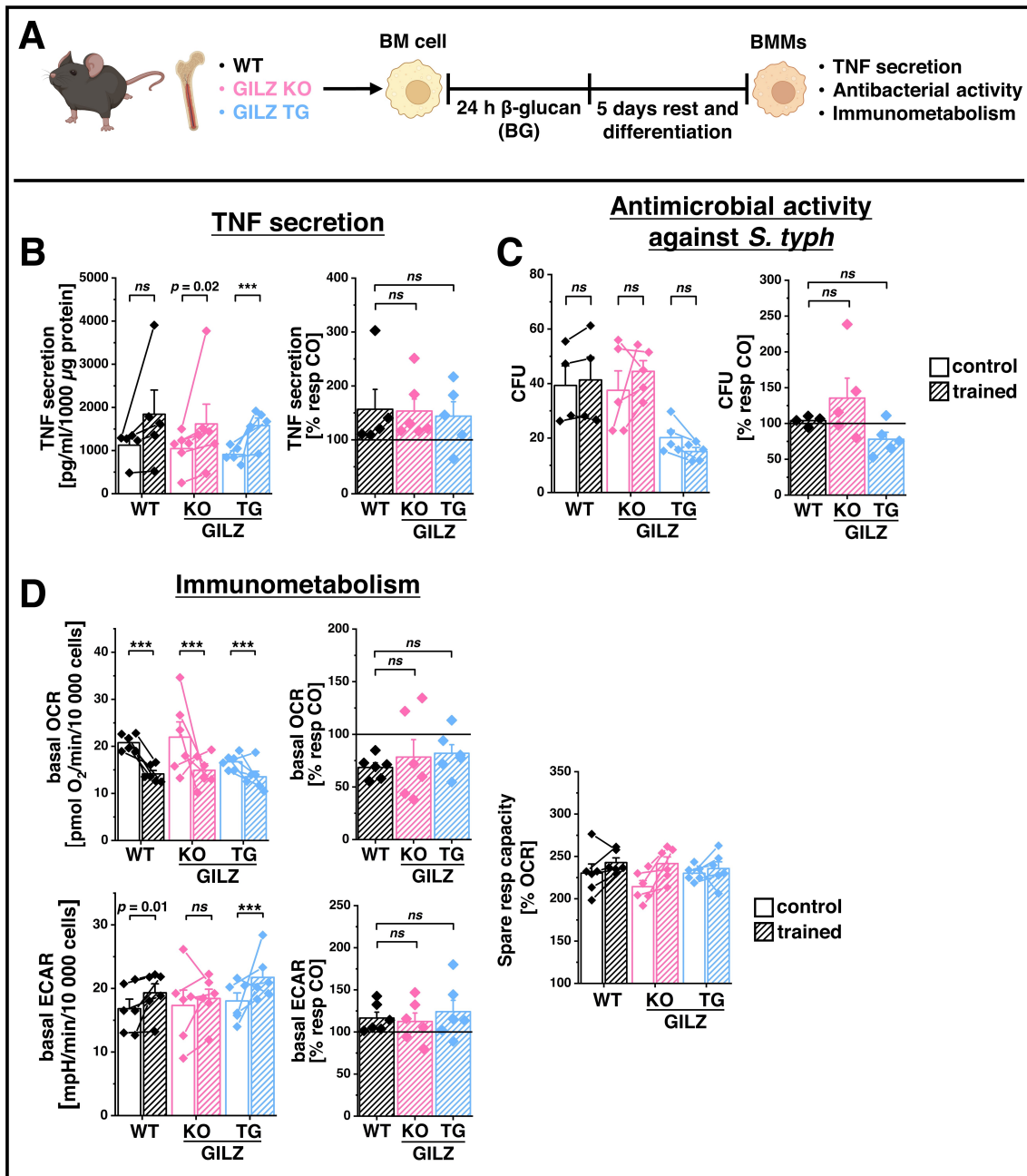


**Figure 14: Training macrophage progenitor cells**

(A) Experimental protocol. (B) TNF secretion of WT, GILZ KO, and GILZ TG BMMs treated with 10 ng/ml LPS (24 h) measured by ELISA normalized to cell protein content, relative to respective control cells from the same preparation (n = 5-6 BMM preparations per group). (C) Colony-forming units (CFU) after 6 h infection with *S. typhimurium*, relative to respective control cells from the same preparation (n = 5-6 BMM preparations per group). (D) Basal oxygen consumption rate (OCR), extracellular acidification rate (ECAR), and spare respiratory capacity of trained BMMs were measured with the Seahorse XFe96 Analyzer (n = 5-6 BMM preparations per group). Each dot represents one independent biological replicate (mean  $\pm$  SEM), and connected dots represent paired samples indicating the respective untreated control. *p* values were generated from one-way ANOVA comparison between groups, followed by Bonferroni *post-hoc* tests. \*\*\* *p* < 0.0001

### 3.3.2 Structural Diversity of $\beta$ -glucans and their Influence on TRIM

Dectin-1, a C-type lectin receptor, is recognized as the primary receptor for  $\beta$ -glucans, initiating antifungal responses in innate immune cells (Kalia *et al.*, 2021). This receptor can bind various ligands, both microbial and endogenous, leading to versatile Syk- and/or Raf-1-dependent signaling pathways involved in numerous processes (Mata-Martinez *et al.*, 2022). The primary ligands for Dectin-1 are  $\beta$ -1,3-glucans with  $\beta$ -1,6 branching. Key properties such as molecular size, polymer length, branching, and solubility significantly influence Dectin-1 activation. For instance, the characterization of WGP has demonstrated strong activation of Dectin-1 due to their

large particle size and insolubility (Kankkunen *et al.*, 2010). These WGs, extracted from the cell wall of *Saccharomyces cerevisiae*, predominantly consist of long  $\beta$ -1,3-glucose polymers and are identified as Dectin-1 receptor agonists according to the manufacturer.

Dectin-1's pivotal role in initiating trained innate immune memory has renewed interest in this receptor. Upon ligand recognition, the AKT/mTOR/HIF1 $\alpha$  pathway is activated, driving the necessary metabolic shift towards a glycolytic phenotype essential for trained immunity (Cheng *et al.*, 2014). The gold standard in the field of trained immunity research is the highly purified and thoroughly characterized (1 $\rightarrow$ 3,1 $\rightarrow$ 6)- $\beta$ -glucan isolated from *Candida albicans* SC5314 yeast cell walls, provided by the Williams lab at East Tennessee State University. However, we did not use this specific preparation in our study. Recent findings indicate that different Dectin-1 ligands can induce distinct signaling pathways, resulting in varied training phenotypes (Cheng *et al.*, 2024). In our studies, bone marrow and *in vivo* training were conducted using a single batch of commercially available  $\beta$ -glucan preparation (termed 'from baker's yeast'), as utilized by the Divangahi lab, to ensure consistency.

It is important to note that  $\beta$ -glucan training can be reversed when concurrently treated with TLR ligands, due to the activation of NF- $\kappa$ B and AP-1 transcription factors (Cheng *et al.*, 2024). Commercially available  $\beta$ -glucan products are chemically and structurally diverse, containing not only  $\beta$ -glucan but also mannoproteins, lipids, proteins, chitins, and other macromolecules in varying proportions (Goodridge *et al.*, 2011; Ikeda *et al.*, 2008). These impurities can bind TLRs in addition to Dectin-1, possibly explaining the high variability in the extent of macrophage training, particularly in TNF secretion.

The  $\beta$ -glucans used in our study, being commercially sourced, might have contributed to the variability in training we observed. Using the same batch of  $\beta$ -glucan preparation for all experiments helped maintain consistency, but the presence of impurities could explain why in some preparations the training phenotype was more pronounced than in others. In line with the literature, macrophages approximately doubled their TNF secretion in response to LPS stimulation when trained with  $\beta$ -glucans (Cheng *et al.*, 2024; Ding *et al.*, 2023; Domínguez-Andrés *et al.*, 2021). This observation supports the notion that the  $\beta$ -glucan used in our study, despite their variability, effectively induced trained immunity in BMMs.

### 3.3.3 Sex-specific Differences in TRIM

Sex differences, influenced by genes, hormones, and early environmental exposures, undoubtedly affect the incidence of autoimmune diseases, malignancies, infectious disease susceptibility, and vaccine responses (Klein & Flanagan, 2016). Sex-biased immune responses are clearly evidenced by diverse X chromosome-linked mechanisms (Forsyth *et al.*, 2024). Moreover, sex hormones, such as estrogen, progesterone, and testosterone, directly influence immune cell function and inflammatory capacity, driving epigenetic changes that contribute to sexual dimorphism, particularly during hormonal shifts like puberty, pregnancy, menopause, and hormone therapy (Shepherd *et al.*, 2020).

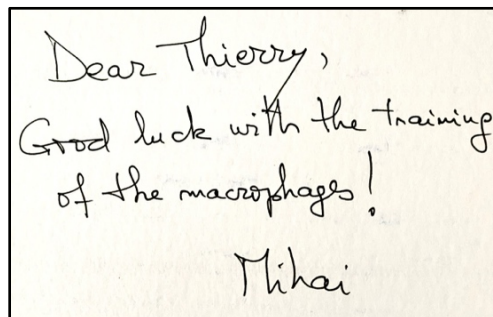
On the other hand, the ImmGen report revealed through RNA and ATAC sequence profiling of immune cells in male and female mice that there were very few differentially expressed genes between male and female immune cells, except in certain tissue-specific macrophage populations (Gal-Oz *et al.*, 2019). Bister *et al.* analyzed endometrial and peripheral blood immune cells from monozygotic twins, revealing that while genetics predominantly shaped peripheral blood immune cells, environmental factors, particularly hormonal contraception, had a stronger influence on the variation observed in endometrial immune cells and soluble proteome, highlighting tissue-specific nonheritable effects on immune system variability (Bister *et al.*, 2024).

Aside from its intended protection against tuberculosis, BCG has been shown to reduce neonatal mortality by decreasing the incidence of sepsis and respiratory infections in several epidemiological studies and randomized trials (Aaby *et al.*, 2011; Biering-Sørensen, Aaby, *et al.*, 2017). In light of the substantial influence of sex differences on immune responses, it is noteworthy that the impact of BCG vaccination varies by sex, with girls experiencing delayed but more sustained benefits compared to boys, particularly in terms of reducing mortality and respiratory infections (Biering-Sørensen, Jensen, *et al.*, 2017; Roth *et al.*, 2006; Stensballe *et al.*, 2005). Similar sex-specific trends have been observed with other live attenuated vaccines such as measles and smallpox, whereas non-live vaccines like diphtheria-tetanus-pertussis and hepatitis B have shown more adverse effects in girls (Aaby *et al.*, 2012; Aaby *et al.*, 2006).

Current research suggests that the induction of trained immunity may be the primary mechanism underlying the broad beneficial effects of BCG, possibly explaining the observed sex-specific responses (Arts *et al.*, 2018; Moorlag *et al.*, 2024). While the production of proinflammatory cytokines after direct stimulation was inhibited, the induction of trained immunity *in vitro* by BCG in human monocytes is not altered by the addition of the important sex hormones estradiol and dihydrotestosterone, nor did they induce training or tolerance in monocytes themselves (de Bree *et al.*, 2018).

Culturing BMMs from both male and female mice in sex-matched serum showed that  $\beta$ -glucan training was less effective in female BMMs cultured with female serum compared to male BMMs cultured with male serum (Earhart *et al.*, 2023). Notably, female BMMs did not exhibit enhanced responses when cultured with male serum instead of female serum. In contrast, male cells trained with female serum secreted significantly fewer inflammatory markers upon restimulation than those trained with male serum. Additionally, Earhart *et al.* found no differences in immune training when using tissue culture media supplemented with FBS, which contains pooled serum from

both sexes or charcoal-stripped FBS, which reduces steroid-based compounds (Cao *et al.*, 2009). BMPCs in our experiments were isolated from male mice only and culture media was supplemented with FBS. These findings suggest that sex-specific differences in serum composition may influence the effectiveness of  $\beta$ -glucan training in macrophages. Given that GILZ expression is modulated by sex hormones - being downregulated by estradiol - it is pertinent to investigate whether using sex-specific media affects the training of macrophages *in vitro* (Whirlledge & Cidlowski, 2013). Moreover, glucocorticoid receptor (GR) expression on circulating leukocytes differs between healthy males and females, with lower leukocyte GR levels in females (Lu *et al.*, 2017). Research has demonstrated a higher hepatic GILZ response in females compared to males due to sex differences in the pharmacokinetic and pharmacodynamic mechanisms controlling GILZ expression by corticosteroids *in vivo* (Ayyar *et al.*, 2019). Additionally, sex-specific cellular heterogeneity in the heart has been highlighted, with GILZ being the most sexually dimorphic macrophage gene (Michel *et al.*, 2022). These studies collectively suggest that GILZ expression is influenced by sex-specific factors and hormonal regulation. Therefore, future studies should consider the impact of sex-specific hormones on GILZ expression and its role in trained immunity. Conducting *in vitro* experiments with sex-specific media and *in vivo* studies could reveal unknown sex-specific differences in the role of GILZ in trained immunity.



Dear Thierry,  
Good luck with the training  
of the macrophages!  
Mihai

**Figure 15:** Inspirational autograph from Prof. Mihai Netea, the leading authority in trained immunity research, written in my lab book at the Keystone Symposium 2022 on Innate Immune Memory in Banff, Canada.

## Chapter 4 Materials and Methods

### 4.1.1 Materials

RPMI-1640 cell culture media (#R0833), 200 mM L-glutamine (#G7513), 1% penicillin/streptomycin (#P4333), Accutase (#A6964), mitomycin C (#10107409001), antimycin A from *Streptomyces* sp. (#A8674), gentamicin (#G1397), dihydroethidium (DHE) (#37291), eplerenone (#E6657), mifepristone (#475838), and gelatin type A (#G1890) were from Sigma-Aldrich. FBS (#P040-37500) and Panexin BMM Serum Substitute (#P04-951SA2) were obtained from PAN Biotech. Ultrapure lipopolysaccharide (LPS) from *E. coli* K12 (#tlrl-pek1ps), nigericin (#tlrl-nig), and ATP (#tlrl-atpl) were purchased from Invivogen. TE buffer (#A0386.1000), and DMSO (#A3672-0250) were from AppliChem, M-CSF (#130-101-705), and premium grade, recombinant mouse interleukin 4 (IL-4) from *E. coli* (#130-097-760) from Miltenyi Biotech, and mouse recombinant interferon gamma (IFN- $\gamma$ , #87389.100) from Biomol. Dexamethasone came as a pharmaceutical-grade injection solution designated for human use (PZN 02740534). Primers for qRT-PCR were purchased from Eurofins Genomics. Other chemicals were obtained from either Sigma-Aldrich or Carl Roth unless stated otherwise.

### 4.1.2 Mice

Animal housing and all experimental procedures were approved by the local animal welfare committee (AZ 2.4.1.1). C57BL/6J mice were housed in individually ventilated cages in a temperature and humidity-controlled room (22-24°C, 45-65 relative humidity) and a 12 h light/dark cycle. Water and food were provided *ad libitum*. Mice were age and sex-matched within experimental sets. B6.129P2-Lyz2<sup>tm1(cre)lfo</sup>/J mice with Cre recombinase expression under the endogenous *Lyz2* promoter of the myeloid cell lineage were considered WT. Crossing these animals with mice bearing loxP sites up and downstream of *Gilz* exon 6 resulted in a myeloid-specific knockout of GILZ (B6.129P2-Tsc22d3<sup>flf</sup> Lyz2<sup>tm1(cre)lfo</sup>/J, GILZ KO). Both strains were described previously (Hoppstädter *et al.*, 2015). In addition, mice bearing a *Tsc22d3/Gilz-1* cDNA knock-in under the control of the ROSA26 promoter preceded by a loxP-flanked stop cassette (Carceller *et al.*, 2016) were crossed with B6.129P2-Lyz2<sup>tm1(cre)lfo</sup>/J mice, resulting in myeloid-specific GILZ overexpression. These animals (BL6Tsc22d3<sup>Rosa26EGFPtg</sup>Lyz2<sup>tm1(cre)lfo</sup>/J) are designated as GILZ overexpressing or transgenic (GILZ TG).

### 4.1.3 Cell Culture Conditions

Cells were cultured in a humidified incubator at 37°C and 5% CO<sub>2</sub> in RPMI-1640 cell culture media supplemented with 10% FBS, 1% 200 mM L-glutamine, and 100 units/ml penicillin/streptomycin (P/S) unless stated otherwise. High salt conditions were achieved by adding sterile, certified endotoxin-free NaCl solution (Sigma Aldrich, #S5150) to cell culture media to increase the NaCl concentration by 40 mM for indicated incubation times.

### 4.1.4 Mouse Genotyping

Genotypes of the GILZ TG mice were tested up until the F2 generation of two homozygous LysM (+/+) RosaGILZ (+/+) breeding pairs. DNA for genotyping reactions was obtained by proteinase K (Roche, #03115836001) digestion in Taq buffer (Genscript, #E00007) of ear biopsies or hairs (1 h, 55 °C).

Table 1 Primers used for mice genotyping.

Name	Primer sequence (5'→3')	Explanation
oIMR3066	CCCAGAAATGCCAGATTACG	oIMR3066 and oIMR3067 detect LysMCre (750bp). oIMR3067 and oIMR3068 detect WT Cre (350bp) at 64 °C annealing temperature.
oIMR3067	CTTGGGCTGCCAGAATTTCTC	
oIMR3068	TTACAGTCGGCCAGGCTGAC	
RosaGILZ_1	AAAGTCGCTCTGAGTTGTTAT	RosaGILZ_1 and RosaGILZ_2 detect Rosa26GILZ (300bp). RosaGILZ_2 and RosaGILZ_3 detect WT GILZ (600bp).
RosaGILZ_2	GCGAAGAGTTTGTCTAACC	
RosaGILZ_3	GGAGCGGGAGAAATGGATATG	

The presence of LysM-Cre in the offspring DNA was tested by PCR with Kapa2G Fast HS Genotyping Mix (Kapa Biosystems, #KM5606) with the primers depicted in Table 1. The PCR reaction comprised 3 min at 95°C, 40 cycles of 15 s at 95°C, 15 s at the primer-specific annealing temperature, and 20 s at 72°C, followed by 2 min at 72°C. The primer-specific annealing temperature for oIMR3067 and oIMR3068 is 64°C, and for oIMR3066 and oIMR3067 is 62°C.

The presence of the *Tsc22d3/Gilz-1* cDNA knock-in under the control of the ROSA26 promoter was tested by qRT-PCR with HOT FIREPol EvaGreen qPCR Mix Plus (no ROX) (Solis Biodyne, #082500020) and the primers listed in Table 1. The PCR protocol comprised 15 min at 95°C, 40 cycles of 30 s at 95°C, 30 s at the primer-specific annealing temperature, and 30 s at 72°C. The primer-specific annealing temperature for RosaGILZ\_1 and RosaGILZ\_2 is 56°C, and for RosaGILZ\_1 and RosaGILZ\_3 is 64°C. For all genotyping reactions, specific PCR products were detected by melting curve analysis and agarose gel electrophoresis against a negative and positive control.

#### 4.1.5 Generation of BMMs

Bone marrow-derived macrophages (BMMs) were obtained from 10- to 23-week-old WT, GILZ KO, and GILZ TG mice as described previously (Hoppstädter *et al.*, 2016). Mice were sacrificed, and femurs and tibias were removed. The bone marrow (BM) was flushed out with cell culture medium using a 27G cannula and passed through a 100  $\mu$ m cell strainer before erythrocyte lysis in hypotonic buffer (155 mM NH<sub>4</sub>Cl, 10 mM KHCO<sub>3</sub>, 1 mM Na<sub>2</sub>EDTA) at 37°C for 3 min. Cells were either resuspended in FBS with 10% DMSO for cryopreservation or in cell culture medium supplemented with M-CSF (50 ng/ml) for differentiation to BMMs (BMM medium). Cryopreserved cells were cooled to -80°C using the MrFrosty™ device (Thermo Scientific, #5100-0001) and transferred into liquid nitrogen for long-term storage. Bone marrow cells were incubated overnight in 30 ml of BMM medium in a T75 flask. On the next day, non-adherent cells were transferred to a fresh cell culture flask and incubated for 5 more days in 45 ml of BMM medium in a T175 flask. Subsequently, cells were washed once with PBS, detached with Accutase, and counted using the LUNA-FL™ Automated Fluorescence Cell Counter (Logos Biosystems) with Acridine Orange/Propidium Iodide staining according to the manufacturer's protocol. The viable cell count was used to calculate seeding densities. All cell preparations had a viability of at least 95%. BMMs were seeded and treated in BMM medium according to the specified conditions for each assay. While *Gilz* was absent in GILZ KO BMMs, its expression in GILZ TG BMMs exceeded the endogenous expression by about 10-fold (Figure 3).

#### 4.1.6 RNA Sequencing (RNA-Seq)

For transcriptome analysis of BMMs from WT, GILZ KO, and GILZ TG mice, next-generation sequencing (NGS) was performed as described previously (Hoppstädter *et al.*, 2021). 500,000 BMMs (1 ml/well) were seeded in a 12-well plate and treated for 4 h with LPS (100 ng/ml) on the next day. RNA was isolated using the High Pure RNA Isolation Kit (Roche, #11828665001) according to the manufacturer's protocol and stored at -80°C. All RNA samples used for further analysis had an RNA integrity number > 9 according to the analysis in a 2100 Bioanalyzer (Agilent) using the RNA 6000 Nano Kit (Agilent, #5067-1513). Libraries were prepared from 500 ng RNA. Poly(A) enrichment was performed on the input total RNA using the NEBNext Poly(A) mRNA Magnetic Isolation Module (New England Biolabs, #E7490) according to the manufacturer's instructions. The cDNA library preparation was conducted with the NEBNext Ultra Directional RNA Library Prep Kit for Illumina (New England Biolabs, #E7420) by Hanna S. Schymik as recommended by the supplier. In brief, first- and second-strand cDNA synthesis was performed, followed by adapter ligation and PCR amplification of the final library (12 cycles). PCR cleanup was performed using Agencourt AM-Pure XP beads (Beckmann Coulter, #A63881). Libraries were sequenced for 1x 75 nt on a NextSeq500 (Illumina) sequencer by Dr. Gilles Gasparoni.

#### 4.1.7 RNA-Seq Data Processing and Analysis

Raw reads were demultiplexed and subjected to quality control through FastQC v0.11.2. Read processing was performed with grape-nf pipeline (v1.1.3) using Nextflow (v20.10.0) and mapped to GRC38mm10 assembly. The counts obtained after alignment were used to analyze differential expression using DESeq2 v1.40.2. Principle component analysis was performed using the CPM values of all annotated protein-coding genes. All analyses were conducted in the R programming language. DESeq2 analysis revealed differentially expressed genes (DEGs,  $p < 0.05$ ) in the comparisons of GILZ KO vs. WT, GILZ TG vs. WT, and GILZ KO vs. GILZ TG under both untreated and LPS-treated conditions. Subsequently, TPM values of the DEGs from all three contrasts were subjected to k-Means unsupervised clustering using iDEP 1.12, independently for untreated and LPS-treated cells (Ge *et al.*, 2018). All data processing and analyses, except for the unsupervised clustering, were performed by Dr. Gilles Gasparoni. Processed and raw data were deposited in the Gene Expression Omnibus (GEO) database under the accession code GSE254137.

#### 4.1.8 RNA isolation, Reverse Transcription, and qRT-PCR

Cells were stored at -80°C after the indicated treatment until RNA was isolated using the High Pure RNA Isolation Kit (Roche, #11828665001) or the Direct-Zol RNA Miniprep Kit (ZymoResearch, #R2052) according to the manufacturer's protocol. Reverse transcription was performed using the High-Capacity cDNA Kit (Thermo Scientific, #4368813) according to the manufacturer's protocol using 300-500 ng of RNA per reaction. RT products were diluted in TE buffer (AppliChem, #A0386.1000).

Table 2 Primers used for qRT-PCR.

Gene	Transcript RefSeq (NCBI)	Forward sequence (5'→3')	Reverse sequence (5'→3')
<i>Arg1</i>	NM_007482.3	ACAAGACAGGGCTCCTTTTCAG	GGCTTATGGTTACCCTCCCG
<i>Arg2</i>	NM_009705.3	ATCCCCCTCCCTGCCAATCAT	CTAGCTTCTTCTGTCCCCGA
<i>Gilz</i>	NM_010286.4	GCTGCTTGAGAAGAACTCCCA	GAACTTTTCCAGTTGCTCGGG
<i>Il10</i>	NM_010548.2	GCCCAGAAATCAAGGAGCAT	GAAATCGATGACAGCGCCT
<i>Mrc1</i>	NM_008625.2	TTCAGCTATTGGACGCGAGG	GAATCTGACACCCAGCGGAA
<i>Nfat5</i>	NM_133957.3	AGCTGGAAATGGAACATTGGA	CGCACAACATAGGGCTCTTCT
<i>Nlrp3</i>	NM_145827.3	AGCCTTCCAGGATCCTCTTC	CTTGGGCAGCAGTTTCTTTC
<i>Nos2</i>	NM_010927.3	CTTCTGGACATTACGACCC	TACTCTGAGGGCTGACACAA
<i>Ppia</i>	NM_008907.1	GCGTCTCCTTCGAGCTGTTT	CACCTTGGCACATGAATCCT
<i>Sgk1</i>	NM_001161850.2	CGGTGGACTGGTGGTGTCTT	GTCGTACATCTCAGCCGTGTTT
<i>Slc6a12</i>	NM_001381904.1	AGAAGCTTTACCTCGCCTGTGATG	CGTGGATGCCCGATGTAATAC
<i>Tnf</i>	NM_008361.3	CCATTCTGAGTTCTGCAAAGG	AGGTAGGAAGGCCTGAGATCTTATC
<i>Vegfa</i>	NM_001287058.1	CCACCATGCCAAGTGGTCCC	ACCAGGGTCTCAATCGGACG
<i>Ym1</i>	NM_009892.4	AAAGCCAGCAGAAGCTCTCCA	GAAGAATTGCCAGACCTGTGAC

The qRT-PCR reactions were prepared in technical duplicates or triplicates using HOT FIREPol EvaGreen qPCR Mix Plus (no ROX) (Solis Biodyne, #082500020) according to the manufacturer's protocol as described previously (Hoppstädter *et al.*, 2021; Valbuena-Perez *et al.*, 2020) except that half of the recommended volumes were used. The qRT-PCR reactions were performed in a CFX96 Real-time PCR Detection system (Bio-Rad) using the primers listed in Table 2. The qRT-PCR protocol comprised 15 min at 95°C and 40 cycles of 15 s at 95°C, 20 s at 60°C, and 20 s at 72°C. Quantification was achieved by calculating starting quantities using a standard dilution of a pGEM<sup>®</sup>-T Easy Vector plasmid (Promega, #A137A) containing the PCR product or by the  $2^{-\Delta\Delta Cq}$  method normalized to *Ppia*.

#### 4.1.9 pHrodo™ Phagocytosis Assay

50,000 BMMs (150 µl/well) were seeded into a 96-well plate and incubated overnight. pHrodo™ Red *S. aureus* Bioparticles™ (Thermo Scientific, #A10010) were suspended in PBS and treated in an ultrasonic water bath for 15 min at 37°C before adding 5 µl of a 1 µg/µl dilution to each well. Real-time imaging was started immediately in the Incucyte<sup>®</sup> S3 Live-Cell Analysis System (Essen BioScience) in the brightfield and red fluorescence channel (10x objective lens, 400 ms acquisition time). The phagocytic capacity was calculated as the total red object integrated intensity (RCU × µm<sup>2</sup>/Image) normalized to cell confluency [%] at the start of the assay as described previously (Linnenberger *et al.*, 2021).

#### 4.1.10 Salmonella enterica and Escherichia coli Infection Assay

*Salmonella enterica* subsp. *enterica* serotype *Typhimurium* (NCTC<sup>®</sup> 12023) (Helaine *et al.*, 2010) and *Escherichia coli* TOP10 (Invitrogen™) were cultured overnight in LB at 37°C in an orbital shaker. Bacteria were washed once in PBS and resuspended in BMM media without P/S supplementation to infect BMMs at a multiplicity of infection (MOI) of 20 with *S. typhimurium* and an MOI of 100 with *E. coli*. Bacterial cell count was determined by OD<sub>600</sub> measurement assuming that an OD<sub>600</sub> of 1 equates to 10<sup>9</sup> colony-forming units (CFU) in the overnight bacterial culture. BMMs were seeded the day before infection in a 24-well plate (250,000 cells/well, 0.5 ml). Infection was synchronized by centrifuging for 5 min at 300 × g and maintained for 30 min. After the infection, BMMs were washed twice with PBS and cultured in cell culture media containing 100 µg/ml gentamicin for 90 min to kill extracellular bacteria, after which the gentamicin concentration was reduced to 10 µg/ml. BMMs were lysed in 200 µl Triton-X 100 (1% in water) after a total incubation time of 3 h for *E. coli* and the indicated time for *S. typhimurium* specific to the assay. Lysis was stopped by adding 800 µl LB media. The bacterial load of the infected BMMs was determined by serially diluting the lysates 1:10 in PBS (200 µl) and plating them out on LB (100 µl per agar plate) as described previously (Hoppstädter *et al.*, 2019). Plates were incubated for 24 h at 37°C and CFUs were counted using ImageJ (Version 1.53k) (Schneider *et al.*, 2012).

#### 4.1.11 Griess Assay

NO production was assessed by Griess assay as previously described (Linnenberger *et al.*, 2021). 250,000 BMMs (0.5 ml/well) were seeded in 24-well plates or 50,000 BMMs (150 µl/well) in 96-well plates the day before. On the next day, cells were treated as described before 100 µl of supernatant was incubated for 10 min at room temperature with 90 µl 1% sulfanilamide in 5% phosphoric acid, then 90 µl 1% N-1-naphthylethylenediamine dihydrochloride (NED) was added and incubated for 5 min until absorbance was measured at λ = 560 nm in a GloMax<sup>®</sup> Discover Microplate Reader (Promega). Absolute concentrations were determined by measuring a NaNO<sub>2</sub> standard curve in parallel for each assay. Data were normalized to protein contents measured by the Pierce™ BCA Protein Assay Kit according to the manufacturer's protocol (Thermo Scientific, #23227).

#### 4.1.12 Real-time Caspase-3/7 Activity and Cytotoxicity Detection

50,000 BMMs (150  $\mu$ l/well) were seeded in 96-well plates and incubated overnight. To induce pyroptosis, cells were treated for 4 h with LPS (100 ng/ml) and subsequently with ATP (2 mM). Culture media was supplemented with 4  $\mu$ M CellEvent™ Caspase-3/7 Green Detection Reagent (Invitrogen, #C10723) and 0.25  $\mu$ M Incucyte® Cytotox Red Reagent (Essen BioScience, #4632) as described previously (Dahlem *et al.*, 2020). Real-time imaging was started immediately after LPS treatment using the Incucyte® S3 Live-Cell Analysis System (Essen BioScience) in brightfield, red, and green fluorescence channels (10x objective lens, 300 ms acquisition time for the green channel and 400 ms for the red channel). Total red and green object integrated intensities in red or green calibrated units (GCU or RCU x  $\mu$ m<sup>2</sup>/Image) was normalized to the initial cell confluency [%] in each well. Background fluorescence at the beginning of the assay was uniformly set to 0 for all wells. Spectral unmixing was set to 1.5% removal of red signal from green as recommended by the manufacturer.

#### 4.1.13 ELISA

500,000 BMMs (1 ml/well) were seeded in 12-well plates or 75,000 BMMs (150  $\mu$ l/well) in 96-well plates and incubated overnight. Cells were treated as indicated before supernatants were stored at -80°C. TNF and IL-1 $\beta$  secretion was measured by ELISA (BioLegend #430904, and #432604 respectively) according to the manufacturer's protocol. Supernatants were diluted 1:25 in ELISA assay diluent. Data were normalized to protein contents measured by the Pierce™ BCA Protein Assay Kit according to the manufacturer's protocol (Thermo Scientific, #23227) if indicated.

#### 4.1.14 Detection of Reactive Oxygen Species (ROS)

50,000 BMMs (150  $\mu$ l/well) were seeded in 96-well plates and incubated overnight. Cells were treated for 4 h with LPS (100 ng/ml). Then, culture medium was exchanged to medium containing ATP (2 mM) and 10  $\mu$ M dihydroethidium (DHE). Real-time imaging was started immediately in the Incucyte® S3 Live-Cell Analysis System (Essen BioScience) in the brightfield and red fluorescence channels (10x objective lens, 400 ms acquisition time) upon ATP treatment. Total ROS production was determined as the total red object integrated intensity in red calibrated units (RCU x  $\mu$ m<sup>2</sup>/Image) after 30 min normalized to cell confluency [%] at the start of the assay. For the detection of mitochondrial ROS production, cells were incubated with 5  $\mu$ M red MitoSOX™ mitochondrial superoxide indicator (Invitrogen, #M36008) in PBS with 2% FCS. ATP (2 mM) or antimycin A (AA, 10  $\mu$ M) were added as indicated.

#### 4.1.15 Agilent Seahorse Cell Mito Stress and Glycolysis Stress Test

50,000 BMMs (150  $\mu$ l/well) were seeded in Seahorse 96-well cell culture plates (Agilent, #103793-100) the day before the assay. The Mito Stress test (Agilent, #103015-100) and Glycolysis Stress Test (Agilent, #103020-100) were performed according to the recommendations in the manufacturer's protocol in a Seahorse XFe96 Analyzer (Agilent). OCR and ECAR measurements were normalized to cell count as determined in a Cytation 1 Cell Imaging Reader (BioTek) from brightfield images taken after the assay using the Gen5 software (Version 3.14) as described previously (Dahlem *et al.*, 2020).

#### 4.1.16 Quantification of Mitochondrial DNA Copy Number

Mitochondrial DNA (mtDNA) copy number was determined based on a protocol by (Quiros *et al.*, 2017). Briefly, DNA was extracted from 250,000 BMMs cultured in 0.5 ml of BMM media per well (12-well plate) using the DNA Mini Prep Plus kit (ZymoResearch, #D4069) as per the manufacturer's instructions. Subsequently, qRT-PCR was employed to measure the gene expressions of *mt16S*, *mtND1*, and *Hk2*, utilizing primer sequences adapted from the referenced publication. The mitochondrial DNA (mtDNA) copy number was calculated as the ratio between mtDNA content (mean expression of *mt16S* and *mtND1*) and nuclear DNA (nDNA) represented by *Hk2* expression.

#### 4.1.17 Flow Cytometry

10<sup>6</sup> BMMs (2 ml/well) were seeded in 6-well plates. On the next day, cells were detached by gently scraping the wells with a cell scraper (TPP®), resuspended in 2% FCS-containing PBS, stained for 45 min at 37°C with 0.1  $\mu$ M MitoTracker Green FM and Deep Red FM (Invitrogen, #M22426 and #M7514 respectively), and washed with 2% FCS-containing PBS. Flow cytometry measurements were performed using an LSRFortessa™ (BD Biosciences) operated by FACS Diva 8.0.1 (BD Biosciences). In each measurement, at least 50,000 events were recorded. MFI of unstained control cells was subtracted from corresponding stained cells, and background-subtracted MFI values for WT cells were set as 100%. The pseudocolor plots were generated utilizing FlowJo 10.10.0 software.

#### 4.1.18 BMM-Conditioned Media

BMM-conditioned media for migration and proliferation assays were generated by incubating 10<sup>6</sup> BMMs in a 6-well format with 3 ml per well of BMM medium for 24 h starting at the time of seeding. To assess matrix metalloproteinase (MMP) activity, 75,000 BMMs were incubated in a 96-well format with 150  $\mu$ l of BMM media containing Panexin BMM serum substitute instead of FBS for 24 h, starting at the time of seeding.

#### 4.1.19 Cell Migration and Proliferation Assays

Cell migration and proliferation capacity were measured using the Incucyte<sup>®</sup> S3 Live-Cell Analysis System (Essen BioScience) as described previously (Chanda *et al.*, 2024; Dahlem *et al.*, 2020).

To assess migration capacity, L929 cells (ATCC: CCL-1<sup>TM</sup>) were seeded (50,000 cells per well in 100  $\mu$ l medium) in 96-well ImageLock<sup>TM</sup> plates (Essen BioScience, #BA-04856) and grown to full confluency overnight. Cells were cultured as described above. On the next day, cells were treated for 2 h with 5  $\mu$ g/ml mitomycin C and washed with PBS before every well was scratched uniformly using the WoundMaker<sup>TM</sup> (Essen BioScience). Detached cells were removed by washing with PBS before BMM-conditioned medium was added to the cells (100  $\mu$ l/well). Plates were immediately placed into the Incucyte<sup>®</sup> S3 Live-Cell Analysis System (Essen BioScience) and imaged for relative wound closure [%] at indicated time points.

To assess proliferation capacity, L929 cells were seeded (5,000 cells/well, 100  $\mu$ l) and incubated overnight. On the next day, the medium was replaced by BMM-conditioned medium (100  $\mu$ l/well). Cell confluency was measured over time in the Incucyte<sup>®</sup> S3 Live-Cell Analysis System (Essen BioScience) and normalized to starting confluency in each well.

#### 4.1.20 Gelatin Zymography

Matrix metalloproteinase (MMP) activity was measured as previously described (Toth & Fridman, 2001). In brief, 100  $\mu$ l of the BMM-conditioned media supernatants were mixed with 4x loading buffer (250 mM Tris pH = 6.8, 40% glycerol, 8% SDS, and 0.01% bromophenol blue in water) and incubated for 15 minutes at room temperature. Then, 45  $\mu$ l of the resulting sample were loaded onto a 10-well 1.0 mm 10% SDS-acrylamide gel containing 1 mg/ml gelatin, and electrophoresis was performed. Gels were washed extensively in Triton-X 100 (2.5% in water) to remove SDS and after a 72-hour incubation at 37°C in a buffer conducive to enzyme activity (50 mM Tris, 5 mM CaCl<sub>2</sub> and 0.02% Brij-35 in water), the gel was stained with Coomassie solution (40% methanol, 10% acetic acid, and 0.01% Coomassie R250 in water) for 90 minutes. After brief incubation in a destaining solution (20% acetic acid, and 10% methanol in water), specific MMP activities, indicating gelatin degradation as clear bands on a dark background, were assessed based on their molecular weights. Conditioned media from each individual biological replicate were measured in technical duplicates. Gels were scanned with an Odyssey<sup>®</sup> CLx Infrared Imaging System (LI-COR Biosciences) and inverted to enhance visibility, presenting bands in black against a white background. Signals were quantified using the Odyssey<sup>®</sup> Image Studio software (Version 5.2).

#### 4.1.21 L929-conditioned Media

The murine fibroblast cell line L929 (ATCC: CCL-1) was cultured for 7 days in a 175 cm<sup>2</sup> flask containing 5.5x10<sup>6</sup> cells (on day 0) in 50 ml of complete BMM media. The conditioned media was filtered through a bottle-top sterile filter (0.2  $\mu$ m pore size) and stored at -80°C.

#### 4.1.22 Western Blot

BMMs (2 ml/well) were seeded in 6-well plates at a density of 10<sup>6</sup> cells per well. After treatment, cells were lysed in 200  $\mu$ l of lysis buffer (1 M Tris, pH 6.8, 2.5 ml; 10% SDS, 5 ml; glycerol, 5 ml; water, 28 ml;  $\beta$ -mercaptoethanol, 2.5 ml; a few crystals of bromophenol blue) supplemented with cOmplete Protease Inhibitor Cocktail (Roche, #04693124001), and stored at -80°C. The lysates were sonicated with 5 impulses using a Sonifier 250 (Branson) with a duty cycle of 20 and output control of 2 on ice, followed by heating at 95°C for 5 minutes. For SDS-PAGE, 50  $\mu$ l of lysate was loaded per lane on a standard 10-well, 1.5 mm polyacrylamide gel, initially run for 5 minutes, after which an additional 50  $\mu$ l per lane was added. The gel was a 5-10% gradient gel using Rotiphorese<sup>®</sup> Gel 30 with a crosslink-ratio of 37.5:1 (Carl Roth, #3029). Electrophoresis was conducted for a total of 90 minutes (30 minutes at 100 V and 60 minutes at 120 V). The running buffer consisted of Tris (3.0 g), glycine (14.4 g), 10% SDS solution (10 ml), and water to 1000 ml.

Protein transfer onto a 0.2  $\mu$ m PVDF membrane (Amersham Hybond LFP Western Blotting Membrane, GE Healthcare, #10600022) was performed over 17 hours at 4°C with an ice pack in the chamber, using a current of 80 mA. All materials, including the membrane, were soaked in methanol and equilibrated in transfer buffer, which contained glycine (14.4 g), Tris (3.0 g), methanol (200 ml), and water to 1000 ml. Blocking was conducted for 2 hours in Blocking Buffer (Rockland, #MB-070). The membrane was cut at the 35 kDa marker band to stain the lower part with anti-GILZ antibody and the upper part with anti- $\alpha$ -tubulin antibody.

Primary antibodies (GILZ at 1:1000, tubulin at 1:2000) were prepared in RBB buffer and incubated in a 4-well plate (3 ml/well) for 22-24 hours at 4°C. The primary antibodies used were GILZ monoclonal antibody (clone CFMKG15) (eBioscience, #14-4033-82) and monoclonal anti- $\alpha$ -tubulin antibody produced in mouse clone DM1A, ascites fluid (Sigma-Aldrich, #T9026).

Secondary antibody incubation was performed after four 5-minute washes with TBST. The secondary antibodies were IRDye<sup>®</sup> 800CW goat anti-mouse IgG (LI-COR, #926-32210) for tubulin and IRDye<sup>®</sup> 800CW goat anti-rabbit IgG (LI-COR, #926-32211) for GILZ, used at a 1:10000 dilution (in 3 ml RBB in a 4-well plate). Incubation with secondary antibodies was performed for 120 minutes at room temperature, followed by two 5-minute washes in TBST and two 5-minute washes in TBS. Gels were scanned using the Odyssey<sup>®</sup> CLx Infrared Imaging System (LI-COR Biosciences). The gel after protein transfer was stained with Coomassie for 1.5 hours and destained overnight to verify the transfer.



For HRP detection, Goat anti-rat IgG (H+L) Secondary Antibody, HRP (Thermo Scientific, #31470) was used at 0.4 µg/ml in RBB for 1 hour at room temperature. After three washes with TBST and three washes with TBS, Clarity™ Western ECL Substrate (Bio-Rad, #1705060) was added, and chemiluminescence was immediately scanned under auto exposure settings using the ChemiDoc™ MP Imaging System (Bio-Rad).

#### 4.1.23 *In vitro* BMM β-glucan Training

Fully differentiated BMMs were trained by treatment with dispersible whole glucan particles WGP (Invivogen, #ttrl-wgp) at the indicated concentrations and incubation times.

BM cells were trained by treatment with 5 µg/ml β-glucan from baker's yeast (Sigma Aldrich, #G5011) for 24 h. The powder was stored at 4°C as recommended by the manufacturer. It was resuspended for each experiment in PBS at a concentration of 1 mg/ml and homogenized by passing it through a 0.4 x 20 mm Sterican® cannula (Braun, PZN 02050864) until the solution appeared milky white without agglomerates visible by the eye.

BM cells were harvested from the tibias and femurs of WT, GILZ KO and GILZ TG mice as described above. Cells were passed through a 0.8 x 40 mm Sterican® cannula (Braun, PZN 02050806) and passed through a 100 µm pore size cell strainer (Greiner, #542000) to remove cell clumps, and resuspended in BMM media containing 30% L929-conditioned media as the source for M-CSF. Cells of one individual mouse were then split into 43% for control and 57% for β-glucan-treated cells to account for small cell toxicity. Training consisted of 24 h treatment of the freshly isolated bone marrow cells with 5 µg/ml β-glucan in 30 ml of 30% L929-conditioned BMM media in a T175 flask. Subsequently, the adherent and non-adherent cells were washed twice with PBS and further differentiated in 45 ml of 30% L929-conditioned BMM media in a T175 flask for additional 5 days. Cells were then seeded for assays as described above in 30% L929-conditioned BMM media.

#### 4.1.24 *In vivo* Induction of Trained Innate Immunity

All experiments involving animals were approved by the McGill University Animal Care Committee in accordance with the guidelines set out by the Canadian Council on Animal Care. Six-month-old male C57Bl6/J WT mice were injected intraperitoneally with 100 µl of 5 mg/ml β-glucan from baker's yeast (Sigma Aldrich, #G5011), resulting in 500 µg per mouse, or with PBS as a control using TB syringes (BD, #309626). Seven days later, mice were injected intraperitoneally with 100 µl of 1 mg/ml LPS (Sigma Aldrich, #L2654), resulting in 100 µg per mouse, or PBS as a control using TB syringes (BD, #309626). After 4 hours, 1 ml of blood and the lungs of each mouse were harvested.

Lungs were perfused with PBS and digested in 2 ml of cell culture media containing 150 U of Collagenase IV (Sigma-Aldrich, #C5138) for 60 minutes at 37°C. Two ml of ACK lysis buffer (Gibco, #A10492-01) was then added to each preparation and incubated for 2 minutes at room temperature before lysis was stopped by the addition of PBS. Cells were centrifuged and resuspended in 1 ml of cell culture media, then counted with a hemocytometer using 1:40 Trypan Blue (Gibco, #15250061).

Cell culture media consisted of RPMI 1640 (Gibco, #11875-093) supplemented with 10% FBS (Wisent, #080150), 2 mM L-glutamine (Gibco, #25030-081), 1 mM sodium pyruvate (Gibco, #11360-070), 100 U/ml penicillin and 100 mg/ml streptomycin (Anti-Anti, Gibco, #15240-062), 2% HEPES (Gibco, #15630-080), 1% MEM non-essential amino acids (Gibco, #11140-050), 1% MEM essential amino acids (Gibco, #11130-051), and 70 mM sodium hydroxide.

Four million cells were stained for flow cytometry. Cells were stained in 100 µl of Fixable Viability Dye eFluor™ 506 (1:1000 in PBS, eBioscience™, #65-0866-18) for 30 minutes at 4°C. After washing in FACS buffer (BD Pharmingen™, #554656), cells were stained in 50 µl of antibody mix (1:100 in FACS buffer) for 30 minutes at 4°C. The antibodies used were CD3-FITC (BD Pharmingen™, #553061, clone 145-2C11), CD19-BUV395 (BD Horizon™, #563557, clone 1D3), Ly6G-PerCP-eFluor™ 710 (eBioscience™, #46-9668-82, clone 1A8-Ly6G), F4/80-APC-eFluor™ 780 (eBioscience™, #47-4801-80, clone BM8), CD45.2-BUV737 (BD Horizon™, #612779, clone 104), CD11b-BV605 (BD Horizon™, #563015, clone M1/70), Siglec-F-BV786 (BD OptiBuild™, #740956, clone E50-2440), Ly-6C-APC-Cy™7 (BD Pharmingen™, #560596, clone AL-21), and Fc block (eBioscience™, #14-0161-82). Cells were washed in FACS buffer, resuspended in 100 µl of 1% PFA, and stored at 4°C until measurement.

Flow cytometry was performed using an LSR Fortessa X-20 (BD Biosciences) with BD FACSDiva (version 8.0.1) in FACSFlow™ Sheath Fluid (BD Biosciences, #342003). Measurements were conducted in polystyrene round-bottom tubes with cell-strainer caps (Corning, #352235). At least 500,000 events were measured per staining. The threshold was set to 5,000 events/sec. Each staining was verified using its respective FMO control. Compensation was performed using 20 µl of UltraComp eBeads™ compensation beads (Invitrogen, #01-2222-42) and 1.5 µl of antibodies in sheath buffer. Data analysis was conducted using FlowJo (version 10.10).

Blood was harvested by cardiac puncture and collected in BD Microtainer® SST™ tubes (BD, #365967) for cytokine analysis in the serum. TNF and IL-6 levels were measured by ELISA using mouse TNF and IL-6 DuoSet ELISA kits (R&D Systems, #DY410-05 and #DY406-05, respectively) according to the manufacturer's protocol in Nunc MaxiSorp™ clear flat-bottom 96-well plates (Invitrogen, #44-2404-21). The wash buffer was 0.05% Tween® 20 in PBS, reagent diluent was 1% Bovine Serum Albumin Fraction V (Roche, #10735094001) in PBS, substrate solution was a 1:1 mixture of Peroxidase Substrate (TMB) (Thermo Scientific, #1854050) and Peroxide

Solution (Thermo Scientific, #1854060), and stop solution was 2N sulfuric acid. Serum samples were diluted 1:1 in reagent diluent for analysis.

#### 4.1.25 RAW-Blue™ Reporter Cells

NF- $\kappa$ B activation was measured using the mouse macrophage reporter cell line RAW-Blue™ (Invivogen, #raw-sp). According to the manufacturer, the cells stably express a secreted embryonic alkaline phosphatase (SEAP) gene inducible by NF- $\kappa$ B and AP-1 transcription factors, making NF- $\kappa$ B and AP-1 activation detectable using QUANTI-Blue™, a SEAP detection medium. 100,000 RAW-Blue™ cells (200  $\mu$ l/well) were seeded in 96-well plates according to the manufacturer's protocol and treated as indicated for 24 h. Subsequently, 20  $\mu$ l of the supernatant was incubated with 180  $\mu$ l QUANTI-Blue™ detection medium for 2.5 h at 37°C and absorbance was measured at  $\lambda = 600$  nm in a GloMax® Discover Microplate Reader (Promega).

#### 4.1.26 Data Representation and Statistics

Visualization, advanced analysis, and all statistical tests were performed in Origin Lab 2018b and in GraphPad Prism (Version 10.1). Data are presented as means  $\pm$  standard error of the mean (bars). Each dot within the bar graphs represents one independent cell preparation from one biological replicate or mice. The mean of two groups was tested for statistical significance using the Mann-Whitney *U*-test. Statistical significance across all genotypes (mean of 3 groups) was assessed through one-way ANOVA (for single time point comparisons) and two-way ANOVA (for multiple time points) both followed by Bonferroni *post-hoc* tests.

## Publications

ORCID iD: <https://orcid.org/0009-0009-0859-7773>

1. Hoppstädter J, Valbuena-Perez JV, Linnenberger R, Dahlem C, **Legroux TM**, Hecksteden A, Tse WKF, Flamini S, Andreas A, Herrmann J, Herr C, Müller R, Meyer T, Bals R, Riccardi C, Bruscoli S, Kiemer AK. *Glucocorticoid Induced Leucine Zipper (GILZ) Mediates Statin-Induced Muscle Damage*. FASEB Journal, 2020, [doi:10.1096/fj.201902557RRR](https://doi.org/10.1096/fj.201902557RRR)
2. Wiesenthal AA, **Legroux TM**, Richter C, Junker BH, Hecksteden A, Kessler SM, Hoppstädter J, Kiemer AK. *Endotoxin Tolerance Acquisition and Altered Hepatic Fatty Acid Profile in Aged Mice*. Biology, 2023, [doi:10.3390/biology12040530](https://doi.org/10.3390/biology12040530)
3. **Legroux TM**, Schymik HS, Gasparoni G, Libert C, Mohammadi S, Walter J, Diesel B, Hoppstädter J, Kiemer AK. *Immunomodulation by Glucocorticoid-Induced Leucine Zipper in Macrophages: Enhanced Phagocytosis, Protection from Pyroptosis, and Altered Mitochondrial Function*. Frontiers in Immunology, 2024, [doi:10.3389/fimmu.2024.1396827](https://doi.org/10.3389/fimmu.2024.1396827)
4. Mashayekhi V, Schomisch A, Rasheed S, Aparicio-Puerta E, Risch T, Yildiz D, Koch M, Both S, Ludwig N, **Legroux TM**, Keller A, Müller R, Fuhrmann G, Hoppstädter J, Kiemer AK. *The RNA Binding Protein IGF2BP2/IMP2 Alters the Cargo of Cancer Cell-derived Extracellular Vesicles Supporting Tumor-associated Macrophages*. Cell Communication & Signaling, 2024, [doi:10.1186/s12964-024-01701-y](https://doi.org/10.1186/s12964-024-01701-y)

## Curriculum Vitae

**Not included in the published version.**

## Acknowledgements

In this chapter of my life called PhD studies, I am deeply grateful to the many individuals who have contributed to my journey.

First and foremost, I extend my heartfelt thanks to Prof. Alexandra K. Kiemer for providing me with the opportunity to take my first steps in academic research. Your guidance has not only shaped me as a scientist but also as a person. Five years ago, your encouragement to submit my scholarship application changed the course of my life, something for which I will always be grateful.

I also want to sincerely thank Jessica and Britta for their unwavering support and invaluable guidance.

A special mention to Prof. Andriy Luzhetskyy, who, as scientific advisor, not only provided academic insights but also fostered a friendly bond that I deeply value.

I would also like to extend my gratitude to the *Studienstiftung des deutschen Volkes* for their financial and ideational support during my PhD in various seminar vacations and my stay in Canada. Their support has been invaluable.

I cherish the many amazing memories and camaraderie shared with Arefeh, Alex, Ali, Amanda, Anna, Annika, Astrid, Beate, Charlotte, Daria, Erwan, Eva, Eugene, Gilles, Hanna, Iris, Jan, Kim, Kinza, Kira, Kostya, Lisa, Marlon, Matti, Maz, Miriam, Muriel, Natja, Rebecca, Renata, Renaud, Richard, Salma, Saeed, Mr. Schneider, Shilpee, Simon, Tarek, Theo, Vanessa, Vida, and Dr. Zapp. You all have made my PhD journey immensely pleasant and memorable. Thank you for being a significant part of it.

Sorry for not going into too much detail; some stories are best kept private! 😊

Lastly, I am deeply grateful for the unconditional love and unwavering trust of my friends, family, and my partner, Denise.

## References (categorized)

### General References and GILZ

- Ayrolidi, E., & Riccardi, C. (2009). Glucocorticoid-Induced Leucine Zipper (GILZ): A New Important Mediator of Glucocorticoid Action. *FASEB Journal*, 23(11), 3649-3658. <https://doi.org/10.1096/fj.09-134684>
- Ayyar, V. S., DuBois, D. C., Almon, R. R., & Jusko, W. J. (2019). Modeling Corticosteroid Pharmacokinetics and Pharmacodynamics, Part III: Estrous Cycle and Estrogen Receptor-Dependent Antagonism of Glucocorticoid-Induced Leucine Zipper (GILZ) Enhancement by Corticosteroids. *Journal of Pharmacology and Experimental Therapeutics*, 370(2), 337-349. <https://doi.org/10.1124/jpet.119.257543>
- Bruscoli, S., Donato, V., Velardi, E., Di Sante, M., Migliorati, G., Donato, R., & Riccardi, C. (2010). Glucocorticoid-Induced Leucine Zipper (GILZ) and Long GILZ Inhibit Myogenic Differentiation and Mediate Anti-Myogenic Effects of Glucocorticoids. *Journal of Biological Chemistry*, 285(14), 10385-10396. <https://doi.org/10.1074/jbc.M109.070136>
- Bruscoli, S., Riccardi, C., & Ronchetti, S. (2022). GILZ as a Regulator of Cell Fate and Inflammation. *Cells*, 11(1), 122. <https://doi.org/10.3390/cells11010122>
- Cappetta, D., De Angelis, A., Flamini, S., Cozzolino, A., Bereshchenko, O., Ronchetti, S., Cianflone, E., Gagliardi, A., Ricci, E., Rafaniello, C., Rossi, F., Riccardi, C., Berrino, L., Bruscoli, S., & Urbanek, K. (2021). Deficit of Glucocorticoid-Induced Leucine Zipper Amplifies Angiotensin-Induced Cardiomyocyte Hypertrophy and Diastolic Dysfunction. *Journal of Cellular and Molecular Medicine*, 25(1), 217-228. <https://doi.org/10.1111/jcmm.15913>
- Carceller, E., Ballegeer, M., Deckers, J., Riccardi, C., Bruscoli, S., Hochepped, T., Libert, C., & Perez, P. (2016). Overexpression of Glucocorticoid-Induced Leucine Zipper (GILZ) Increases Susceptibility to Imiquimod-Induced Psoriasis and Involves Cutaneous Activation of TGF- $\beta$ 1. *Scientific Reports*, 6, 38825. <https://doi.org/10.1038/srep38825>
- Chanda, S., Lepikhov, K., Dahlem, C., Schymik, H. S., Hoppstädter, J., Geber, A.-K., Wagner, K., Kessler, S. M., Empting, M., & Kiemer, A. K. (2024). Gene Editing and Small Molecule Inhibitors of the RNA Binding Protein IGF2BP2/IMP2 Show Its Potential as an Anti-Cancer Drug Target. *Frontiers in Bioscience-Landmark*, 29(1), 41. <https://doi.org/10.31083/j.fbl2901041>
- Cohen, N., Mouly, E., Hamdi, H., Maillot, M. C., Pallardy, M., Godot, V., Capel, F., Balian, A., Naveau, S., Galanaud, P., Lemoine, F. M., & Emilie, D. (2006). GILZ Expression in Human Dendritic Cells Redirects Their Maturation and Prevents Antigen-Specific T Lymphocyte Response. *Blood*, 107(5), 2037-2044. <https://doi.org/10.1182/blood-2005-07-2760>
- Dahlem, C., Siow, W. X., Lopatniuk, M., Tse, W. K. F., Kessler, S. M., Kirsch, S. H., Hoppstädter, J., Vollmar, A. M., Muller, R., Luzhetskyy, A., Bartel, K., & Kiemer, A. K. (2020). Thiogolgamide a, a New Anti-Proliferative Anti-Tumor Agent, Modulates Macrophage Polarization and Metabolism. *Cancers (Basel)*, 12(5), 1288. <https://doi.org/10.3390/cancers12051288>
- Ellouze, M., Vigouroux, L., Tcherakian, C., Woerther, P. L., Guguin, A., Robert, O., Surenaud, M., Tran, T., Calmette, J., Barbin, T., Perlemuter, G., Cassard, A. M., Launay, P., Maxime, V., Annane, D., Levy, Y., & Godot, V. (2020). Overexpression of GILZ in Macrophages Limits Systemic Inflammation While Increasing Bacterial Clearance in Sepsis in Mice. *European Journal of Immunology*, 50(4), 589-602. <https://doi.org/10.1002/eji.201948278>
- Foster, S. L., Hargreaves, D. C., & Medzhitov, R. (2007). Gene-Specific Control of Inflammation by TLR-Induced Chromatin Modifications. *Nature*, 447(7147), 972-978. <https://doi.org/10.1038/nature05836>
- Ge, S. X., Son, E. W., & Yao, R. (2018). iDEP: An Integrated Web Application for Differential Expression and Pathway Analysis of RNA-Seq Data. *BMC Bioinformatics*, 19(1), 534. <https://doi.org/10.1186/s12859-018-2486-6>
- Hamdi, H., Godot, V., Maillot, M., Prejean, M. V., Cohen, N., Krzysiek, R., Lemoine, F. M., Zou, W., & Emilie, D. (2007). Induction of Antigen-Specific Regulatory T Lymphocytes by Human Dendritic Cells Expressing the Glucocorticoid-Induced Leucine Zipper. *Blood*, 110(1), 211-219. <https://doi.org/10.1182/blood-2006-10-052506>
- Helaine, S., Thompson, J. A., Watson, K. G., Liu, M., Boyle, C., & Holden, D. W. (2010). Dynamics of Intracellular Bacterial Replication at the Single Cell Level. *Proceedings of the National Academy of Sciences*, 107(8), 3746-3751. <https://doi.org/10.1073/pnas.1000041107>
- Hoppstädter, J., Dembek, A., Höring, M., Schymik, H. S., Dahlem, C., Sultan, A., Wirth, N., Al-Fityan, S., Diesel, B., Gasparoni, G., Walter, J., Helms, V., Huwer, H., Simon, M., Liebisch, G., Schulz, M. H., & Kiemer, A. K. (2021). Dysregulation of Cholesterol Homeostasis in Human Lung Cancer Tissue and Tumour-Associated Macrophages. *EBioMedicine*, 72, 103578. <https://doi.org/10.1016/j.ebiom.2021.103578>
- Hoppstädter, J., Diesel, B., Linnenberger, R., Hachenthal, N., Flamini, S., Minet, M., Leidinger, P., Backes, C., Grasser, F., Meese, E., Bruscoli, S., Riccardi, C., Huwer, H., & Kiemer, A. K. (2019). Amplified Host Defense by Toll-Like Receptor-Mediated Downregulation of the Glucocorticoid-Induced Leucine Zipper (GILZ) in Macrophages. *Front Immunol*, 9, 3111. <https://doi.org/10.3389/fimmu.2018.03111>

- Hoppstädter, J., Hachenthal, N., Valbuena-Perez, J. V., Lampe, S., Astanina, K., Kunze, M. M., Bruscoli, S., Riccardi, C., Schmid, T., Diesel, B., & Kiemer, A. K. (2016). Induction of Glucocorticoid-Induced Leucine Zipper (GILZ) Contributes to Anti-Inflammatory Effects of the Natural Product Curcumin in Macrophages. *Journal of Biological Chemistry*, 291(44), 22949-22960. <https://doi.org/10.1074/jbc.M116.733253>
- Hoppstädter, J., Kessler, S. M., Bruscoli, S., Huwer, H., Riccardi, C., & Kiemer, A. K. (2015). Glucocorticoid-Induced Leucine Zipper: A Critical Factor in Macrophage Endotoxin Tolerance. *Journal of Immunology*, 194(12), 6057-6067. <https://doi.org/10.4049/jimmunol.1403207>
- Legroux, T. M., Schymik, H. S., Gasparoni, G., Mohammadi, S., Walter, J., Libert, C., Diesel, B., Hoppstädter, J., & Kiemer, A. K. (2024). Immunomodulation by Glucocorticoid-Induced Leucine Zipper in Macrophages: Enhanced Phagocytosis, Protection from Pyroptosis, and Altered Mitochondrial Function. *Frontiers in Immunology*, 15, 1396827. <https://doi.org/10.3389/fimmu.2024.1396827>
- Linnenberger, R., Hoppstädter, J., Wrublewsky, S., Ampofo, E., & Kiemer, A. K. (2021). Statins and Bempedoic Acid: Different Actions of Cholesterol Inhibitors on Macrophage Activation. *International Journal of Molecular Sciences*, 22(22), 12480. <https://doi.org/10.3390/ijms222212480>
- Lu, K. D., Radom - Aizik, S., Haddad, F., Zaldivar, F., & Kraft, M. (2017). Glucocorticoid Receptor Expression on Circulating Leukocytes Differs between Healthy Male and Female Adults. *Journal of Clinical and Translational Science*, 1(2), 108-114. <https://doi.org/10.1017/cts.2016.20>
- Malaise, O., Relic, B., Charlier, E., Zeddou, M., Neuville, S., Deroyer, C., Gillet, P., Louis, E., Malaise, M. G., & de Seny, D. (2016). Glucocorticoid-Induced Leucine Zipper (GILZ) Is Involved in Glucocorticoid-Induced and Mineralocorticoid-Induced Leptin Production by Osteoarthritis Synovial Fibroblasts. *Arthritis Research & Therapy*, 18(1), 219. <https://doi.org/10.1186/s13075-016-1119-6>
- Medzhitov, R., Schneider, D., & Soares, M. P. (2012). Disease Tolerance as a Defense Strategy. *Science*, 335(6071), 936-941. <https://doi.org/10.1126/science.1214935>
- Michel, N. A., Ljubojević-Holzer, S., Bugger, H., & Zirlik, A. (2022). Cellular Heterogeneity of the Heart. *Frontiers in Cardiovascular Medicine*, 9, 868466. <https://doi.org/10.3389/fcvm.2022.868466>
- Mozaffari, M. S. (2020). Role of GILZ in the Kidney and the Cardiovascular System: Relevance to Cardiorenal Complications of Covid-19. *Journal of Pharmacology and Experimental Therapeutics*, 375(3), 398-405. <https://doi.org/10.1124/jpet.120.000243>
- Ortega - Gómez, A., Perretti, M., & Soehnlein, O. (2013). Resolution of Inflammation: An Integrated View. *EMBO Molecular Medicine*, 5(5), 661-674. <https://doi.org/https://doi.org/10.1002/emmm.201202382>
- Quiros, P. M., Goyal, A., Jha, P., & Auwerx, J. (2017). Analysis of mtDNA/nDNA Ratio in Mice. *Current Protocols in Mouse Biology*, 7(1), 47-54. <https://doi.org/10.1002/cpmo.21>
- Rashmi, P., Colussi, G., Ng, M., Wu, X., Kidwai, A., & Pearce, D. (2017). Glucocorticoid-Induced Leucine Zipper Protein Regulates Sodium and Potassium Balance in the Distal Nephron. *Kidney International*, 91(5), 1159-1177. <https://doi.org/10.1016/j.kint.2016.10.038>
- Schneider, C. A., Rasband, W. S., & Eliceiri, K. W. (2012). NIH Image to ImageJ: 25 Years of Image Analysis. *Nature Methods*, 9(7), 671-675. <https://doi.org/10.1038/nmeth.2089>
- Shi, X. M., Shi, W., Li, Q., Song, B., Wan, M., Bai, S., & Cao, X. (2003). A Glucocorticoid - Induced Leucine - Zipper Protein, GILZ, Inhibits Adipogenesis of Mesenchymal Cells. *Embo Reports*, 4(4), 374-380. <https://doi.org/10.1038/sj.embor.embor805>
- Soundararajan, R., Wang, J., Melters, D. P., & Pearce, D. (2010). Glucocorticoid-Induced Leucine Zipper 1 Stimulates the Epithelial Sodium Channel by Regulating Serum- and Glucocorticoid-Induced Kinase 1 Stability and Subcellular Localization. *Journal of Biological Chemistry*, 285(51), 39905-39913. <https://doi.org/10.1074/jbc.m110.161133>
- Souza, J. A. M., Carvalho, A. F. S., Grossi, L. C., Zaidan, I., de Oliveira, L. C., Vago, J. P., Cardoso, C., Machado, M. G., Souza, G. V. S., Queiroz-Junior, C. M., Morand, E. F., Bruscoli, S., Riccardi, C., Teixeira, M. M., Tavares, L. P., & Sousa, L. P. (2022). Glucocorticoid-Induced Leucine Zipper Alleviates Lung Inflammation and Enhances Bacterial Clearance During Pneumococcal Pneumonia. *Cells*, 11(3), 532. <https://doi.org/10.3390/cells11030532>
- Toth, M., & Fridman, R. (2001). Assessment of Gelatinases (MMP-2 and MMP-9) by Gelatin Zymography. *Methods Mol Med*, 57, 163-174. <https://doi.org/10.1385/1-59259-136-1:163>
- Vago, J. P., Galvão, I., Negreiros-Lima, G. L., Teixeira, L. C. R., Lima, K. M., Sugimoto, M. A., Moreira, I. Z., Jones, S. A., Lang, T., Riccardi, C., Teixeira, M. M., Harris, J., Morand, E. F., & Sousa, L. P. (2020). Glucocorticoid-Induced Leucine Zipper Modulates Macrophage Polarization and Apoptotic Cell Clearance. *Pharmacological Research*, 158, 104842. <https://doi.org/10.1016/j.phrs.2020.104842>
- Valbuena-Perez, J. V., Linnenberger, R., Dembek, A., Bruscoli, S., Riccardi, C., Schulz, M. H., Meyer, M. R., Kiemer, A. K., & Hoppstädter, J. (2020). Altered Glucocorticoid Metabolism Represents a Feature of Macroph-Aging. *Aging Cell*, 19(6), e13156. <https://doi.org/https://doi.org/10.1111/acer.13156>
- Venanzi, A., Di Sante, M., Bruscoli, S., Biagioli, M., Sorcini, D., Cimino, M., Frammartino, T., Bereshchenko, O., Franconi, F., & Riccardi, C. (2014). Recombinant Long-Glucocorticoid-Induced Leucine Zipper (L-

- GILZ) Protein Restores the Control of Proliferation in Gilz KO Spermatogonia. *European Journal of Pharmaceutical Sciences*, 63, 22-28. <https://doi.org/10.1016/j.ejps.2014.06.013>
- Whirlledge, S., & Cidlowski, J. A. (2013). Estradiol Antagonism of Glucocorticoid-Induced GILZ Expression in Human Uterine Epithelial Cells and Murine Uterus. *Endocrinology*, 154(1), 499-510. <https://doi.org/10.1210/en.2012-1748>
- High Salt-induced Inflammation**
- Belden, Z., Deuliis, J. A., Dobre, M., & Rajagopalan, S. (2017). The Role of the Mineralocorticoid Receptor in Inflammation: Focus on Kidney and Vasculature. *American Journal of Nephrology*, 46(4), 298-314. <https://doi.org/10.1159/000480652>
- Berry, M. R., Mathews, R. J., Ferdinand, J. R., Jing, C., Loudon, K. W., Wlodek, E., Dennison, T. W., Kuper, C., Neuhofer, W., & Clatworthy, M. R. (2017). Renal Sodium Gradient Orchestrates a Dynamic Antibacterial Defense Zone. *Cell*, 170(5), 860-874 e819. <https://doi.org/10.1016/j.cell.2017.07.022>
- Binger, K. J., Gebhardt, M., Heinig, M., Rintisch, C., Schroeder, A., Neuhofer, W., Hilgers, K., Manzel, A., Schwartz, C., Kleinewietfeld, M., Voelkl, J., Schatz, V., Linker, R. A., Lang, F., Voehringer, D., Wright, M. D., Hubner, N., Dechend, R., Jantsch, J., . . . Müller, D. N. (2015). High Salt Reduces the Activation of IL-4- and IL-13-Stimulated Macrophages. *Journal of Clinical Investigation*, 125(11), 4223-4238. <https://doi.org/10.1172/jci80919>
- Ellison, D. H., & Welling, P. (2021). Insights into Salt Handling and Blood Pressure. *The New England Journal of Medicine*, 385(21), 1981-1993. <https://doi.org/10.1056/NEJMra2030212>
- Fraccarollo, D., Thomas, S., Scholz, C. J., Hilfiker-Kleiner, D., Galuppo, P., & Bauersachs, J. (2019). Macrophage Mineralocorticoid Receptor Is a Pleiotropic Modulator of Myocardial Infarct Healing. *Hypertension*, 73(1), 102-111. <https://doi.org/10.1161/HYPERTENSIONAHA.118.12162>
- Furman, D., Campisi, J., Verdin, E., Carrera-Bastos, P., Targ, S., Franceschi, C., Ferrucci, L., Gilroy, D. W., Fasano, A., Miller, G. W., Miller, A. H., Mantovani, A., Weyand, C. M., Barzilai, N., Goronzy, J. J., Rando, T. A., Effros, R. B., Lucia, A., Kleinstreuer, N., & Slavich, G. M. (2019). Chronic Inflammation in the Etiology of Disease across the Life Span. *Nature Medicine*, 25, 1822-1832. <https://doi.org/10.1038/s41591-019-0675-0>
- Geisberger, S., Bartolomeus, H., Neubert, P., Willebrand, R., Zasada, C., Bartolomeus, T., McParland, V., Swinnen, D., Geuzens, A., Maifeld, A., Krampert, L., Vogl, M., Mähler, A., Wilck, N., Markó, L., Tilic, E., Forslund, S. K., Binger, K. J., Stegbauer, J., . . . Müller, D. N. (2021). Salt Transiently Inhibits Mitochondrial Energetics in Mononuclear Phagocytes. *Circulation*, 144(2), 144-158. <https://doi.org/10.1161/circulationaha.120.052788>
- Guimarães, G. R., Almeida, P. P., de Oliveira Santos, L., Rodrigues, L. P., de Carvalho, J. L., & Boroni, M. (2021). Hallmarks of Aging in Macrophages: Consequences to Skin Inflammaging. *Cells*, 10(6), 1323. <https://www.mdpi.com/2073-4409/10/6/1323>
- Hamad, I., Cardilli, A., Côrte-Real, B. F., Dyczko, A., Vangronsveld, J., & Kleinewietfeld, M. (2022). High-Salt Diet Induces Depletion of Lactic Acid-Producing Bacteria in Murine Gut. *Nutrients*, 14(6), 1171. <https://www.mdpi.com/2072-6643/14/6/1171>
- Hernansanz-Agustín, P., Choya-Foces, C., Carregal-Romero, S., Ramos, E., Oliva, T., Villa-Piña, T., Moreno, L., Izquierdo-Álvarez, A., Cabrera-García, J. D., Cortés, A., Lechuga-Vieco, A. V., Jadiya, P., Navarro, E., Parada, E., Palomino-Antolín, A., Tello, D., Acín-Pérez, R., Rodríguez-Aguilera, J. C., Navas, P., . . . Martínez-Ruiz, A. (2020). Na(+) Controls Hypoxic Signalling by the Mitochondrial Respiratory Chain. *Nature*, 586(7828), 287-291. <https://doi.org/10.1038/s41586-020-2551-y>
- Huang, L., Trieu, K., Yoshimura, S., Neal, B., Woodward, M., Campbell, N. R. C., Li, Q., Lackland, D. T., Leung, A. A. C., Anderson, C. A. M., MacGregor, G. A., & He, F. J. (2020). Effect of Dose and Duration of Reduction in Dietary Sodium on Blood Pressure Levels: Systematic Review and Meta-Analysis of Randomised Trials. *BMJ*, 368(m315). <https://doi.org/10.1136/bmj.m315>
- Hunter, R. W., Dhaun, N., & Bailey, M. A. (2022). The Impact of Excessive Salt Intake on Human Health. *Nature Reviews Nephrology*, 18(5), 321-335. <https://doi.org/10.1038/s41581-021-00533-0>
- Ip, W. K., & Medzhitov, R. (2015). Macrophages Monitor Tissue Osmolarity and Induce Inflammatory Response through NLRP3 and NLRC4 Inflammasome Activation. *Nature Communications*, 6, 6931. <https://doi.org/10.1038/ncomms7931>
- Jantsch, J., Schatz, V., Friedrich, D., Schröder, A., Kopp, C., Siegert, I., Maronna, A., Wendelborn, D., Linz, P., Binger, Katrina J., Gebhardt, M., Heinig, M., Neubert, P., Fischer, F., Teufel, S., David, J.-P., Neufert, C., Cavallaro, A., Rakova, N., . . . Titze, J. (2015). Cutaneous Na<sup>+</sup> Storage Strengthens the Antimicrobial Barrier Function of the Skin and Boosts Macrophage-Driven Host Defense. *Cell Metabolism*, 21(3), 493-501. <https://doi.org/https://doi.org/10.1016/j.cmet.2015.02.003>
- Jung, S. M., Kim, Y.-K., Kim, J., Jung, H., Yi, H., Rim, Y. A., Park, N., Kwok, S. K., & Park, S. H. (2019). Sodium Chloride Aggravates Arthritis Via Th17 Polarization. *Yonsei Medical Journal*, 60(1), 88. <https://doi.org/10.3349/ymj.2019.60.1.88>



- Kleinewietfeld, M., Manzel, A., Titze, J., Kvakana, H., Yosef, N., Linker, R. A., Müller, D. N., & Hafler, D. A. (2013). Sodium Chloride Drives Autoimmune Disease by the Induction of Pathogenic Th17 Cells. *Nature*, 496(7446), 518-522. <https://doi.org/10.1038/nature11868>
- Kopp, C., Linz, P., Wachsmuth, L., Dahlmann, A., Horbach, T., Schofl, C., Renz, W., Santoro, D., Niendorf, T., Müller, D. N., Neininger, M., Cavallaro, A., Eckardt, K. U., Schmieder, R. E., Luft, F. C., Uder, M., & Titze, J. (2012). <sup>23</sup>Na Magnetic Resonance Imaging of Tissue Sodium. *Hypertension*, 59(1), 167-172. <https://doi.org/10.1161/HYPERTENSIONAHA.111.183517>
- Krampert, L., Ossner, T., Schröder, A., Schatz, V., & Jantsch, J. (2023). Simultaneous Increases in Intracellular Sodium and Tonicity Boost Antimicrobial Activity of Macrophages. *Cells*, 12(24), 2816. <https://doi.org/10.3390/cells12242816>
- Laube, M., Riedel, D., Ackermann, B., Haase, M., & H. Thome, U. (2020). Glucocorticoids Equally Stimulate Epithelial Na<sup>+</sup> Transport in Male and Female Fetal Alveolar Cells. *International Journal of Molecular Sciences*, 21(1), 57. <https://www.mdpi.com/1422-0067/21/1/57>
- Linz, P., Santoro, D., Renz, W., Rieger, J., Ruehle, A., Ruff, J., Deimling, M., Rakova, N., Müller, D. N., Luft, F. C., Titze, J., & Niendorf, T. (2015). Skin Sodium Measured with <sup>23</sup>Na MRI at 7.0 T. *NMR in Biomedicine*, 28(1), 54-62. <https://doi.org/https://doi.org/10.1002/nbm.3224>
- López-Otín, C., Blasco, M. a. A., Partridge, L., Serrano, M., & Kroemer, G. (2013). The Hallmarks of Aging. *Cell*, 153(6), 1194-1217. <https://doi.org/10.1016/j.cell.2013.05.039>
- Machnik, A., Neuhofer, W., Jantsch, J., Dahlmann, A., Tammela, T., Machura, K., Park, J. K., Beck, F. X., Müller, D. N., Derer, W., Goss, J., Ziomber, A., Dietsch, P., Wagner, H., van Rooijen, N., Kurtz, A., Hilgers, K. F., Alitalo, K., Eckardt, K. U., . . . Titze, J. (2009). Macrophages Regulate Salt-Dependent Volume and Blood Pressure by a Vascular Endothelial Growth Factor-C-Dependent Buffering Mechanism. *Nature Medicine*, 15(5), 545-552. <https://doi.org/10.1038/nm.1960>
- McDonald, J., Graves, J., Waldman, A., Lotze, T., Schreiner, T., Belman, A., Greenberg, B., Weinstock - Guttman, B., Aaen, G., Tillema, J. M., Hart, J., Lulu, S., Ness, J., Harris, Y., Rubin, J., Candee, M., Krupp, L., Gorman, M., Benson, L., . . . Waubant, E. (2016). A Case-Control Study of Dietary Salt Intake in Pediatric-Onset Multiple Sclerosis. *Multiple Sclerosis and Related Disorders*, 6, 87-92. <https://doi.org/10.1016/j.msard.2016.02.011>
- Miranda, P. M., De Palma, G., Serkis, V., Lu, J., Louis-Auguste, M. P., McCarville, J. L., Verdu, E. F., Collins, S. M., & Bercik, P. (2018). High Salt Diet Exacerbates Colitis in Mice by Decreasing Lactobacillus Levels and Butyrate Production. *Microbiome*, 6(1), 57. <https://doi.org/10.1186/s40168-018-0433-4>
- Miyauchi, H., Geisberger, S., Luft, F. C., Wilck, N., Stegbauer, J., Wiig, H., Dechend, R., Jantsch, J., Kleinewietfeld, M., Kempa, S., & Müller, D. N. (2024). Sodium as an Important Regulator of Immunometabolism. *Hypertension*, 81(3), 426-435. <https://doi.org/doi:10.1161/HYPERTENSIONAHA.123.19489>
- Mozaffarian, D., Fahimi, S., Singh, G. M., Micha, R., Khatibzadeh, S., Engell, R. E., Lim, S., Danaei, G., Ezzati, M., Powles, J., Global Burden of Diseases, N., & Chronic Diseases Expert, G. (2014). Global Sodium Consumption and Death from Cardiovascular Causes. *The New England Journal of Medicine*, 371(7), 624-634. <https://doi.org/10.1056/NEJMoa1304127>
- Müller, D. N., Wilck, N., Haase, S., Kleinewietfeld, M., & Linker, R. A. (2019). Sodium in the Microenvironment Regulates Immune Responses and Tissue Homeostasis. *Nature Reviews Immunology*, 19(4), 243-254. <https://doi.org/10.1038/s41577-018-0113-4>
- Müller, L., Nasr, A. R., Jux, B., Makdissi, N., Trowbridge, J. W., Schmidt, S. V., Schultze, J. L., Quast, T., Schulte-Schrepping, J., Kolanus, W., & Mass, E. (2024). Differential Impact of High-Salt Levels in Vitro and in Vivo on Macrophage Core Functions. *Molecular Biology Reports*, 51(1), 343. <https://doi.org/10.1007/s11033-024-09295-x>
- Neubert, P., Homann, A., Wendelborn, D., Bär, A. L., Krampert, L., Trum, M., Schröder, A., Ebner, S., Weichselbaum, A., Schatz, V., Linz, P., Veelken, R., Schulte-Schrepping, J., Aschenbrenner, A. C., Quast, T., Kurts, C., Geisberger, S., Kunzelmann, K., Hammer, K., . . . Jantsch, J. (2020). NCX1 Represents an Ionic Na<sup>+</sup> Sensing Mechanism in Macrophages. *PLOS Biology*, 18(6), e3000722. <https://doi.org/10.1371/journal.pbio.3000722>
- Neubert, P., Weichselbaum, A., Reitinger, C., Schatz, V., Schroder, A., Ferdinand, J. R., Simon, M., Bar, A. L., Brochhausen, C., Gerlach, R. G., Tomiuk, S., Hammer, K., Wagner, S., van Zandbergen, G., Binger, K. J., Müller, D. N., Kitada, K., Clatworthy, M. R., Kurts, C., . . . Jantsch, J. (2019). Hif1a and Nfat5 Coordinate Na<sup>(+)</sup>-Boosted Antibacterial Defense Via Enhanced Autophagy and Autolysosomal Targeting. *Autophagy*, 15(11), 1899-1916. <https://doi.org/10.1080/15548627.2019.1596483>
- O'Donnell, M., Mente, A., Rangarajan, S., McQueen, M. J., Wang, X., Liu, L., Yan, H., Lee, S. F., Mony, P., Devanath, A., Rosengren, A., Lopez-Jaramillo, P., Diaz, R., Avezum, A., Lanas, F., Yusuf, K., Iqbal, R., Ilow, R., Mohammadifard, N., . . . Investigators, P. (2014). Urinary Sodium and Potassium Excretion, Mortality, and Cardiovascular Events. *New England Journal of Medicine*, 371(7), 612-623. <https://doi.org/10.1056/NEJMoa1311889>

- Rakova, N., Jüttner, K., Dahlmann, A., Schröder, A., Linz, P., Kopp, C., Rauh, M., Goller, U., Beck, L., Agureev, A., Vassilieva, G., Lenkova, L., Johannes, B., Wabel, P., Moissl, U., Vienken, J., Gerzer, R., Eckardt, K. U., Müller, D. N., . . . Titze, J. (2013). Long-Term Space Flight Simulation Reveals Infradian Rhythmicity in Human Na(+) Balance. *Cell Metabolism*, 17(1), 125-131. <https://doi.org/10.1016/j.cmet.2012.11.013>
- Shapiro, L., & Dinarello, C. A. (1995). Osmotic Regulation of Cytokine Synthesis in Vitro. *Proceedings of the National Academy of Sciences*, 92(26), 12230-12234. <https://doi.org/10.1073/pnas.92.26.12230>
- Sposito, F., Northey, S., Charras, A., McNamara, P. S., & Hedrich, C. M. (2023). Hypertonic Saline Induces Inflammation in Human Macrophages through the NLRP1 Inflammasome. *Genes & Immunity*, 24(5), 263-269. <https://doi.org/10.1038/s41435-023-00218-7>
- Titze, J., Dahlmann, A., Lerchl, K., Kopp, C., Rakova, N., Schröder, A., & Luft, F. C. (2014). Spooky Sodium Balance. *Kidney International*, 85(4), 759-767. <https://doi.org/https://doi.org/10.1038/ki.2013.367>
- Titze, J., Maillet, A., Lang, R., Gunga, H. C., Johannes, B., Gauquelin-Koch, G., Kihm, E., Larina, I., Gharib, C., & Kirsch, K. A. (2002). Long-Term Sodium Balance in Humans in a Terrestrial Space Station Simulation Study. *American Journal of Kidney Diseases*, 40(3), 508-516. <https://doi.org/10.1053/ajkd.2002.34908>
- Wilck, N., Balogh, A., Marko, L., Bartolomaeus, H., & Muller, D. N. (2019). The Role of Sodium in Modulating Immune Cell Function. *Nature Reviews Nephrology*, 15(9), 546-558. <https://doi.org/10.1038/s41581-019-0167-y>
- Wilck, N., Matus, M. G., Kearney, S. M., Olesen, S. W., Forslund, K., Bartolomaeus, H., Haase, S., Mahler, A., Balogh, A., Marko, L., Vvedenskaya, O., Kleiner, F. H., Tsvetkov, D., Klug, L., Costea, P. I., Sunagawa, S., Maier, L., Rakova, N., Schatz, V., . . . Muller, D. N. (2017). Salt-Responsive Gut Commensal Modulates T(H)17 Axis and Disease. *Nature*, 551(7682), 585-589. <https://doi.org/10.1038/nature24628>
- Wu, C., Yosef, N., Thalhamer, T., Zhu, C., Xiao, S., Kishi, Y., Regev, A., & Kuchroo, V. K. (2013). Induction of Pathogenic Th17 Cells by Inducible Salt-Sensing Kinase SGK1. *Nature*, 496(7446), 513-517. <https://doi.org/10.1038/nature11984>
- Zhang, W. C., Zheng, X. J., Du, L. J., Sun, J. Y., Shen, Z. X., Shi, C., Sun, S., Zhang, Z., Chen, X. Q., Qin, M., Liu, X., Tao, J., Jia, L., Fan, H. Y., Zhou, B., Yu, Y., Ying, H., Hui, L., Liu, X., . . . Duan, S. Z. (2015). High Salt Primes a Specific Activation State of Macrophages, M(Na). *Cell Research*, 25(8), 893-910. <https://doi.org/10.1038/cr.2015.87>
- Zhang, X., Zhang, Z., Zhao, Y., Jin, L., Tai, Y., Tang, Y., Geng, S., Zhang, H., Zhai, Y., Yang, Y., Pan, P., He, P., Fang, S., Sun, C., Chen, Y., Zhou, M., Liu, L., Wang, H., Xu, L., . . . Zhang, L. (2024). Sodium Chloride Promotes Macrophage Pyroptosis and Aggravates Rheumatoid Arthritis by Activating SGK1 through Gaba Receptors Slc6a12. *International Journal of Biological Sciences*, 20(8), 2922-2942. <https://doi.org/10.7150/ijbs.93242>
- Trained Innate Immunity**
- Aaby, P., Benn, C. S., Nielsen, J., Lisse, I. M., Rodrigues, A., & Ravn, H. (2012). Testing the Hypothesis That Diphtheria–Tetanus–Pertussis Vaccine Has Negative Non-Specific and Sex-Differential Effects on Child Survival in High-Mortality Countries. *BMJ Open*, 2(3), e000707. <https://doi.org/10.1136/bmjopen-2011-000707>
- Aaby, P., Jensen, H., & Walraven, G. (2006). Age-Specific Changes in the Female–Male Mortality Ratio Related to the Pattern of Vaccinations: An Observational Study from Rural Gambia. *Vaccine*, 24(22), 4701-4708. <https://doi.org/10.1016/j.vaccine.2006.03.038>
- Aaby, P., Roth, A., Ravn, H., Napirna, B. M., Rodrigues, A., Lisse, I. M., Stensballe, L. G., Diness, B. R., Lausch, K. R., Lund, N., Biering-Sørensen, S., Whittle, H., & Benn, C. S. (2011). Randomized Trial of BCG Vaccination at Birth to Low-Birth-Weight Children: Beneficial Nonspecific Effects in the Neonatal Period? *The Journal of Infectious Diseases*, 204(2), 245-252. <https://doi.org/10.1093/infdis/jir240>
- Arts, R. J., Joosten, L. A., & Netea, M. G. (2016). Immunometabolic Circuits in Trained Immunity. *Seminars in Immunology*, 28(5), 425-430. <https://doi.org/https://doi.org/10.1016/j.smim.2016.09.002>
- Arts, R. J., Novakovic, B., Ter Horst, R., Carvalho, A., Bekkering, S., Lachmandas, E., Rodrigues, F., Silvestre, R., Cheng, S. C., Wang, S. Y., Habibi, E., Goncalves, L. G., Mesquita, I., Cunha, C., van Laarhoven, A., van de Veerdonk, F. L., Williams, D. L., van der Meer, J. W., Logie, C., . . . Netea, M. G. (2016). Glutaminolysis and Fumarate Accumulation Integrate Immunometabolic and Epigenetic Programs in Trained Immunity. *Cell Metabolism*, 24(6), 807-819. <https://doi.org/10.1016/j.cmet.2016.10.008>
- Arts, R. J. W., Carvalho, A., Rocca, C. L., Palma, C., Rodrigues, F., Silvestre, R., Kleinnijenhuis, J., Lachmandas, E., Gonçalves, L. G., Belinha, A., Cunha, C., Oosting, M., Joosten, L. A. B., Matarese, G., Crevel, R. v., & Netea, M. G. (2016). Immunometabolic Pathways in BCG-Induced Trained Immunity. *Cell Reports*, 17(10), 2562-2571. <https://doi.org/10.1016/j.celrep.2016.11.011>
- Arts, R. J. W., Moorlag, S. J. C. F. M., Novakovic, B., Li, Y., Wang, S.-Y., Oosting, M., Kumar, V., Xavier, R. J., Wijmenga, C., Joosten, L. A. B., Reusken, C., Benn, C. S., Aaby, P., Koopmans, M., Stunnenberg, H. G., Crevel, R. v., & Netea, M. G. (2018). BCG Vaccination Protects against Experimental Viral Infection in Humans through the Induction of Cytokines Associated with Trained Immunity. *Cell Host & Microbe*, 23(1), 89-100.e105. <https://doi.org/10.1016/j.chom.2017.12.010>

- Bekkering, S., Arts, R. J. W., Novakovic, B., Kourtzelis, I., Heijden, C. D. C. C. v. d., Li, Y., Popa, C., Horst, R. t., Tuijl, J. v., Netea - Maier, R. T., Veerdonk, F. L. v. d., Chavakis, T., Joosten, L. A. B., Meer, J. W. M. v. d., Stunnenberg, H., Riksen, N. P., & Netea, M. G. (2018). Metabolic Induction of Trained Immunity through the Mevalonate Pathway. *Cell*, *172*, 135–146. <https://doi.org/10.1016/j.cell.2017.11.025>
- Bekkering, S., Blok, B. A., Joosten, L. A., Riksen, N. P., van Crevel, R., & Netea, M. G. (2016). In Vitro Experimental Model of Trained Innate Immunity in Human Primary Monocytes. *Clinical and Vaccine Immunology*, *23*(12), 926-933. <https://doi.org/10.1128/cvi.00349-16>
- Bekkering, S., Domínguez-Andrés, J., Joosten, L. A. B., Riksen, N. P., & Netea, M. G. (2021). Trained Immunity: Reprogramming Innate Immunity in Health and Disease. *Annual Review of Immunology*, *39*(1), 667-693. <https://doi.org/10.1146/annurev-immunol-102119-073855>
- Benjaskulluecha, S., Boonmee, A., Haque, M., Wongprom, B., Pattarakankul, T., Pongma, C., Sri-Ngern-Ngam, K., Keawvilai, P., Sukdee, T., Saechue, B., Kueanjinda, P., & Palaga, T. (2024). O(6)-Methylguanine DNA Methyltransferase Regulates Beta-Glucan-Induced Trained Immunity of Macrophages Via Farnesoid X Receptor and Ampk. *iScience*, *27*(1), 108733. <https://doi.org/10.1016/j.isci.2023.108733>
- Beura, L. K., Hamilton, S. E., Bi, K., Schenkel, J. M., Odumade, O. A., Casey, K. A., Thompson, E. A., Fraser, K., Rosato, P. C., Filali - Mouhim, A., Sékaly, R. P., Jenkins, M. K., Vezys, V., Haining, W. N., Jameson, S. C., & Masopust, D. (2016). Normalizing the Environment Recapitulates Adult Human Immune Traits in Laboratory Mice. *Nature*, *532*(7600), 512-516. <https://doi.org/10.1038/nature17655>
- Biering-Sørensen, S., Aaby, P., Lund, N., Monteiro, I., Jensen, K. J., Eriksen, H. B., Schaltz - Buchholzer, F., Jørgensen, A. S. P., Rodrigues, A., Fisker, A. B., & Benn, C. S. (2017). Early BCG-Denmark and Neonatal Mortality among Infants Weighing <math>\geq 2500\text{ G}</math>: A Randomized Controlled Trial. *Clinical Infectious Diseases*, *65*(7), 1183-1190. <https://doi.org/10.1093/cid/cix525>
- Biering-Sørensen, S., Jensen, K. J., Monterio, I., Ravn, H., Aaby, P., & Benn, C. S. (2017). Rapid Protective Effects of Early BCG on Neonatal Mortality among Low Birth Weight Boys: Observations from Randomized Trials. *The Journal of Infectious Diseases*, *217*(5), 759-766. <https://doi.org/10.1093/infdis/jix612>
- Bister, J., Filipovic, I., Sun, D., Crona-Guterstam, Y., Cornillet, M., Ponzetta, A., Michaëlsson, J., Gidlöf, S., Ivarsson, M. A., Strunz, B., & Björkström, N. K. (2024). Tissue-Specific Nonheritable Influences Drive Endometrial Immune System Variation. *Science Immunology*, *9*(94), eadj7168. <https://doi.org/doi:10.1126/sciimmunol.adj7168>
- Bonilla, F. A., & Oettgen, H. C. (2010). Adaptive Immunity. *Journal of Allergy and Clinical Immunology*, *125*(2), S33-S40. <https://doi.org/10.1016/j.jaci.2009.09.017>
- Cao, Z., West, C., Norton-Wenzel, C. S., Rej, R., Davis, F. B., Davis, P. J., & Rej, R. (2009). Effects of Resin or Charcoal Treatment on Fetal Bovine Serum and Bovine Calf Serum. *Endocrine Research*, *34*(4), 101-108. <https://doi.org/10.3109/07435800903204082>
- Cheng, Q. J., Farrell, K., Fenn, J., Ma, Z., Makanani, S. K., & Siemsen, J. (2024). Dectin-1 Ligands Produce Distinct Training Phenotypes in Human Monocytes through Differential Activation of Signaling Networks. *Scientific Reports*, *14*(1), 1454. <https://doi.org/10.1038/s41598-024-51620-8>
- Cheng, S.-C., Scicluna, B. P., Arts, R. J. W., Gresnigt, M. S., Lachmandas, E., Giamarellos-Bourboulis, E. J., Kox, M., Manjeri, G. R., Wagenaars, J. A. L., Cremer, O. L., Leentjens, J., van der Meer, A. J., van de Veerdonk, F. L., Bonten, M. J., Schultz, M. J., Willems, P. H. G. M., Pickkers, P., Joosten, L. A. B., van der Poll, T., & Netea, M. G. (2016). Broad Defects in the Energy Metabolism of Leukocytes Underlie Immunoparalysis in Sepsis. *Nature Immunology*, *17*(4), 406-413. <https://doi.org/10.1038/ni.3398>
- Cheng, S. C., Quintin, J., Cramer, R. A., Shepardson, K. M., Saeed, S., Kumar, V., Giamarellos-Bourboulis, E. J., Martens, J. H., Rao, N. A., Aghajani-refah, A., Manjeri, G. R., Li, Y., Ifrim, D. C., Arts, R. J., van der Veer, B. M., Deen, P. M., Logie, C., O'Neill, L. A., Willems, P., . . . Netea, M. G. (2014). mTOR- and Hif-1 $\alpha$ -Mediated Aerobic Glycolysis as Metabolic Basis for Trained Immunity. *Science*, *345*(6204), 1250684. <https://doi.org/10.1126/science.1250684>
- Christ, A., Günther, P., Lauterbach, M. A., Duewell, P., Biswas, D., Pelka, K., Scholz, C. J., Oosting, M., Haendler, K., Baßler, K., Klee, K., Schulte-Schrepping, J., Ulas, T., Moorlag, S. J. C. F. M., Kumar, V., Park, M. H., Joosten, L. A. B., Groh, L., Riksen, N. P., . . . Latz, E. (2018). Western Diet Triggers NLRP3-Dependent Innate Immune Reprogramming. *Cell*, *172*(1-2), 162-175.e114. <https://doi.org/10.1016/j.cell.2017.12.013>
- Cirovic, B., de Bree, L. C. J., Groh, L., Blok, B. A., Chan, J., van der Velden, W., Bremmers, M. E. J., van Crevel, R., Handler, K., Picelli, S., Schulte-Schrepping, J., Klee, K., Oosting, M., Koeken, V., van Ingen, J., Li, Y., Benn, C. S., Schultze, J. L., Joosten, L. A. B., . . . Schlitzer, A. (2020). BCG Vaccination in Humans Elicits Trained Immunity Via the Hematopoietic Progenitor Compartment. *Cell Host & Microbe*, *28*(2), 322-334 e325. <https://doi.org/10.1016/j.chom.2020.05.014>
- Covián, C., Ríos, M., Berrios, R. V., Bueno, S. M., & Kalergis, A. M. (2021). Induction of Trained Immunity by Recombinant Vaccines. *Frontiers in Immunology*, *11*, 611946. <https://doi.org/10.3389/fimmu.2020.611946>

- de Bree, L. C. J., Janssen, R., Aaby, P., van Crevel, R., Joosten, L. A. B., Benn, C. S., & Netea, M. G. (2018). The Impact of Sex Hormones on BCG-Induced Trained Immunity. *Journal of Leukocyte Biology*, *104*(3), 573-578. <https://doi.org/10.1002/JLB.5MA0118-027R>
- De Silva, N. S., & Klein, U. (2015). Dynamics of B Cells in Germinal Centres. *Nature Reviews Immunology*, *15*(3), 137-148. <https://doi.org/10.1038/nri3804>
- Ding, C., Shrestha, R., Zhu, X., Geller, A. E., Wu, S., Woeste, M. R., Li, W., Wang, H., Yuan, F., Xu, R., Chariker, J. H., Hu, X., Li, H., Tieri, D., Zhang, H. G., Rouchka, E. C., Mitchell, R., Siskind, L. J., Zhang, X., . . . Yan, J. (2023). Inducing Trained Immunity in Pro-Metastatic Macrophages to Control Tumor Metastasis. *Nature Immunology*, *24*(2), 239-254. <https://doi.org/10.1038/s41590-022-01388-8>
- Divangahi, M., Aaby, P., Khader, S. A., Barreiro, L. B., Bekkering, S., Chavakis, T., van Crevel, R., Curtis, N., DiNardo, A. R., Dominguez-Andres, J., Duivenvoorden, R., Fanucchi, S., Fayad, Z., Fuchs, E., Hamon, M., Jeffrey, K. L., Khan, N., Joosten, L. A. B., Kaufmann, E., . . . Netea, M. G. (2021). Trained Immunity, Tolerance, Priming and Differentiation: Distinct Immunological Processes. *Nature Immunology*, *22*(1), 2-6. <https://doi.org/10.1038/s41590-020-00845-6>
- Domínguez-Andrés, J., Arts, R. J. W., Bekkering, S., Bahrar, H., Blok, B. A., de Bree, L. C. J., Bruno, M., Bulut, Ö., Debisarun, P. A., Dijkstra, H., Cristina dos Santos, J., Ferreira, A. V., Flores-Gomez, D., Groh, L. A., Grondman, I., Helder, L., Jacobs, C., Jacobs, L., Jansen, T., . . . Netea, M. G. (2021). In vitro Induction of Trained Immunity in Adherent Human Monocytes. *STAR Protocols*, *2*(1), 100365. <https://doi.org/https://doi.org/10.1016/j.xpro.2021.100365>
- Domínguez-Andrés, J., Joosten, L. A. B., & Netea, M. G. (2019). Induction of Innate Immune Memory: The Role of Cellular Metabolism. *Current Opinion in Immunology*, *56*, 10-16. <https://doi.org/https://doi.org/10.1016/j.coi.2018.09.001>
- Domínguez - Andrés, J., Novakovic, B., Li, Y., Scicluna, B. P., Gresnigt, M. S., Arts, R. J. W., Oosting, M., Moorlag, S. J. C. F. M., Groh, L., Zwaag, J., Koch, R. M., Horst, R. t., Joosten, L. A. B., Wijmenga, C., Michelucci, A., Poll, T. v. d., Kox, M., Pickkers, P., Kumar, V., & Stunnenberg, H. (2019). The Itaconate Pathway Is a Central Regulatory Node Linking Innate Immune Tolerance and Trained Immunity. *Cell Metabolism*, *29*(1), 211-220.e215. <https://doi.org/10.1016/j.cmet.2018.09.003>
- Earhart, A. P., Karasseva, N. G., Storey, K. M., Olthoff, B., Sarker, M. B., Laffey, K. G., Lange, M. J., Rector, R. S., Schulz, L. C., Gil, D., Neuhauser, C. M., & Schrum, A. G. (2023). Lower Female Survival from an Opportunistic Infection Reveals Progesterone-Driven Sex Bias in Trained Immunity. *Cell Reports*, *42*(8), 113007. <https://doi.org/10.1016/j.celrep.2023.113007>
- Fanucchi, S., Dominguez-Andres, J., Joosten, L. A. B., Netea, M. G., & Mhlanga, M. M. (2021). The Intersection of Epigenetics and Metabolism in Trained Immunity. *Immunity*, *54*(1), 32-43. <https://doi.org/10.1016/j.immuni.2020.10.011>
- Forsyth, K. S., Jiwrajka, N., Lovell, C. D., Toothacre, N. E., & Anguera, M. C. (2024). The Connexion between Sex and Immune Responses. *Nature Reviews Immunology*, *24*, 487-502. <https://doi.org/10.1038/s41577-024-00996-9>
- Gal-Oz, S. T., Maier, B., Yoshida, H., Seddu, K., Elbaz, N., Czysz, C., Zuk, O., Stranger, B. E., Ner-Gaon, H., & Shay, T. (2019). Immgen Report: Sexual Dimorphism in the Immune System Transcriptome. *Nature Communications*, *10*(1), 4295. <https://doi.org/10.1038/s41467-019-12348-6>
- Geckin, B., Konstantin Fohse, F., Dominguez-Andres, J., & Netea, M. G. (2022). Trained Immunity: Implications for Vaccination. *Current Opinion in Immunology*, *77*, 102190. <https://doi.org/10.1016/j.coi.2022.102190>
- Goodridge, H. S., Reyes, C. N., Becker, C. A., Katsumoto, T. R., Ma, J., Wolf, A. J., Bose, N., Chan, A. S., Magee, A. S., Danielson, M. E., Weiss, A., Vasilakos, J. P., & Underhill, D. M. (2011). Activation of the Innate Immune Receptor Dectin-1 Upon Formation of a 'Phagocytic Synapse'. *Nature*, *472*(7344), 471-475. <https://doi.org/10.1038/nature10071>
- Gourbal, B., Pinaud, S., Beckers, G. J. M., Van Der Meer, J. W. M., Conrath, U., & Netea, M. G. (2018). Innate Immune Memory: An Evolutionary Perspective. *Immunological Reviews*, *283*(1), 21-40. <https://doi.org/https://doi.org/10.1111/imr.12647>
- Hajishengallis, G., Netea, M. G., & Chavakis, T. (2023). Innate Immune Memory, Trained Immunity and Nomenclature Clarification. *Nature Immunology*, *24*(9), 1393-1394. <https://doi.org/10.1038/s41590-023-01595-x>
- Hole, C. R., Wager, C. M. L., Castro-Lopez, N., Campuzano, A., Cai, H., Wozniak, K. L., Wang, Y., & Wormley, F. L., Jr. (2019). Induction of Memory-Like Dendritic Cell Responses in Vivo. *Nature Communications*, *10*(1), 2955. <https://doi.org/10.1038/s41467-019-10486-5>
- Hu, Z., Lu, S. H., Lowrie, D. B., & Fan, X. Y. (2022). Trained Immunity: A Yin-Yang Balance. *MedComm*, *3*(1), e121. <https://doi.org/10.1002/mco2.121>
- Ikeda, Y., Adachi, Y., Ishii, T., Miura, N., Tamura, H., & Ohno, N. (2008). Dissociation of Toll-Like Receptor 2-Mediated Innate Immune Response to Zymosan by Organic Solvent-Treatment without Loss of Dectin-1 Reactivity. *Biological and Pharmaceutical Bulletin*, *31*(1), 13-18. <https://doi.org/10.1248/bpb.31.13>

- Kalafati, L., Kourtzelis, I., Schulte-Schrepping, J., Li, X., Hatzioannou, A., Grinenko, T., Hagag, E., Sinha, A., Has, C., Dietz, S., Domingues, A. M. d. J., Nati, M., Sormendi, S., Neuwirth, A., Chatzigeorgiou, A., Ziogas, A., Lesche, M., Dahl, A., Henry, I., . . . Chavakis, T. (2020). Innate Immune Training of Granulopoiesis Promotes Anti-Tumor Activity. *Cell*, 183(3), 771-785. <https://doi.org/10.1016/j.cell.2020.09.058>
- Kalia, N., Singh, J., & Kaur, M. (2021). The Role of Dectin-1 in Health and Disease. *Immunobiology*, 226(2), 152071. <https://doi.org/https://doi.org/10.1016/j.imbio.2021.152071>
- Kankkunen, P., Teirilä, L., Rintahaka, J., Alenius, H., Wolff, H., & Matikainen, S. (2010). (1,3)-B-Glucans Activate Both Dectin-1 and NLRP3 Inflammasome in Human Macrophages. *The Journal of Immunology*, 184(11), 6335-6342. <https://doi.org/10.4049/jimmunol.0903019>
- Katzmarski, N., Domínguez-Andrés, J., Cirovic, B., Renieris, G., Ciarlo, E., Le Roy, D., Lepikhov, K., Kattler, K., Gasparoni, G., Händler, K., Theis, H., Beyer, M., van der Meer, J. W. M., Joosten, L. A. B., Walter, J., Schultze, J. L., Roger, T., Giamarellos-Bourboulis, E. J., Schlitzer, A., & Netea, M. G. (2021). Transmission of Trained Immunity and Heterologous Resistance to Infections across Generations. *Nature Immunology*, 22(11), 1382-1390. <https://doi.org/10.1038/s41590-021-01052-7>
- Kaufmann, E., Landekic, M., Downey, J., Chronopoulos, J., Teimouri Nezhad, S., Tran, K., Vinh, D. C., Barreiro, L. B., & Divangahi, M. (2022). Lack of Evidence for Intergenerational Inheritance of Immune Resistance to Infections. *Nature Immunology*, 23(2), 203-207. <https://doi.org/10.1038/s41590-021-01102-0>
- Klein, S. L., & Flanagan, K. L. (2016). Sex Differences in Immune Responses. *Nature Reviews Immunology*, 16(10), 626-638. <https://doi.org/10.1038/nri.2016.90>
- Kleinnijenhuis, J., Quintin, J., Preijers, F., Benn, C. S., Joosten, L. A. B., Jacobs, C., Loenhout, J. v., Xavier, R. J., Aaby, P., Meer, J. W. M. v. d., Crevel, R. v., & Netea, M. G. (2013). Long-Lasting Effects of BCG Vaccination on Both Heterologous Th1/Th17 Responses and Innate Trained Immunity. *Journal of Innate Immunity*, 6(2), 152-158. <https://doi.org/10.1159/000355628>
- Kleinnijenhuis, J., Quintin, J., Preijers, F., Joosten, L. A. B., Ifrim, D. C., Saeed, S., Jacobs, C., Loenhout, J. v., Jong, D. d., Stunnenberg, H. G., Xavier, R. J., Meer, J. W. M. v. d., Crevel, R. v., & Netea, M. G. (2012). Bacille Calmette-Guérin Induces NOD2-Dependent Nonspecific Protection from Reinfection Via Epigenetic Reprogramming of Monocytes. *Proceedings of the National Academy of Sciences*, 109(43), 17537-17542. <https://doi.org/10.1073/pnas.1202870109>
- Lau, C. M., Adams, N. M., Geary, C. D., Weizman, O.-E., Rapp, M., Pritykin, Y., Leslie, C. S., & Sun, J. C. (2018). Epigenetic Control of Innate and Adaptive Immune Memory. *Nature Immunology*, 19(9), 963-972. <https://doi.org/10.1038/s41590-018-0176-1>
- Mata-Martinez, P., Bergon-Gutierrez, M., & Del Fresno, C. (2022). Dectin-1 Signaling Update: New Perspectives for Trained Immunity. *Frontiers in Immunology*, 13, 812148. <https://doi.org/10.3389/fimmu.2022.812148>
- Medzhitov, R. (2001). Toll-Like Receptors and Innate Immunity. *Nature Reviews Immunology*, 1(2), 135-145. <https://doi.org/10.1038/35100529>
- Moorlag, S., Folkman, L., Ter Horst, R., Krausgruber, T., Barreca, D., Schuster, L. C., Fife, V., Matzaraki, V., Li, W., Reichl, S., Mourits, V. P., Koeken, V., de Bree, L. C. J., Dijkstra, H., Lemmers, H., van Cranenbroek, B., van Rijssen, E., Koenen, H., Joosten, I., . . . Bock, C. (2024). Multi-Omics Analysis of Innate and Adaptive Responses to BCG Vaccination Reveals Epigenetic Cell States That Predict Trained Immunity. *Immunity*, 57(1), 171-187 e114. <https://doi.org/10.1016/j.immuni.2023.12.005>
- Moorlag, S., Khan, N., Novakovic, B., Kaufmann, E., Jansen, T., van Crevel, R., Divangahi, M., & Netea, M. G. (2020). B-Glucan Induces Protective Trained Immunity against Mycobacterium Tuberculosis Infection: A Key Role for IL-1. *Cell Rep*, 31(7), 107634. <https://doi.org/10.1016/j.celrep.2020.107634>
- Netea, M. G., Domínguez-Andrés, J., Barreiro, L. B., Chavakis, T., Divangahi, M., Fuchs, E., Joosten, L. A. B., van der Meer, J. W. M., Mhlanga, M. M., Mulder, W. J. M., Riksen, N. P., Schlitzer, A., Schultze, J. L., Stabell Benn, C., Sun, J. C., Xavier, R. J., & Latz, E. (2020). Defining Trained Immunity and Its Role in Health and Disease. *Nature Reviews Immunology*, 20(6), 375-388. <https://doi.org/10.1038/s41577-020-0285-6>
- Netea, M. G., & Meer, J. W. M. v. d. (2017). Trained Immunity: An Ancient Way of Remembering. *Cell Host & Microbe*, 21(3), 297-300. <https://doi.org/10.1016/j.chom.2017.02.003>
- Netea, Mihai G., Quintin, J., & van der Meer, Jos W. M. (2011). Trained Immunity: A Memory for Innate Host Defense. *Cell Host & Microbe*, 9(5), 355-361. <https://doi.org/https://doi.org/10.1016/j.chom.2011.04.006>
- Netea, M. G., Schlitzer, A., Placek, K., Joosten, L. A. B., & Schultze, J. L. (2019). Innate and Adaptive Immune Memory: An Evolutionary Continuum in the Host's Response to Pathogens. *Cell Host & Microbe*, 25(1), 13-26. <https://doi.org/10.1016/j.chom.2018.12.006>
- Ochando, J., Mulder, W. J. M., Madsen, J. C., Netea, M. G., & Duivenvoorden, R. (2023). Trained Immunity — Basic Concepts and Contributions to Immunopathology. *Nature Reviews Nephrology*, 19(1), 23-37. <https://doi.org/10.1038/s41581-022-00633-5>
- Quintin, J., Saeed, S., Martens, J. H. A., Giamarellos-Bourboulis, E. J., Ifrim, D. C., Logie, C., Jacobs, L., Jansen, T., Kullberg, B. J., Wijmenga, C., Joosten, L. A. B., Xavier, R. J., van der Meer, J. W. M., Stunnenberg,

- H. G., & Netea, M. G. (2012). Candida Albicans Infection Affords Protection against Reinfection Via Functional Reprogramming of Monocytes. *Cell Host & Microbe*, 12(2), 223-232. <https://doi.org/10.1016/j.chom.2012.06.006>
- Riksen, N. P., Bekkering, S., Mulder, W. J. M., & Netea, M. G. (2023). Trained Immunity in Atherosclerotic Cardiovascular Disease. *Nature Reviews Cardiology*, 20(12), 799-811. <https://doi.org/10.1038/s41569-023-00894-y>
- Robinson, K. A., Akbar, N., Baidžajevas, K., & Choudhury, R. P. (2023). Trained Immunity in Diabetes and Hyperlipidemia: Emerging Opportunities to Target Cardiovascular Complications and Design New Therapies. *FASEB Journal*, 37(11), e23231. <https://doi.org/https://doi.org/10.1096/fj.202301078R>
- Rosshart, S. P., Herz, J., Vassallo, B. G., Hunter, A., Wall, M., Badger, J. H., McCulloch, J. A., Anastasakis, D. G., Sarshad, A. A., Leonardi, I., Collins, N., Blatter, J., Han, S. W., Tamoutounour, S., Potapova, S., Claire, M., Yuan, W., Sen, S. K., Dreier, M. S., . . . Rehermann, B. (2019). Laboratory Mice Born to Wild Mice Have Natural Microbiota and Model Human Immune Responses. *Science*, 365(6452). <https://doi.org/10.1126/science.aaw4361>
- Roth, A., Sodemann, M., Jensen, H., Poulsen, A., Gustafson, P., Weise, C. F., Gomes, J., Djana, Q., Jakobsen, M. D., Garly, M. L., Rodrigues, A., & Aaby, P. (2006). Tuberculin Reaction, BCG Scar, and Lower Female Mortality. *Epidemiology*, 17(5), 562-568. <https://doi.org/10.1097/01.ede.0000231546.14749.ab>
- Saeed, S., Quintin, J., Kerstens, H. H., Rao, N. A., Aghajani-refah, A., Matarese, F., Cheng, S. C., Ratter, J., Berentsen, K., van der Ent, M. A., Sharifi, N., Janssen-Megens, E. M., Ter Huurne, M., Mandoli, A., van Schaik, T., Ng, A., Burden, F., Downes, K., Frontini, M., . . . Stunnenberg, H. G. (2014). Epigenetic Programming of Monocyte-to-Macrophage Differentiation and Trained Innate Immunity. *Science*, 345(6204), 1251086. <https://doi.org/10.1126/science.1251086>
- Saz-Leal, P., Del Fresno, C., Brandi, P., Martínez-Cano, S., Dungan, O. M., Chisholm, J. D., Kerr, W. G., & Sancho, D. (2018). Targeting Ship-1 in Myeloid Cells Enhances Trained Immunity and Boosts Response to Infection. *Cell Reports*, 25(5), 1118-1126. <https://doi.org/10.1016/j.celrep.2018.09.092>
- Shepherd, R., Cheung, A. S., Pang, K., Saffery, R., & Novakovic, B. (2020). Sexual Dimorphism in Innate Immunity: The Role of Sex Hormones and Epigenetics. *Frontiers in Immunology*, 11, 604000. <https://doi.org/10.3389/fimmu.2020.604000>
- Stensballe, L. G., Nante, E., Jensen, I. P., Kofoed, P. E., Poulsen, A., Jensen, H., Newport, M. J., Marchant, A., & Aaby, P. (2005). Acute Lower Respiratory Tract Infections and Respiratory Syncytial Virus in Infants in Guinea-Bissau: A Beneficial Effect of BCG Vaccination for Girls. *Vaccine*, 23(10), 1251-1257. <https://doi.org/10.1016/j.vaccine.2004.09.006>
- Stražar, M., Mourits, V. P., Koeken, V. A. C. M., Bree, L. C. J. d., Moorlag, S. J. C. F. M., Joosten, L. A. B., Crevel, R. v., Vlamakis, H., Netea, M. G., & Xavier, R. J. (2021). The Influence of the Gut Microbiome on BCG-Induced Trained Immunity. *Genome Biology*, 22(1). <https://doi.org/10.1186/s13059-021-02482-0>
- Sviridov, D., Miller, Y. I., & Bukrinsky, M. I. (2022). Trained Immunity and Hiv Infection. *Frontiers in Immunology*, 13, 903884. <https://doi.org/10.3389/fimmu.2022.903884>
- van der Heijden, C., Noz, M. P., Joosten, L. A. B., Netea, M. G., Riksen, N. P., & Keating, S. T. (2018). Epigenetics and Trained Immunity. *Antioxidants & Redox Signaling*, 29(11), 1023-1040. <https://doi.org/10.1089/ars.2017.7310>
- van Leent, M. M. T., Priem, B., Schrijver, D. P., de Dreu, A., Hofstraat, S. R. J., Zwolsman, R., Beldman, T. J., Netea, M. G., & Mulder, W. J. M. (2022). Regulating Trained Immunity with Nanomedicine. *Nature Reviews Materials*, 7(6), 465-481. <https://doi.org/10.1038/s41578-021-00413-w>
- Vivier, É., Rautlet, D. H., Moretta, A., Caligiuri, M. A., Zitvogel, L., Lanier, L. L., Yokoyama, W. M., & Ugolini, S. (2011). Innate or Adaptive Immunity? The Example of Natural Killer Cells. *Science*, 331(6013), 44-49. <https://doi.org/10.1126/science.1198687>
- Walachowski, S., Tabouret, G., Fabre, M., & Foucras, G. (2017). Molecular Analysis of a Short-Term Model of B-Glucans-Trained Immunity Highlights the Accessory Contribution of GM-CSF in Priming Mouse Macrophages Response. *Frontiers in Immunology*, 8, 1089. <https://doi.org/10.3389/fimmu.2017.01089>
- Yona, S., Kim, K. W., Wolf, Y., Mildner, A., Varol, D., Breker, M., Strauss-Ayali, D., Viukov, S., Guilliams, M., Misharin, A., Hume, D. A., Perlman, H., Malissen, B., Zelzer, E., & Jung, S. (2013). Fate Mapping Reveals Origins and Dynamics of Monocytes and Tissue Macrophages under Homeostasis. *Immunity*, 38(1), 79-91. <https://doi.org/10.1016/j.immuni.2012.12.001>